COUPLING OF BACKBARRIER SHORELINES TO GEOMORPHOLOGICAL PROCESSES

A Thesis

by

SARAH MARGARET TRIMBLE

Submitted to the Office of Graduate Studies of
Texas A&M University
in partial fulfillment of the requirements for the degree of

MASTER OF SCIENCE

Approved by:

Chair of Committee,	Christopher Houser
Committee Members,	Anthony Filippi
	Rick Giardino
Head of Department,	Vatche Tchakarian

August 2013

Major Subject: Geography

ABSTRACT

Recent evidence suggests that backbarrier structure may act as an historical record of island development, and that backbarrier shorelines can be used as a proxy of an island's past and future transgressive response to sea-level rise. The structure and stability of back-barrier shorelines are dependent on the geologic framework, defined here as the combination of nearshore topography, underlying geology, and modern geomorphologic forces. This antecedent framework controls and influences the present morphology, nearshore dynamics, and rates of transgression in response to sea-level rise while also acting as a feedback to the estuary ecology on the bayside. It is therefore surprising that our understanding of backbarrier geomorphology is limited. There is a need for an established link between process regimes and an island's geomorphological history. This thesis bridges the current intellectual gap.

The primary hypothesis of this project is that shorelines and bathymetric isolines share quantitative shape signatures indicative of their shared morphological past. To establish this link, the backbarrier shorelines of four United States National Seashores (Fire Island, NY; Assateague Island, MD; Santa Rosa Island, FL; and North Padre Island, TX) are digitized from aerial imagery using the marshline as the shoreline indicator to ensure the inclusion of (vital, sometimes inundated) ecosystems and sediment storage. The alongshore variation of this backbarrier shoreline, the mainland shoreline, lagoon bathymetry, and nearshore bathymetry are each quantified through wavelet analysis and their shape signatures are examined for spatial correspondence.

Large and small scale variations are identified and attributed to the geomorphologic controls operating on the same scale and alongshore variation. The result is an improved understanding of how the geologic framework controls backbarrier shoreline shape, which is essentially an expression of the underlying geology.

ACKNOWLEDGEMENTS

I would like to thank my committee chair, Dr. Houser, and my committee members, Dr. Filippi and Dr. Giardino, for their guidance and feedback. Their support was critical to my completion of the research presented here.

I am also thankful for the friends and colleagues who made my experience at Texas A&M University so memorable. The advice and support this community provided in the office (and after hours) have made me an Aggie for life. I also want to extend my gratitude to Dr. Houser, Dr. Brannstrom, and the Department of Geography for awarding me the Research Assistantships that made it financially possible for me to complete my research, and to the National Science Foundation and Texas SeaGrant for providing those grants. Thanks are also due to the US Department of Veterans Affairs for their financial assistance, and to my father, Lieutenant Colonel Edward Trimble, for earning that assistance through his continued service to this country for more than 25 years. His example of service to others is only outshined by his persistent reminders to prioritize the things in life which are truly most valuable.

Finally, I want to express my gratitude to my entire family for their eternal patience, especially my mother. I could not have reached this point without their boundless love and encouragement.

TABLE OF CONTENTS

Page

LIST OF FIGURES

Page

LIST OF TABLES

Page

CHAPTER I

INTRODUCTION AND STUDY SITE DESCRIPTION

Introduction

Barrier islands lie along most of the United States' Gulf and East Coasts (Dickinson, Berryhill and Holmes 1972). The dynamic nature of these landforms often conflicts with increasing development along the coast. Studies of coastal erosion are increasingly pertinent in the United States, where 50% of the population lives in coastal counties and recent storms have caused serious economic and personal loss (Crossett et al. 2004; Sallenger et al. 2009: New York Times 2012; Anderson 2013). The effects of Hurricane Sandy on New Jersey and Hurricane Katrina's impact on the Gulf Coast are recent examples (Goodnough 2005; Navarro 2012; New York Times 2012; Anderson 2013). The protective role barrier islands may play in mitigating storm damage has recently become a popular focus of science (Navarro 2012). Evidence also suggests that barrier islands absorb the destructive impact of storms and that wider islands perform this protective role better than narrower ones (Leatherman 1979; Stone and McBride 1998; Claudino-Sales, Wang, and Horwitz 2008; Houser, Hapke, and Hamilton 2008).

The ecosystem that develops on wider islands between the beach and the lagoon, hereafter referred to as the back-barrier, provides critical habitat for endangered wildlife and vegetation (Moore et al. 1990). The back-barrier also has cultural or aesthetic value and a measureable positive impact on the landscape (such as improving water quality; Kennish 2001). The ecosystems that form along the back-barrier are some of the most

biologically productive in the world, capable of providing critical habitat to filter feeders, fish, and waterfowl species (Edgar et al. 2000; Kennish 2001; Courrat et al. 2009). There is also evidence that sheltered, low-energy coasts like those on the sound-facing back-barrier are also some of the most densely populated and some of the most heavily eroding in the United States, providing further reason to investigate and preserve them (Morton, Miller, and Moore 2004; National Research Council 2007). The changing climate, sea-level rise, and a continued growth in the global population all put greater strain on fragile, critical coastal systems, including those present in the back-barrier, where "[a]n inability to expand with relative sea level rise (so called 'coastal squeeze,' French 2006), and disintegration of protective barrier islands (McBride et al. 1995; McBride and Byrnes 1997; Penland et al.2005)" are increasingly threatened by the combination of anthropogenic forces and climate change. Investigations into how these systems have responded to similar stresses in the past are vital for understanding and predicting their future response.

If societies are to continue to build and expand in coastal areas, they must learn to live with and manage complex shorelines. Learning to do so will require realistic models of the large-scale behavior of coastal systems, and to achieve such models we must first understand the detailed geologic framework controlling barrier island geomorphology. As used throughout this thesis, the term 'geologic framework' is in reference to the structure as described by Riggs, Cleary and Snyder (1994), the bathymetry and geology "underlying the shoreface and the inner shelf, as well as the physical dynamics operating within and upon regional segments of the shoreface

system." This includes the slope of the nearshore, ridges and swales in the bathymetry, and the presence of paleo-channels submerged in the nearshore. Alongshore variation in these features alters the approaching waves that would rework the island under normal conditions and storm conditions, and thereby contributes to the shaping of the barrier island.

For ocean-facing beaches, the effect of tall, well-established dunes is known to mitigate the impacts of storm level forces and prevent overwash (Sallenger 2000). When storm runup on the beach is sufficient to exceed the dune crest elevation (or berm crest, if there is no dune) then overwash, breaching, or inundation will occur and the pre-storm island will potentially be unable to recover to its previous elevation, such as narrow Santa Rosa Island, FL experienced following multiple storm impacts in 2005 (Sallenger 2000). Should these processes occur, the back-barrier shoreline may receive new deposits of sand but lose vegetation in the process. The ability of the island to rebuild a dune line will be determined by the volume of its sediment supply from the nearshore to the beach. Where this supply is abundant and the island is already wide, such as at North Padre Island, the scarping of the established dune does not result in overwash or inundation but leads instead to blowouts, which funnel excess sand into the back-barrier. This process also builds the island vertically and potentially smothers existing vegetation, but in comparison to an overwash event the 'throat' of a blowout will be narrow and close more quickly due to the abundant sediment supply.

The frequency and magnitude of storm events are predicted to increase with continued climate change, and sea-level is also predicted to rise (Kemp et al. 2011).

These shifts will increase the impact potential of all storm types, and an improved knowledge of historical changes is needed to predict how US barrier coasts will respond. Recent evidence suggests that backbarrier structure may act as an historical record of island development, and that backbarrier shorelines can be used as a proxy of an island's past and future transgressive response to sea-level rise. Specifically, the structure and stability of back-barrier shorelines are dependent on the geomorphological record of overwash, breaching, and prevailing winds (etc.), but are also a feedback to the estuary ecology (Ashton et al. 2009; Claudino-Sales, Wang, and Horwitz 2008; Houser, Hapke, and Hamilton 2008).

While storm impact regimes may be well defined for ocean-facing coasts (Sallenger 2000), process regimes in the back-barrier are not yet as well defined. Recent research has shown that when low-energy coasts of elongated water bodies, such as the back-barrier coasts along the sound, are exposed to deepwater waves they experience an increase in local instability (Ashton et al. 2009). This fetch-limiting feedback leads to the segmentation of the water body, a process which can have negative effects on water ecology, back-barrier vegetation, and maintenance of the intra-coastal waterway present behind the barrier islands of the US Gulf and East coasts (Ashton et al. 2009).

Recent evidence suggests this antecedent morphology, and the geomorphological history in general, are recorded in the back-barrier of islands (Houser, Hapke, and Hamilton 2008), which is in turn dependent on the geologic framework (Riggs, Cleary and Snyder 1994; Houser 2012). In other words, there is a multi-scale feedback in which the response of barrier islands to storms defines and is defined by the geologic

framework. Unfortunately, the methods typically used to determine an island's morphological past and historical response to sea-level rise (such as GPR or seismic surveys) are spatially limited in their application. To construct a history using these methods scientists must survey specific transects and interpolate the trends that fall between them; this is a difficult task to complete for an entire barrier island (which can be more than 30 km in length).

The methodology tested by this thesis attempts to fill these intellectual and methodological gaps by coupling shoreline shape features to nearshore geological framework. The shape signature of the back-barrier shoreline of four islands is empirically identified and coupled to each island's nearshore geologic structure, as well as the geomorphological profile assembled from the ample literature available for each island. These methods can then be applied to new locations in future research projects; investigators will be able to quantify the back-barrier shoreline shape of unstudied or poorly understood barrier islands and deduce information about that island's geomorphologic history. Understanding the correspondence between shoreline shape signatures and known morphological processes will extend geologic surveys and actuate projects on less-investigated barrier islands. The project could also lead to the connection of back-barrier morphological characteristics to vegetation density and ecosystem formation. Such results will have positive implications for the restoration, preservation, management, and development of National Seashores and other barrier islands in which the public has a vested interest. The thesis will bridge intellectual gaps by extending geologic surveys in both time and space, and offering evidence that (as

theorized) the geomorphological history of barrier islands may be recorded in the back-barrier.

The primary hypothesis of this study is that the primary mechanisms responsible for the development and evolution of the back-barrier shoreline will generate an empirically identifiable shape signature indicative of that particular geomorphology. If the back-barrier shoreline is controlled by the geologic framework, then the scales of variation in its shape will be directly related to the offshore bathymetry and in some cases, also the mainland shoreline. Vectors will share signatures, and islands with similar geologic framework will share patterns. If the back-barrier shoreline is shaped independently of the geologic framework, there will not be shared variations beyond those that occur by chance (red noise). To test the hypothesis, four objectives must be completed:

1. Build extensive profiles for four US National Seashores with an extensive geomorphological literature.
2. Acquire imagery for each location and digitize the back-barrier shoreline of each study site.
3. Quantify the shoreline shape signature of each island, using wavelet analysis to empirically identify the length frequency and alongshore variation of features in the back-barrier shoreline, the mainland shoreline, and isobaths in the lagoon and nearshore.

4. Demonstrate correspondence between these shape signatures and observed geomorphological processes (or lack thereof).

In the last half century, research in coastal geomorphology has exhibited a continuous interest in the geologic history and morphological formation of barrier islands, but the present literature repeatedly examines the same islands; the result is a well-researched and understood morphological history of certain US barrier coasts. This project capitalizes on this in-depth knowledge of limited locations by building profiles for four, heavily-researched, US barrier island systems. By focusing on islands already possessing an extensive, peer-reviewed literature, patterns in shoreline shape can be reasonably associated with the physical and morphological characteristics as determined by previous observation of each island. The findings presented by the existing literature represent known facts for each study site, and these provide potential reasons for certain shape characteristics.

In addition, each of these four islands are relatively undeveloped National Seashores. Despite some permitted human activity, such as camping, hiking, or beach driving, the features and changes in these environments can be reasonably attributed to geomorphic forces and geomorphological history, as opposed to anthropogenic development, because these influences contribute far less to the shape features persistent at the scale examined. The selection process for these study sites and the extensive profile of each study site immediately follows this introduction. This section accomplishes objective one (see above).

Chapter II follows, and describes the methods by which the different shoreline and isobath vectors were acquired and analyzed. It details the accomplishment of the second and third objectives, including the specifics of the Geographic Information Science (hereafter referred to as GIS) methods, and the analysis by which the shape signatures were extracted. Two final chapters provide the results and a discussion of these results, as well as concluding remarks for the thesis as a whole.

Study site selection

Barrier islands form on broad, gently sloping coasts all over the world; they make up approximately 5,700 kilometers of the world's coasts. Roughly 3,200 of those kilometers are barrier islands along the eastern and gulf coasts of the United States (US) (Dickinson, Berryhill and Holmes 1972). The geomorphology of these islands is controlled by wind and wave forces that combine to create gently sloped beaches facing the ocean and complex shorelines facing the lagoon. Cross-sections of barrier islands that form on passive continental margins like the East and Gulf Coasts of the US will vary depending on the nearshore geologic framework (Riggs, Cleary and Snyder 1994). The internal structure of barrier islands is controlled by climate, tidal range, sediment supply, and this underlying geology (Dickinson, Berryhill and Holmes 1972; Riggs, Cleary and Snyder 1994). A cross section from ocean to sounds has a typical profile that varies by island according to each barrier's sediment, geologic framework, and geomorphology. Generally, the gently sloping beaches facing the ocean progress into dunes, which give way to vegetated flats or marshes that transition to the shallow lagoon

separating the island from the mainland, and the mainland on the other side is typically very flat and low lying (Rosati, Dean and Stone 2010). This thesis investigates the shape signature of the lagoon-facing back-barrier coastline of these islands. For consistency, the barrier islands chosen for this study are along US coasts.

Many of these islands are developed, with roads, permanent structures, and high levels of human activity. An increased human presence influences the geomorphology of sensitive coastal systems; this is especially true for back-barrier marsh environments (Kennish 2001). Because this study seeks to improve our knowledge of the link between geomorphic process and back-barrier structure, another criterion for selection was a lack of permanent development. This led the investigator to focus on National Seashores and other state or federally-protected lands. As preserved land, National Seashores are relatively undeveloped, and their shape signatures can be reasonably attributed to geomorphologic forces and geomorphology, as opposed to human construction. Choosing to examine National Seashores also allows for conclusions from this study to have a potential impact on management decisions. "Coastal managers, especially in the federally managed lands (i.e.., Fire Island National Seashore) […] rely on science to better understand coastal processes and better manage and protect coastal resources" (Hapke et al. 2010).

A major criterion for selection was for an extensive literature detailing each site's geomorphological history, physical characteristics, and environmental importance. Fortunately, National Seashores are common study sites for many reasons – including those already mentioned. This requirement for extensive previous study was perhaps the

most limiting criterion, because research tends to repeatedly investigate the same locations, and many islands initially considered proved to have too few peer reviewed publications exploring their geomorphological and geologic history.

The shape signatures coupled to the geomorphological profiles are vectors derived from remotely sensed imagery. Availability of imagery was an additional criterion in selection of study sites. Thorough investigation of imagery availability and cost of images determined that four US National Seashores have both an extensive literature and high resolution imagery taken within the last decade (since 2002) that can be acquired at no cost. The selected islands are (from north to south): Fire Island National Seashore, Assateague Island National Seashore, Santa Rosa National Seashore, and Padre Island National Seashore (Figure 1). The in-depth profile gleaned from the literature of each barrier island is offered below. Two of these National Seashores are on the Gulf of Mexico and two are located on the Eastern seaboard. The study sites are evenly split between the two coasts to ensure that multiple barrier island types are represented, and to broaden the application of results.

Figure 1 Map of all four study site locations, indicated by red boxes on the above map of the United States.

Fire Island National Seashore, New York, US

Fire Island is a 50 km long barrier island on the northeastern coast of the United States. It comprises the central portion of the barrier island system that runs along the southern shore of Long Island, New York (Figure 2; Schwab et al. 2000). Since 1960, Fire Island has attracted the attention of scientists, politicians, and engineers because changes to its landscape (such as coastal erosion) have significant impacts on the local economy, which is largely dependent on tourism and coastal attractions (Schwab et al. 2000). The island is popular with tourists due to its national and state parks, vacation communities, a popular fishing industry, and close proximity to a densely populated

mainland (Long Island and New York City; Schwab et al. 2000). Each of these industries may be negatively impacted by erosion of the coast, and consequently Fire Island has been a frequent subject of research into its sediment budget and related topics, and has a dense peer-reviewed literature covering its modern geomorphology and geologic history.

Figure 2 Map of Fire Island National Seashore (FIIS), one of the four study sites. FIIS is a barrier off the coast of Long Island, part of the state of New York and situated along the northeastern Atlantic Coast of the United States.

Geologic history

Long Island, the mainland which Fire Island fronts, is made of glacial deposits laid down during the last ice age. These sediments were deposited during the Holocene as the climate warmed, the glaciers retreated, sea-level rose, and rivers and streams drained morraines (Hapke et al. 2010). As a result, today's Fire Island is composed of glacial deposits sourced from moraine headlands on Long Island and outwash deposits submerged offshore (Leatherman, 1985; Hapke et al. 2010). The beach sediments of western Long Island consist of rounded, well-sorted medium and fine sand quartz sands with grain sizes that vary from 0.1 to 0.5 mm, though some coarser grains (sizes 1.5 to 2.0 mm) are present; shell fragments are also common. In the marshes of the back-barrier sediments are fine-grained, organic-rich muds and peats interleaved with overwash deposits of coarser grained sand from the beach (Scileppi and Donnelly 2007). The salt-marsh in the back-barrier has accumulated at a rate of roughly 1 mm/year over the last millennium (Rampino and Sanders 1980; Donnelly et al. 2004; Scileppi and Donnelly 2007).

Accumulation in the back-barrier is almost entirely the result of overwash events recorded as geophysical evidence in and sediment cores. They show "that the entire Fire Island barrier system has migrated landward continuously, albeit intermittently, for the past 10,000 years" (Williams 1976; Swift and Moslow 1982; Leatherman and Allen 1985; Schwab et al. 2000). In the last 3,500 years, numerous strong hurricanes have impacted the region, though no major hurricanes have impacted Fire Island since 1893, and until Hurricane Sandy in 2012 no serious washover events had occurred for at least

150 years (Scileppi and Donnelly 2007; NPS 2013f). Overwash caused by storm events has had a substantial influence on the geomorphology of Fire Island throughout geologic history. Cores taken from drowned back-barrier deposits indicate that the barrier island was once located 2 km farther out to sea, and has transgressed at an average rate of 0.28 m per year in the last 7,000 years (Rampino and Sanders 1981; Scileppi and Donnelly 2007). This migration landward is driven in part by the episodic overwash events, which cause inlet and tidal delta formation (Leatherman 1983, 1985; Hennessy and Zarillo 1987; Scileppi and Donnelly 2007).

In the Moriches and Shinnecock Bays located behind the eastern half of Fire Island (north of the boundary of the National Seashore), most of the "littoral sand transport into the lagoons and relict flood-tidal deltas" is the result of inlet breaches. These deposits are additional evidence of the island's transgression, as are the many outcrops of tidal marsh sediments on the upper shoreface (Schwab et al. 2000). "In ontrast, over the past ~1000 years, most of Fire Island west of Watch Hill has experienced in-place submergence" (Sanders and Kumar 1975a; Rampino and Sanders 1981a; Leatherman 1985; Leatherman and Allen 1985; quote from Schwab et al. 2000).

Recent history (last 200 years)

Dating of sediment cores is a common method for reconstructing a history of hurricane impact (Scileppi and Donnelly 2007). If a hurricane makes landfall its "waves and storm surge can overtop coastal barriers, depositing sandy overwash fans" on backbarrier salt marshes, tidal flats, or within coastal ponds and long-term records form when organic-rich sediments re-accumulate "over storm-induced deposits, preserving

coarse overwash layers" (Redfield, 1965, 1972; Emery, 1969; McCaffrey and Thompson, 1980; Bricker-Urso et al., 1989; Roman et al., 1997; Orson et al., 1998; Liu and Fearn, 1993, 2000; Donnelly, 2005; quotes from Scileppi and Donnelly 2007). In their study of cores from spatially distinct marshes in the Fire Island back-barrier, Scileppi and Donnelly (2007) determined that: (a) similarity in overwash records suggests major storms with high surges transport coarse sediment to all back-barrier areas of Fire Island, and (b) that between 1788 and 2007, only 3 storms produced storm surge significant enough to overwash Fire Island (3 m or higher).

The hurricane record determined from overwash deposits and pollen dating within the cores showed that since 1900 multiple severe winter storms and hurricanes have impacted the region (such as hurricanes Gloria in 1985 and Sandy in 2012), causing inundation levels of maximum 1.5 – 2.0 m above mean sea level (MSL; Scileppi and Donnelly 2007). Between 1900 and 2012 10 hurricanes passed within 100 nautical miles (185.2 km) of Fire Island. The strongest storms were category 2, and the most direct storms were an unnamed system in 1938, Belle (1976), Gloria (1985), and Sandy (2012). Hurricane Sandy overwashed and breached Fire Island, but this storm is not accounted for in the analysis presented here, because the most recent imagery and the bathymetry data were all collected prior to 2012. As mentioned above, sediment cores from the backbarrier show no overwash incidents between 1954 and 2010. This suggests that the shape signatures examined in this study are drawn from several decades over which the back-barrier shoreline did not have significant change – and is therefore indicative of the

preceding history/Holocene geomorphological environment and not recent anthropogenic changes.

Overwash of a barrier island may carve channels through the dune system or add sediment to the island, so they are part of the driving force behind both the division of Fire Island by inlet formation and increases in island elevation (Leatherman, 1985; Hapke et al. 2010). The eastern and western halves of Fire Island have responded differently to storm events in the last 150 years, possibly due to nearshore bathymetry. The eastern half of the island "has migrated landward through inlet formation and subsequent marsh accretion on the bay side," while the western half has no historical inlets, and "does not appear to be migrating landward at the same rate as the eastern portion of the island" (Hapke et al. 2010). This difference may be due in part to ridge and swale topography in the nearshore, within 20 km of the ocean-facing beach (Hapke et al. 2010). The origin of this ridge and swale pattern is unknown.

In their study of spatial correspondence between overwash fan deposits, historical shoreline change rates, and bathymetry, Hapke et al. (2010) suggested that the offshore ridges control the wave shoaling that leads to breaching and overwash deposits at Fire Island. Troughs in the nearshore bathymetry are spatially correlated with zones that have exhibited net accretion over the last 75 years due to wave action that is focused by the ridges onto certain parts of the beach, and preferentially erodes those areas more than beach sections spatially correlated with swales (Hapke et al. 2010). This is especially true for the western half of the island, where the ridges are attached to the shore, and the trend over the last 75 years has been accretion. Where the ridges are not

attached (in the eastern half) shoreline change is dominated by erosion and is not variable alongshore (Hapke et al. 2010).

Though the island has narrowed by erosion on both the bayside and oceanside in recent decades, it has not migrated a large distance in the last thousand years and so in modern geologic history, Fire Island has been geologically stable (Leatherman 1983, 1985; Panageotou and Leatherman 1986; Scileppi and Donnelly 2007). The backbarrier of Fire Island appears "to be sensitive to only the most severe hurricanes" (Scileppi and Donnelly 2007). The sedimentary record exhibits overwash deposits only during years when strong hurricanes impacted the island, suggesting that "the barrier system has acted as a filter, overtopped extensively only by exceptionally high storm surges" (Scileppi and Donnelly 2007). The backbarrier shoreline as it exists today has remained largely unchanged except where a limited sediment supply has led to erosion.

Modern history (last 60 years)

Fire Island National Seashore was established in 1964 under Public Law 88-587. It contains 42 km of the 50 km long barrier island. On average, the island is only 0.5 km wide. It is separated from Long Island by the Great South Bay (NPS 2013b). The island is relatively undeveloped and so for the last 50 years the physical landscape has remained in a relatively unchanged, natural state. Beach nourishment projects have been carried out on the western half of the island, but these efforts and added material did not significantly alter shoreline change trends as tracked over a 74-year period (Hapke et al. 2010).

Today the island is bound by two artificially maintained inlets: Moriches Inlet at the north end and Fire Island Inlet on the south. Moriches inlet was formed by a storm in 1931 is now artificially maintained by jetties constructed in 1954 (Schwab et al. 2000; Hapke et al. 2010). Fire Island Inlet formed ages before and has migrated more than 7.5 km since 1825, but has been artificially maintained at its present location by jetties constructed in 1941. No new inlets breached Fire Island between 1827 and 2012, but the prior breaching of the island laid the sedimentary deposits which now form the wider west end of the island (Nordstrom and Jackson 2005). In 2012 Hurricane Sandy breached Fire Island in two locations: at Old Inlet (within the Otis Pike Fire Island High Dune Wilderness) and in Smith Point County Park (NPS 2013b). Because this investigator does not have the precise location of the Smith Point County Park breach, it cannot be determined if that breach is spatially correlated with a nearshore ridge, but the breach at Old Inlet does not spatially correlate with the offshore ridges identified in Hapke et al. (2010).

Today, the ocean-facing beach of Fire Island is dominated by a variety of dune forms, some reaching 11-13 m in height (Psuty, Grace, and Pace 2005). Alongshore transport on the ocean side of the island is east to west (Hapke et al. 2010). The beach is microtidal, with a mean tidal range of 1.3 m (Leatherman, 1985). The waves come predominantly from the east/southeast (Hapke et al. 2010). Average nearshore wave height is 1.1 – 1.3 m; average period is 6.3 – 7.1 seconds; storm waves have been recorded as high as 4.1 m (Leatherman and Allen 1985; Hubertz, Thompson and Wang 1996). The average annual storm event creates a storm surge of 0.6 m, and a typical 10-

year storm event has a surge of 1.2 m (Ebersole 1982). Hurricane or tropical storm strength events typically impact Fire Island once or twice per decade – at the same rate as the rest of northeastern US (Schwab et al. 2000).

The western end of the island, from the lighthouse to Fire Island inlet, is a prograding spit with large parallel back-dune ridges (Hapke et al. 2010). The rest of the island contains a variety of dunes interspersed alongshore, including both linear and irregular dunes, blowouts, isolated hummocks, and stabilized, vegetated dunes. The alongshore variation in these dunes can be attributed to the island's geomorphologic history, as breaching and overwash of the foredune is responsible for creating alongshore variation in sediment supply and transport (Psuty, Grace and Pace 2005).

The most common plant species on the island include pitch pine (Pinus rigida), beach grass (Ammophilia breviligulata), wax myrtle (Myrica cerifera), bayberry (M. pensylvanica), shadbush (Amelanchier canadensis), and common greenbrier (Smilax rotundifolia; Psuty, Grace and Pace 2005; NPS 2013b). The only exceptions to these native species are "within the various communities where residents have planted non-indigenous vegetation" (NPS 2013b).

Prior to 2005, little had been written about the low-energy coast on the bayside of Fire Island. The low-energy bay coastline is 49.5 km long. About 17.0 km of that coast is marsh; 24.5 km is beach; and 8.0 km is fronted by marina breakwaters, bulkheads, and docks. "Many bulkheads have been built on the high ground that would normally erode and provide [a sediment source] to nearby beaches, so even the former overwash deposits are unavailable in places" (Nordstrom and Jackson 2005). The wide, irregular

back-barrier coastline along the eastern half of the island, where the mainland shore is closest, “appears to be the result of sedimentary deposits delivered through” the tidal inlets. “The persistence of the irregular shore is due in part to the recent nature of the deposits, the lower energy in the bay waves in this fetch-restricted zone, and the presence of marsh deposits on the shore that are more resistant to wave erosion than the sandy sediments on the higher overwash platforms” (Nordstrom and Jackson 2005).

Tidal range on the bayside is low except near Fire Island Inlet, and tidal range decreases with increasing distance from inlets. Tidal ranges are especially low in the back-barrier, where super-oblique wave angles and longshore current dominate flow. The greatest longshore current velocity recorded in the field was 0.24 m/s despite avg. wind speeds of 11.7 m/s at 71 degrees from shore-normal (Nordstrom 1996).

Fetch distances are narrow in the bay. The most common and frequent winds are nearly perpendicular to shore, but have a fetch length of less than 15 km as they cross the bay. A wind rose for Fire Island is presented in Figure 3. Short fetch combines with shallow water depths (typically less than 2 m even 2 km out from the shore and still only 1 m depth at 1 km out in the lagoon) for small waves that typically break before reaching shore (Nordstrom and Jackson 2005). Significant wave height is less than 0.14 m and periods are less than 2.6 seconds (during onshore winds of 10 m/s) (Nordstrom 1996). Such minimal wind and wave action combine with a steep foreshore (only 3.0 m even at 13 m/s onshore winds) to produce a surf/swash zone so small it is indicative of an estuarine beach (Nordstrom and Jackson 2005).

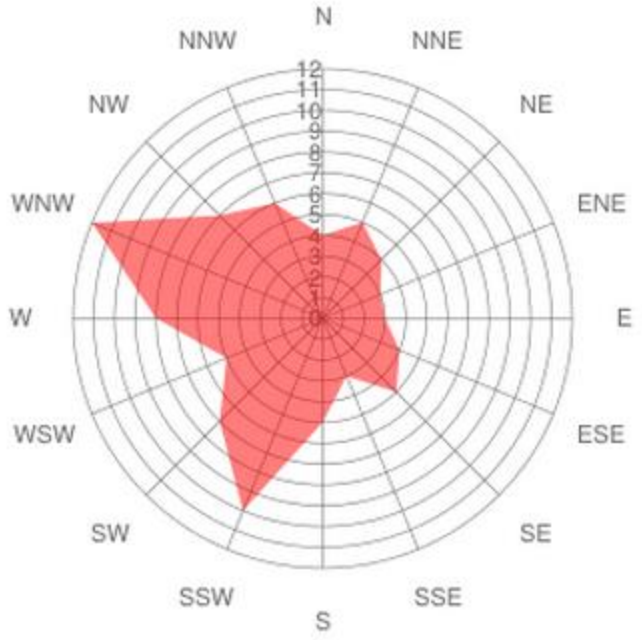

Figure 3 Wind rose for Fire Island, New York; numbers are wind speed in knots and red indicates the direction the wind blows into. The strongest, most persistent winds on an annual basis are from the ESE towards the WNW.

Residential communities located within the National Seashore when it was formed have been allowed to persist, and these are clustered together on the western half of the island. There are 17 communities in total, and in combination with land developed as visitors' centers or other structures by the National Park Service, about 25% of the total land surface in the National Seashore is 'developed' (NPS 2013b). In 2012 FIIS recorded 483,334 visitors, and has averaged 692,553 per year over the last ten years (NPS Stats 2013).

There are no paved public roads within Fire Island National Seashore, so modes of transportation are restricted to water taxis, or walking, bicycles, scooters, rollerskates,

and rollerblades on park boardwalks (NPS 2013e). There are two bridges to Fire Island, one at each end, and the only paced roads on the island lead from these to National Park facilities, but these paved sections are only 5 and 2 km in length (respectively) and do not meet; it is not possible to drive from one end of the island to the other on a paved road. Over-sand driving is permitted for residents or visitors whose destination is one of the grandfathered-in homes on the island.

Assateague Island National Seashore, Maryland, US

Assateague Island National Seashore is a 62 km long barrier island on the mid-Atlantic coast of the United States (Figure 4). The northern 35 km are in the state of Maryland, and the southern 24 are within the bounds of Virginia. Previously part of a longer, more continuous barrier, Ocean City Inlet was cut by a storm in 1933 and effectively severing the island as it remains today, because the inlet has been artificially maintained by jetties constructed in 1933 and completed in 1935 (Mackintosh 1982). The engineering and maintenance of this inlet has caused rapid changes in the rate of erosion and the position of the ocean-facing beach face at Assateague Island because the longshore current here flows north to south and Assateague Island is directly downstream of the jetty. Many peer-reviewed papers have been published on the island's sediment budget and response to storms, made more relevant by Assateague's close proximity to Ocean City, MD (a popular tourist destination) and the major metropolitan areas of Baltimore, MD and Washington, D.C. which make it a popular destination for tourists, on which the local economy is highly dependent. The NPS reported 2,154,859

visitors in 2012, and an average of 2,273,461 per year for the last decade (NPS Park Stats 2013). The rapid changes in the beach at Ocean City Inlet and its popularity as a tourist destination have made Assateague Island National Seashore a frequent subject of geologic and geomorphological study.

Geologic history

Investigation of the influence of the geologic framework on the geomorphology of Assateague Island is not a new idea. In 1985 Demarest and Leatherman mapped the Pleistocene and Holocene shorelines of the region in attempt to link the geologic history of the area with the transgression exhibited by the modern barrier islands along this part of the US Atlantic coast. Their conclusion is that the Pleistocene coastline is most clearly expressed in Maryland by Sinepuxent Neck, the mainland shoreline opposite northern Assateague Island, and that the barrier islands south of Bethany Beach, DE developed in the Holocene seaward from their current location during lower sea levels associated with the last glaciation (Demarest and Leatherman 1985).

The continuous barrier islands along Maryland's coast may have started out as separate islands with many inlets interspersed, but as they transgressed landward with Holocene sea-level rise they attached to an eroding Pleistocene headland just south of Bethany Beach, DE which has provided a steady supply of sediments and formed a continuous barrier along the Maryland coast interrupted only by the artificially maintained inlet at Ocean City, MD (Demarest and Leatherman 1985). Construction of jetties at the Ocean City Inlet at the northern end of Assateague Island in 1935 effectively trapped the littoral drift cell along this part of the coast, leading to a dramatic

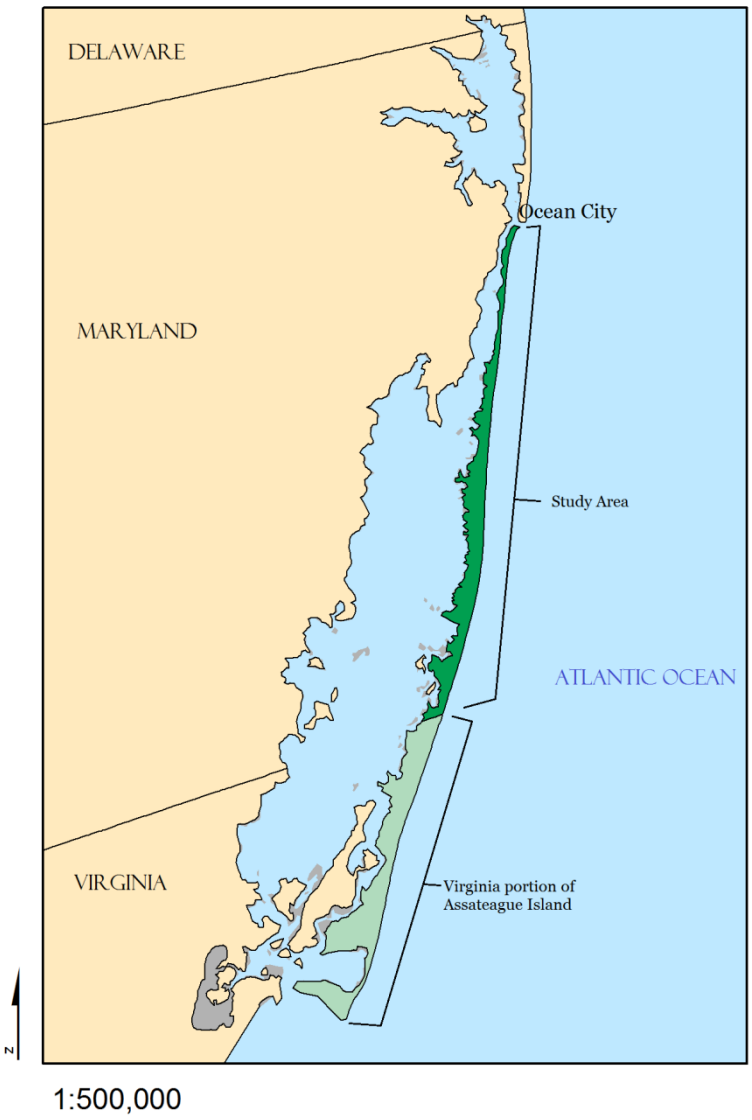

Figure 4 Study area map of Assateague Island National Seashore (ASIS), a barrier island off the coast of Maryland, along the mid-Atlantic coast of the United States.

increase in erosion and causing the oceanward beach face to retreat landward 9 to 12 m per year between 1935 and 1979 (Leatherman 1979). Because Assateague Island is today restricted by the Ocean City Inlet, the bulk of its sediment supply is primarily derived from offshore sands (Mackintosh 1982; Demarest and Leatherman 1985). All of the barrier islands south of Bethany Beach are currently exhibiting transgression toward the mainland, which as it continues will lead to narrower lagoons and a decrease in total wetland area in the back-barrier (Demarest and Leatherman 1985).

These islands "are composed of a thin veneer of sand over a compressible substrate" made of lagoonal muds and marsh deposits laid down when the islands were located farther out in to the Atlantic earlier in the Holocene (Rosati, Dean and Stone 2010). Over time the islands have transgressed overtop of these former deposits through repeated overwash. The washover process, when it happens repetitively over time, can cause any combination of the following: 1) removes sand from the foreshore and dune system to the back-barrier, reducing elevation through removal and compaction while also and increasing vulnerability to future overwash and breaching, 2) alongshore variability in elevation and stability as controlled by variability in subsidence rates of a non-homogenous substrate, and 3) net loss to the sediment budget of the ocean-facing beach (Rosati, Dean and Stone 2010).

Recent history (last 200 years)

Lonsghore currents flowing from Bethany, DE south towards Virginia continuously transport sediments down the Atlantic Coast. During the winter months, frontal storms and other harsh weather events remove sands from the dunes and upper

beachface, depositing it in the nearshore as offshore bars and effectively reducing the width of the beach (CITE a 2nd; NPS 2013a). In the summer milder weather reverses the process, generating gentler waves that carry the sands back onto the beach and restoring the shoreline (CITE a 2nd; NPS 2013a). The island thereby fits Sallenger's overwash regime beach type (2000).

Overwash events, whereby swash is so strong is continues up and over the crest of the most landward berm on the beach (Shepard 1973; Leatherman 1979; Sallenger 2000) often breach the primary dune line, carrying beach sediments into the back-barrier and depositing them in the eolian flats, marsh, or bay. The amount of sediment and the environment it is deposited in are controlled by storm magnitude and island width (Leatherman 1979; Sallenger 2000). At Assateague, large sections of the barrier may be overtopped by waves and swash. These events form sheet-like deposits known as overwash fans which are then only subjected to reworking by the low-energy forces present in the back-barrier normal, and so they can persist as features much longer than forms on the higher-energy ocean-facing coast (Leatherman 1979). It is also possible for repeated overwash deposition can lead to compaction of the substrate. When dredging spoils were placed in the back-barrier of Assateague, the combined weight of these sands and overwash fans caused subsidence, and rate of subsidence was correlated with the rate of accumulation of overburden (Guber and Slingerland 1981, Gayes 1983, Leatherman 1987). This compaction may also be a factor contributing to transgression of the island, by creating a positive feedback whereby overwashed sections become more vulnerable for additional overwash.

As sea levels rise and overwash of the island becomes more frequent (also due in part to shrinking widths for the northern half of the island), Assateague is moving closer to the mainland on the west as a combined result of the forces listed above. Severe storms events, which are becoming more frequent, erode sand from the ocean-facing beaches and carry it across the island where the surge re-deposits them in marshes along the western shore (Kemp et al. 2001, 2009; NPS 2013a). This process is "steadily narrowing the bay that separates the island from the mainland" (NPS 2013a).

Areas of "rapid barrier movement and greatest island width are related to inlet formation and subsequent construction of their flood-tidal deltas" (Leatherman 1979). The washover fans and deposits left by newly breached inlets form bayside 'nodes' of new deposit which then become incised with drainage systems that form overtop of them, draining waters into the sound. Today's nodes appear to coordinate with present and past inlets along the barrier. Accretion that occurs on the bayside during these overwash events can maintain island width (despite retreat in westward in position of the ocean-facing beach) if the island is at least 122 to 213 m wide; at this critical width overwash is "effective in transporting enough material for the island to compensate for shoreline losses" and it will maintaining a minimum width of 122 m (Leatherman 1979). However, revegetation cannot occur under such frequent high-velocity transport, and the establishment of dunes is nearly impossible, so although the spatial width of the island is maintained it does so as a barren flat (highly vulnerable to more overwash events). In contrast, if the island is greater than 213 m in width, overwash cannot penetrate to the bayside to make new deposits, and so any loss of beach width is not mirrored by

accretion on the back-barrier shoreline. This means that vegetation can continue to grow on the bayshore and though the island width may diminish, overwash deposits will instead grow the island vertically (Leatherman 1979).

As a result of this continued transgression, repetitive overwash, and locally restricted sediment budget Assateague Island has developed a cross-shore profile with a much more extensive back-barrier marsh than the other three study sites. This frequent overwash has severely limited the height and extent of both dunes and vegetation. At the northernmost end of Assateague Island, analysis of volume and shoreline position changes for the ocean-facing and back-barrier shorelines show alongshore trends in change of volume and position (Brock, Krabill and Sallenger 2004). Only the northernmost 10 km of Assateague were studied. This part of the island exhibited larger overall volume and transgression at its edges, and volume was maintained as these areas transgressed toward the mainland. For most of the 10 km, movement towards the mainland showed spatial correspondence to volume loss (Brock, Krabill and Sallenger 2004). Aside from affirming that the position of the ocean-facing shoreline is not the best proxy for barrier island stability or transgression, conclusions from the Brock, Krabill and Sallenger study can be expanded for the whole of the study in this thesis to imply that: 1) Leatherman's findings in 1979 were correct, and overwash fans can be eroded and subsided for net loss in the back-barrier, and 2) areas of Assateague that experience positive feedback cycles of overwash occurrence will appear narrow in the alongshore variation in island width from ocean to back-barrier shoreline (Brock, Krabill and Sallenger 2004).

Modern history (last 60 years)

All 19,000 acres (~79 km2) of the 60 km long Assateague Island is designated as a wildlife sanctuary and protected from development, with only a few roads and small building associated with the National Park Service (NPS 2013a). Paved roads do not extend more than 9 km into the island from each access point, and the visitor's centers at end are the only permanent structures on the island. Driving is allowed on 26 km of the ocean-facing beach, from the Maryland access point southward to the state boundary (permit required), but the northern end and the Virginia portion of the island are pedestrian only (Houser 2012; NPS 2013a). Significant beach restoration projects have been attempted at the northern end of Assateague, but as these sands have eroded rapidly and been moved by currents towards the south end of the island (Houser 2012) they have not affected the back-barrier shoreline shape or position.

The park has received nearly 90 million visitors since it was signed into existence in 1965, and today receives 2,273,461 visitors each year (averaged for the last decade; NPS 2013a). Two bridges provide vehicle access to the island, one from the Maryland mainland onto the northern end of the island, and one from Virginia's Chincoteague National Wildlife Refuge (CNWR), a separate island within the sound, onto the southern end of Assateague Island (NPS 2013a).

The island's Atlantic beach is now eroding rapidly at its northern end but also prograding towards the south, because while the Ocean City Inlet jetties successfully maintain the inlet they also block longshore transport from the north while continuing to deposit sediments on the southern end (now taking their supply from the northern end of

the island; Mackintosh 1982). Winds at Assateague blow predominantly toward either the south (along the long axis of the lagoon) or from the southeast into the northwest (see Figure 5).

Assateague Island National Seashore varies in width throughout, from 0.4 to 4 kilometers across. The lagoon varies in width alongshore, and narrows from up to 10 km at the southern end to less than 2 km in the north (and only 0.5 km in the northernmost 500 m, those this area is excluded for all back-barrier shoreline analysis in this thesis). More than half of the island's 79 km^2 area is back-barrier marsh containing near-shore and estuarine waters (NPS 2013a). The beach and dune portion of the island is narrow

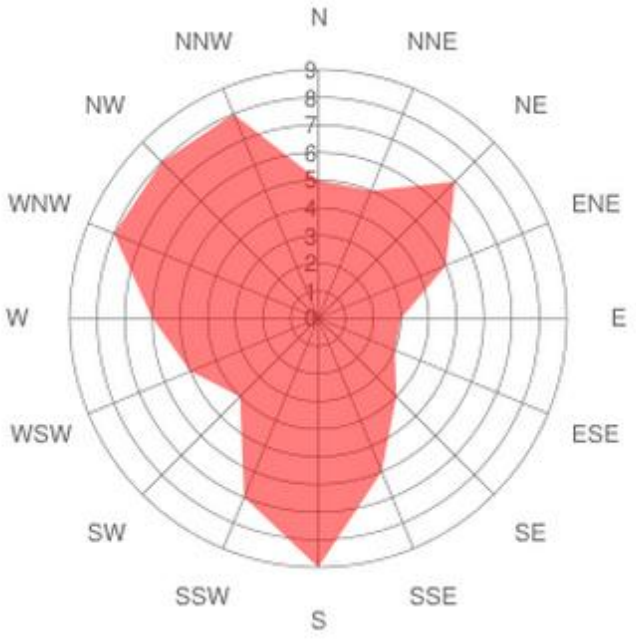

Figure 5 Wind rose data for Assateague Island.

throughout, and regular frontal storms easily alter the shoreline (NPS 2013a). This regular "exposure to salt spray, lack of fresh water, and isolation from the mainland… [have] produced a community of plants and animals uniquely suited to these extremes" (NPS 2013a).

There are distinctly different plant populations clustered together throughout the island as a result of elevation differences (up to 16m between some areas) and differences in proximity to a freshwater source and other water bodies (NPS 2013a). ASIS contains many landscapes. The beach contains both natural and man-made dunes that buffer the inland from salt spray and waves, allowing forests, marshes, beaches, shrublands, and grasslands to thrive (NPS 2013a). In the back-barrier the sheltered, nutrient rich waters of the estuary and bay waters "provide ideal breeding and spawning habitat for many aquatic species," including the blue crab (Callinectes sapidus), which is "commercially important to the local area" (NPS 2013a). The estuary behind Assateague is also an important breeding ground for many species of commercially important fish, including spot (Leiostomus xanthrurus), Atlantic menhaden (Brevoortia tyrannus) and summer flounder (Paralichthys dentatus) (NPS 2013a).

These fauna are an important food source for numerous bird species and other wildlife for which the back-barrier serves as critical habitat and which are important to the local economy. Tens of thousands of shorebirds depend upon the island for "foraging and resting areas during their twice-yearly transcontinental migrations" (NPS 2013a). Each fall, "large flocks of waterfowl such as snow geese (Chen caerulescens)" flock to

Assateague and spend the winter on the sheltered bay, salt marshes, and fallow farm fields on the mainland (NPS 2013a).

In the 1600's colonists introduced large mammals to this environment when they used the island for grazing horses and other livestock. Today bands of wild horses, descendants of the colonists' domesticated animals, number in the between 100 and 150 in a given year and graze on the grasses growing on the island (NPS 2013a). The ponies are a factor for the island's vegetation cover and thereby its geomorphology. They are also a draw for tourists to the park. "While Assateague's wild horses are perhaps the island's best-known inhabitants, other large mammals also roam the park, grazing and browsing on low-lying vegetation" (NPS 2013a). These include the white-tailed deer (Odocoileus virginianus) and the non-native sika deer (Cervus japonica), "a diminutive species of Asian elk introduced to Assateague during the 1920's" (NPS 2013a). The back-barrier is critical habitat for these animals because it provides them with grazing grounds and freshwater ponds.

Santa Rosa Island, Gulf Islands National Seashore, Florida, US

Portions of Santa Rosa Island are part of the Gulf Islands National Seashore, which is the largest National Seashore in the US and includes much of Santa Rosa Island, Perdido Key, and Cat Island in addition to portions of the mainland coast and the entirety of East and West Ship Island, Horn Island, and Petit Bois Island (NPS 2013c). It spans three states and more than 255 km of shoreline. Santa Rosa Island is an 85 km Holocene barrier island that stretches from East Pass near Destin, FL in the east to

Pensacola Inlet in the west (Figure 6). It is the second longest barrier island on the US Gulf Coast, second only to Padre Island on the coast of Texas. Santa Rosa is narrow, measuring only 1.05 km at its maximum width and 106 m at its narrowest points (average width is about 500 m; Claudino-Sales, Wang and Horwitz 2008).

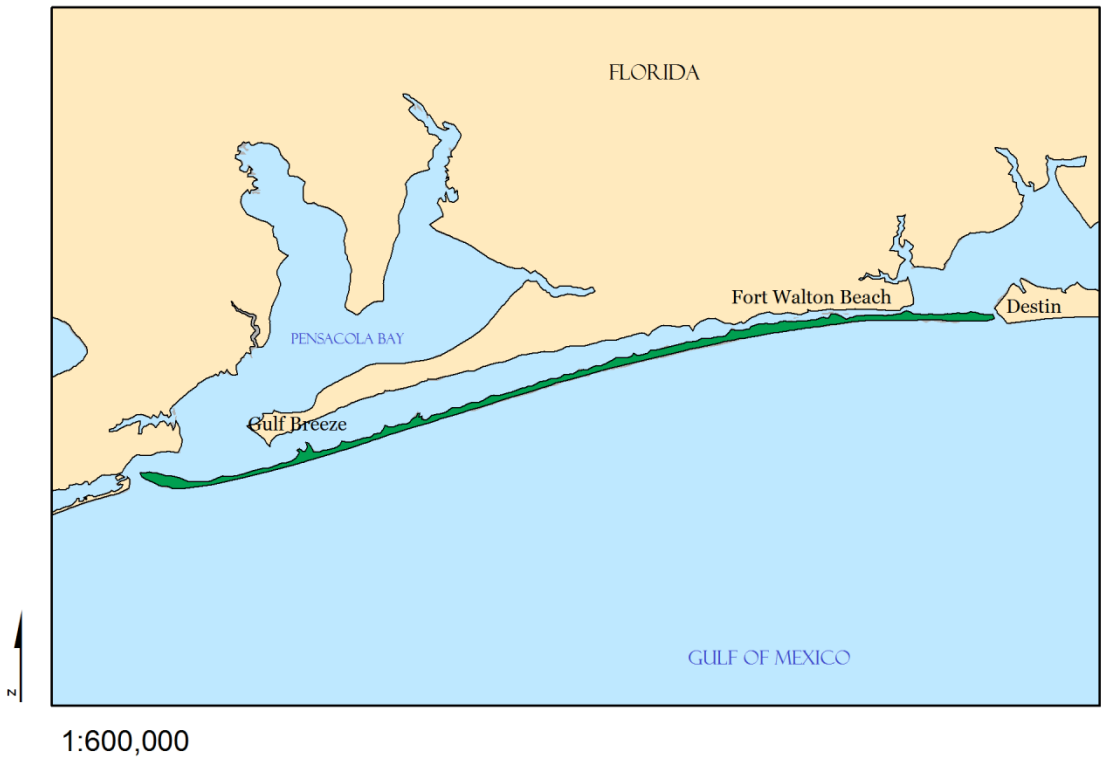

Figure 6 Study area map of Santa Rosa Island, part of the Gulf Islands National Seashore, a series of coastal areas along the northern Gulf Coast of the US states Alabama, Mississippi, and Florida.

Geologic history

Santa Rosa is a wave-dominated Holocene barrier island built over a Pleistocene core from sediments derived from the Pleistocene bluff at Destin and transported by the longshore current, which flows from east to west along this part of the Gulf of Mexico (Otvos 1981; Stone 1991; Stone et al. 1992; Stone and Stapor 1996; Davis Jr. 1997). A series of sinusoidal ridges and troughs exists just offshore for the entire length of the island. These offshore ridges are aligned with the De Soto submarine canyon slightly farther to the east, along a northwest to southeast axis at about 65º with respect to the beach (Stone 1984; Houser, Hapke, and Hamilton 2008). They extend to the 20 m isobath and farther - to offshore distances of 1700 km (Houser, Hapke, and Hamilton 2008). These features were identified as early as 1967 but little is known about their origin and development (Hyne and Goodell 1967). It is widely "hypothesized that these bathymetric features affect the wave energy incident to the coast through attenuation, refraction and defraction" (Cooper and Navas 2004; Schupp et al. 2006; Houser, Hapke and Hamilton 2008). A comparison of bathymetry data collected between 1982 and 2007 showed little to no change in the ridges, despite high storm activity in those years (Houser Hapke and Hamilton 2008).

The ridges and swales generate alognshore variations in wave energy and subsequent beach shape, which in turn controls eolian transport potential from the beach into the foredune (Houser 2012; Houser and Mathew 2011). This results in algonshore variations in dune height within the island. Taller dune heights are clustered in wider sections of the island, corresponding with the point of cusps in the back-barrier and

ridges in the nearshore. These sections also have more gently sloping beaches. The reverse conditions are present in adjacent sections of beach: the narrower sections between cusp tips have lower, discontinuous dunes spatially correlated with swales in the nearshore, and the ocean-facing beaches are steeper (Houser 2012). This alongshore variation results in variabile vulnerability to washover penetration be storms.

Recent history (last 200 years)

The sediments forming Santa Rosa Island are compositionally and texturally homogenous (Claudino-Sales, Wang, and Horwitz 2008). A typical sediment profile from the island is 99% quartz sand, with 75% of those grains having an average diameter between 0.2 and 0.4 mm (Stone and Stapor 1996; Claudino-Sales, Wang, and Horwitz 2008). The lack of diversity in the sediment is evidence of a corresponding lack of a significant terrestrial sediment source (Claudino-Sales, Wang, and Horwitz 2008). "The morphodynamics of Santa Rosa Island [are] largely controlled by the redistribution of sediment from the inner continental shelf, intertidal zone, back beach, dune field and back-barrier bay," whose distribution is largely influenced by extreme storms (Claudino-Sales, Wang, and Horwitz 2008). "The alongshore redistribution of sediment appears to occur within small littoral cells bounded by the back-barrier cuspate headlands along Santa Rosa Sound" (Houser, Hapke and Hamilton 2008).

The island is frequently hit by hurricanes, tropical depressions, and other frontal storm systems, but the gulf shoreline position remains relatively stable in position despite multiple hurricane impacts (Foster et al. 1999; Stapor 1975). "It appears that the alongshore pattern in dune morphology, shoreline erosion and storm impact are

controlled (at a range of length scales) by the transverse ridges on the inner-shelf and the island width, which is realted to the back-barrier cuspate headlands along Santa Rosa Sound" (Houser, Hapke, and Hamilton 2008).

Modern history (last 60 years)

The Santa Rosa area of the Gulf Islands National Seashore received 602,208 visitors for the 2012 fiscal year, 1,076,512 if the count includes visitors to Fort Pickens on the western end of the island (NPS Stats 2013). There are also innumerable numbers of visitors to the areas of Pensacola Beach, Navarre beach, and Fort Walton beach (Figure 6) that are not included in the National Seashore. These areas are quite developed, but the greater proportion of the island remains "pristine" (Claudino-Sales, Wang, and Horwitz 2008). Visitors come for the pristine private and federally preserved shores, with their clear waters and clean beaches (Barrett and Houser 2012). A single paved road runs the length of the island, though it has been reconstructed and moved multiple times in the last 10 years as a result of overwash events caused by storms, including Hurricane Ivan in 2004, which struck land just west of Santa Rosa, and caused a storm surge to overwash at various points along the entire barrier (see Figure 7).

The modern back-barrier shoreline of Santa Rosa, the mainland shoreline of the lagoon, and even that of adjoining Pensacola Bay have a cuspate shape reminiscent of shores present on elongate water bodies all over the world (Ashton et al. 2009). The predominant winds at Santa Rosa blow out of the northwest into the southeast, with a seasonal shift to winds from the southwest into the northeast (see Figure 8). A third axis of regular winds is aimed into the east, directly along the long-axis of the narrow Santa

Figure 7 Aerial photograph taken in the national seashore section of Santa Rosa Island immediately following the impact of Hurricane Ivan in 2005.

Rosa sound. The fetch-limited and shallow lagoon at Santa Rosa restricts the development of waves, so that only those created by winds driving down the long axis of the lagoon are capable of generating the energy necessary to reshape the back-barrier or mainland shores (which are low-energy coasts). Alongshore sediment transport is driven by these waves, and results in the buildup of sediments into cusps that reflect the locally normalized diffusion of wave action. The shoreline shape, once formed, generates a positive feedback where waves maintain the space between cusps but focus their energy on the cap tips, resulting transport that congregates at the tips and grows them further.

Once cusps reach halfway into the lagoon, cusps on opposing coasts begin to migrate toward one another. The ultimate result of this process is a self-organizing energy environment that controls the shape of the back-barrier shoreline (Ashton et al. 2009).

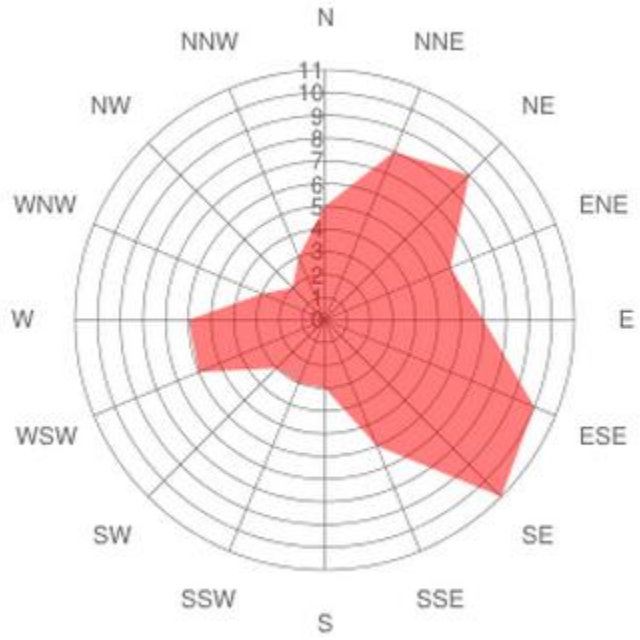

Figure 8 Wind rose data for Santa Rosa Island. Wind rose indicates the direction the wind is blowing into.

Padre Island National Seashore, Texas, US

Padre Island is the longest stretch of undeveloped barrier island coast in the world. Located on the Gulf Coast of Texas, the island is nearly 200 km when measured from the Brazos-Santiago Pass at Post Isabel to the south to Aransas Pass in the north (Figure 9). Padre Island National Seashore is the 112 km middle portion of the island, stretching from the man-made inlet maintained at Port Mansfield in the south (about 55 km north of Port Isabel) to the city boundary of Corpus Christi, TX on the northern end of the island. The area north of Mansfield Pass is commonly referred to as North Padre Island, and is it this area that is studied here. Within the National Seashore (North Padre Island) the width of the island varies from 8 km at its widest to less than 1 km in narrow spots (Weise and White 1980).

Cross-island transects are generally the same for all parts of the island: the gently sloping sandy beach facing the Gulf becomes foredunes and foredune ridges, then vegetated flats with both stable, vegetated dunes and mobile dunes, which eventually give way to sandy wind tidal flats (Weise and White 1980; Morton 1994). Some portions have elevations as high as 3 m (Morton 1994). Its pristine, nearly untouched beaches attract tourists who camping and fish within the National Seashore. There are a high numbers of visitors each year, but very few of these people make it beyond the first 8 km into the island from the beach access road, because you have to have 4-wheel-drive and because it takes significant time to navigate the softer sands deeper into the National Seashore.

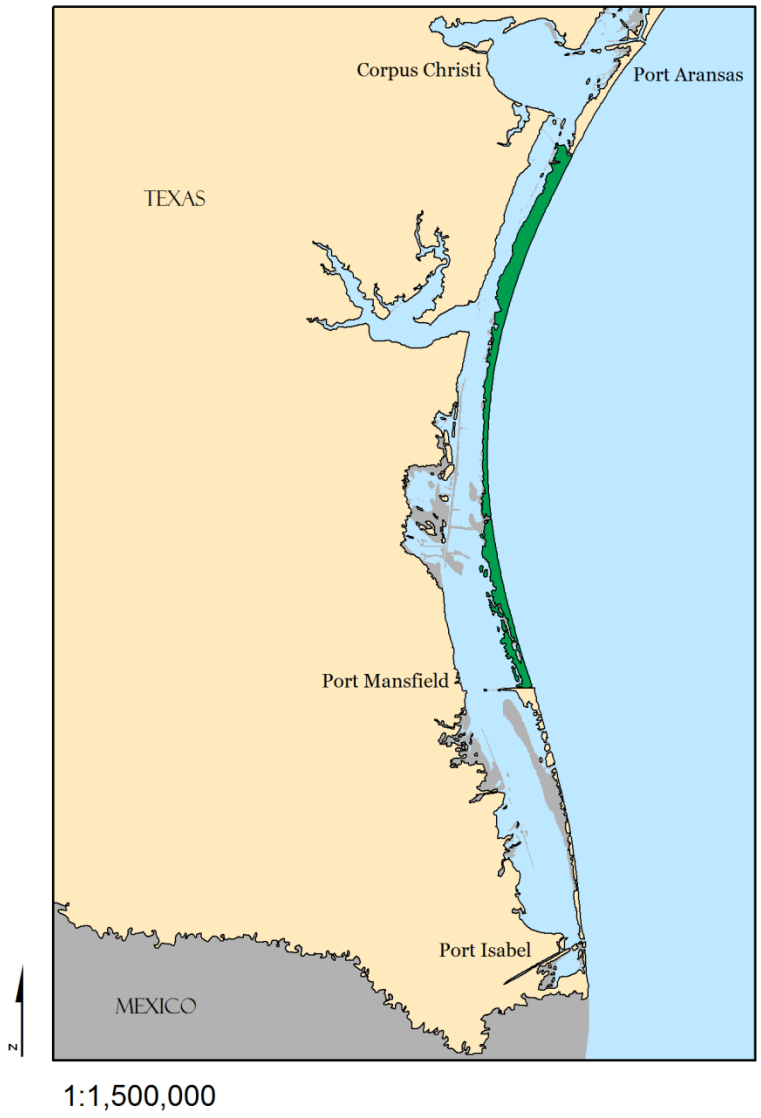

Figure 9 Study area map of Padre Island National Seashore, part of a barrier island that lies along the southern coast of Texas in the Gulf of Mexico.

Geologic history

"Exact positions of sea-level stages or rates of relative sea-level rise between [the late Pleistocene] and about 5,000 B.P. are uncertain. Nevertheless, it is clear that rates of shoreline retreat were so high during rising phases of sea level that barriers either were not well developed or were not widely preserved" (Morton 1994). Sea levels along this part of the gulf did not change as drastically post-deglaciation as other portions of US coastline, such as the previously mentioned Fire Island in the North Atlantic, but sea levels were much lower as recently as 10,000 years ago (Shepard 1956; Weise and White 1980). "During the last Pleistocene glacial stage sea level was lowered approximately 450 feet" and the rivers leading to the Texas coast became deeply entrenched (LeBlanc and Hodgson 1959). "These valleys extended seaward to a shoreline which was probably 80 to 225 km seaward of the present shoreline" (LeBlanc and Hodgson 1959). When the glaciers melted sea-levels rose, drowning the river valleys and their deltas and forming a series of estuaries (LeBlanc and Hodgson 1959; Morton 1994). Approximately 5,000 years B.P., during the later Holocene, "sea-level reached its present position and has remained constant since that time;" the barrier islands along the upper Texas coast formed during this period as "the rate of sea-level rise decreased from an average of 2.0 mm/yr to 0.6 mm/yr" (Shepard 1956; first quote from LeBlanc and Hodgson 1959; Milliken, Andersen, and Rodriguez 2008; second quote from Wallace and Anderson 2013). The rivers and the discharged sediments which formed deltas gulfward of the modern island are the sediments from which today's Padre Island is formed (LeBlanc and Hodgson 1959; Weise and White 1980).

Waves formed across the Gulf of Mexico are focused towards Padre Island because it is located at the westernmost bend of the Gulf (Lohse 1953). The alongshore currents formed by these waves flow in opposing directions, counterclockwise along the US coast in the north and clockwise around the southern portion of the Gulf. These currents meet at approximately 27ºN latitude in a zone of convergence that shifts seasonally but stays between the Mansfield Channel and the northern boundary of the National Seashore (Weise and White 1980; Sirigan and Anderson 1994). This zone of convergence is evidenced by the mineralogy of sediments and shells found on the beach and within sediment cores. Sediment profiles from the southern part of the island match those of rivers to the south, such as the Rio Grande, while profiles from the northern side of the island match rivers to the north, such as the Colorado and the Brazos (Bullard 1942; Hayes 1965; Weise and White 1980). Shells exhibit the same pattern, and are concentrated at the center of the island (Watson 1971). In addition, sediment cores along the central Texas coast lack the high levels of foraminifera expected of bayside deposits and bay deposits upstream in modern rivers and bays are thin. Beach material present in the cores further suggests that Padre Island and its neighbors have transgressed landward with rising sea levels since the postglacial thermal maximum, but the steady supply of sediments has kept the ocean-facing beach either stable or even prograding (Shepard 1956; LeBlanc and Hodgson 1959; Weise and White 1980; Lohse 1953).

The beach is typically wide and gently sloped. Small foredunes at the edge of the backshore are backed by vegetated dune of varied heights, some more than 10 m. Storm surges sometimes scarp the base of these dunes, leading to dune blowouts which

transport large amounts of sand in to the back-barrier (Jewell, in prep). The back-barrier is wide (averaging XX in width) and vegetated for the first XX km. The back-barrier wind tidal flats extend up to XX from the edge of the vegetation.

Recent history (last 200 years)

"There is now strong evidence for historical acceleration in the rate of sea-level rise, which appears to have begun sometime between 1865 and 1892" (Kemp et al. 2009, 2001). "In the northern Gulf of Mexico, sea level is currently rising ~2.0 mm/yr" (Parris et al. 2012). This is 1 mm less per year than the global average, but is approximately "four times the rate for the previous 4,000" years (Milliken, Andersen, and Rodriguez 2008). "The Texas coast is a microtidal, storm-dominated region that is constantly changing as a result of active coastal processes that are directly linked to meteorological events (Morton 1994). The climate for this part of the coast is semi-arid, with less than 64 cm of rainfall each year (LeBlanc and Hodgson 1959; Morton 1994). Local water levels, wave parameters, wind speed, wind direction, and barometric pressure have all been shown to correlate with sediment dynamics on the island (Davis and Fox 1975). For much of the year winds blow predominantly from the east and southeast (from February through September; Prouty and Prouty 1989; CITE wind data). Higher wind velocities blow out of the north and northeast during the months of October through January, but these are often driven by the passing of frontal systems accompanied by rain and so less total transport occurs during these months and in this direction (see Figure 10; Lohse 1955; Weise and White 1980; Prouty and Prouty 1989).

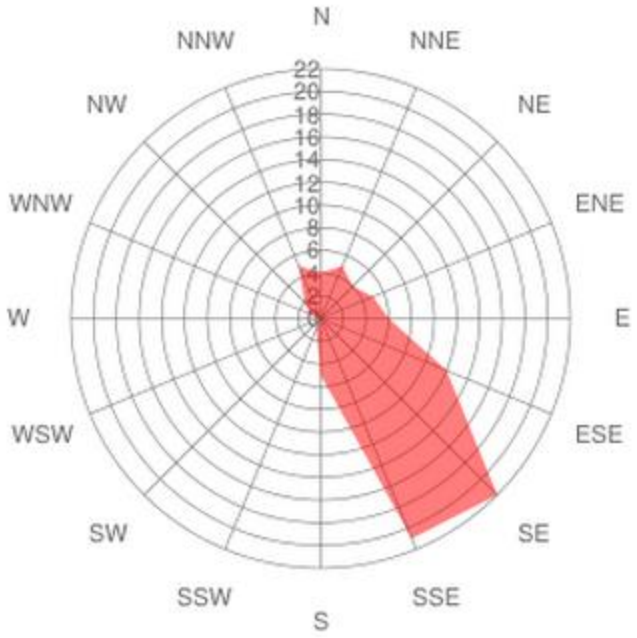

Figure 10 Wind rose data for Padre Island. Wind rose indicates the direction the wind is blowing into.

As most hurricanes entering or originating in the Gulf typically follow a westward path, storm-strength deepwater waves are not uncommon. The broad, shallow bathymetry of the Gulf causes these waves to decompose into low, short-period waves except for along central Padre Island where the offshore gradient is slightly steeper than surrounding areas (Morton 1994). On the gulf-facing beach, nearshore sandbars migrate seaward under strong wind and wave conditions associated with the winter storms and tropical pressure systems, and under low wave energy conditions these bars migrate landward and sometimes weld to the beach (Davis and Fox 1975). By this mechanism the ocean-facing beach recovers from hurricanes and other storms (Morton 1994). In the

last 200 years the ocean-facing beach has regressed seaward 15 to 20 m (Morton 1994). The sediment supply to Padre Island is enough in-excess to cause dune blowouts, wide wind-tidal flats, and even active sand sheets on the mainland side of Laguna Madre (Morton 1994).

Padre Island is an example of an aggradational barrier island because it: a) is wide and thick, b) has a high topographic profile, and c) is formed from sands supplied by interdeltaic bights (Morton 1994). Collectively, these characteristics form an island relatively impervious to overwash (Morton 1994). Instead of washover fans, where the wide island back-barrier lacks dunes it is dominated by barren sand flats (Morton 1994). "These wind-tidal flats are flooded and dried up when the flats are flooded [how often is that?] and dry up when the flats are exposed" (Morton 1994). They are composed of "thin, alternating layers of sand and mud" with more mud present closer to the lagoon (Morton 1994).

Laguna Madre is wide and shallow, at only 1.5 m in maximum depth but up to 11 km wide in parts (Morton 1994). Despite potentially long fetch distances (in comparison to other island back-barrier shorelines, such as at Santa Rosa Island, FL) this shallow environment dictates a very low-energy back-barrier coast. Currents in the shallow Laguna Madre are mostly wind-generated, and so follow the stronger northerly winds, producing net annual transport of sediments towards the south; this is in contrast to the eolian net transport which follows the prevailing winds in a west or northwest direction (Prouty and Prouty 1989). Certain portions of the coast are covered by seagrasses (halodule wrightii, ruppia maritima, and thalassia testuinum; Morton 1994).

Modern history (last 60 years)

Efforts to create a national park on the island began as early as the 1920s, and in 1962 Padre Island National Seashore became protected federal land (Weise and White 1980). Prior to 1962, the uninhabited northern portion of the island was used as a bombing range by the US Navy for a brief period of time (from World War II until 1960; NPS 2013d). Although bridges onto the northern and southern tips of the island were constructed in 1950 and 1954 (respectively), the development of these parts of the island into resorts and condominiums only extended a few kilometers from each entry point before the National Seashore was established (Weise and White 1980). There are no statistics for visitation counts to the ends of the island, which are not part of the NS, but PAIS received 513,855 visitors in 2012 and average of 680,880 per year in the last decade (NPS stats 2013).

The bulk of the island has remained undeveloped. Certain areas have minor oil and gas exploration, and much of it was used for cattle ranching until 1972, when the last cattle were removed, but paved roads and permanent structures are absent from the interior of the park (Weise and White 1980). Permanent development is virtually nonexistent. "Activities of the petroleum companies are carefully planned so that the natural environments are not greatly affected" (Weise and White 1980), and although heavy grazing appears to have affected the vegetation density on the island prior to 1972, the island has since revegetated and any other anthropogenic influences on the geomorphology of the National Seashore are minimal (Weise and White 1980; Prouty and Prouty 1989).

Human influence has greatly influenced the flora and fauna of North Padre Island. There are at least 99 species of naturally occurring flora on North Padre Island, but in the more highly developed ends there may be as many as 117 introduced species (Lonard and Judd 1980). The most common dispersal agent for these species is birds (Lonard and Judd 1980). North Padre Island is a haven for more than 380 bird species (NPS 2013e). It is also a nesting ground for the Kemp's ridley sea turtle, which is the most endangered species of sea turtle (NPS 2013e). The turtle only nests on beaches between Veracruz, Mexico and Mustang Island, TX and after population numbers for the turtle took a dangerous dive in the mid-1990s restoration efforts (largely taking part on North Padre Island) have slowly begun to restore turtle numbers, but numbers are still low and efforts are ongoing (NPS 2013e).

"It is difficult to predict the fate of Padre Island (as determined by natural factors) at a particular location, especially in the zone where longshore currents converge on central Padre" (Weise and White 1980). The interruption and decrease in sediment supply caused by dam destruction and other human activity, rising sea-level, and climate change are causing most of the Texas coast barrier islands to retrograde landward and narrow, but central Padre Island (the lower half of North Padre Island) remains an actively aggrading barrier - at least for now (Weise and White 1980; Morton 1994). An initial shift in climate, "when rainfall decreased during the early Holocene," first reduced the sand supplied to Gulf beaches, which has only decreased more in the past century as reservoirs, flood-control structures, and freshwater diversions further depleted rivers from discharge strength and sediment supply (Morton 1994)

CHAPTER II

METHODS

Introduction

High Resolution Orthoimagery (HRO) provided by the United States Geological Survey (USGS) was used to identify shoreline location along the back-barrier coast and mainland coast of the study sites. The shoreline was visually identified and digitized by the researcher using ESRI's ArcGIS ArcMap interface. The feature captured as the shoreline varied with the alongshore variation of coastline type as detailed below. Bathymetric elevation models as provided by the National Oceanic and Atmospheric Association (NOAA) were used to extract isobaths. Baseline data was acquired from the USGS in the form of Light Detection and Ranging (LiDAR) derived Mean High Water Line (MHWL) position along the United States coast.

Acquisition of Imagery

Imagery for each study site was downloaded via EarthExplorer, a website run by the USGS that offers access to imagery acquired by multiple satellites and imagery collection programs. Some of the data viewable through the EarthExplorer interface can be downloaded at no cost to the user. Each study site in this project is covered by a dataset of images known as High Resolution Orthoimagery (hereafter referred to as HRO). This type of image is created by mosaicking together multiple photographs, which may be natural color (red/green/blue bands or RGB), panchromatic (black-and-

white), or color infrared (RGB-NIR), as long as the pixel resolution of the captured image is equal to or lower than 1 m. The mosaic of photographs is then corrected for topographic displacement or feature displacement (such as hilly terrain or building tilt). The geocorrection process involves calculating the ground-truth location of pixels via sensor geometry, camera tilt, digital elevation models, and ground control points. The result is a uniform-scale image with the high geometric qualities of a map (USGS 2012). The images in this project are of spatial resolution 0.87 m.

The aerial photographs used to produce the HRO in this study were collected during multiple airplane flights and then georectified by independent contractors (the details of acquisition flights for each study site are shown in Table 1. The georectified imagery was then merged into a county-wide single raster of data. This single image was divided into 2 km by 3 km tiles, and these tiles are the data source available at no cost through the USGS EarthExplorer and used in this research. They are made available in a spatially referenced Georeferenced Tagged Image File Format (GeoTIFF). Because they are such high resolution (spatial resolution of a single pixel is 1 foot/0.3 meters or less), and county-specific datasets, the spatial reference is typically a state plane coordinate system in feet. Features digitized from the HRO were digitized within a map document set to the same spatial reference as the HRO. These vectors were then rep-projected into the coordinating state-plane specific projection referenced in meters, as this was the projection assigned to each featuredataset within the DSAS geodatabase. In the HRO dataset, the digital number assigned to each pixel represents its reflection of the red, green, blue, and sometimes infrared bands of the electromagnetic spectrum. Over Santa

Rosa and Assateague, the imagery is 3 band RGB, for Fire Island the imagery is RGB+NIR, and the bands of North Padre Island imagery are unknown but likely to be RGB (as Google Earth rarely displays anything else).

Acquisition of Bathymetry

The bathymetric data used in this research were provided by the National Oceanic and Atmospheric Administration (NOAA). Their Coastal Relief Model (CRM) of the US is made available through the National Geophysical Data Center (NGDC), a website maintained by NOAA. The CRM is the result of compiling multiple bathymetric surveys captured by a wide range of technologies and methods, including multibeam swath sonar and LiDAR (among others). The CRM dataset is of spatial resolution 3 arc seconds, which is equivalent to ~ 80 or 90 m at the latitudes of the study sites of this project. The data used to compile the portions of CRM used here are from the USGS, the U.S. National Ocean Service Hydrographic Database, the U.S. Army Corps of Engineers, and various other academic institutions. The bathymetric data for North Padre Island and Santa Rosa Island are specifically from the International Bathymetric Chart of the Caribbean Sea and the Gulf of Mexico (IBCCA; IBCCA 2013). This international project is sponsored by the Intergovernmental Oceanographic Commission (IOC) of the United Nations Educational, Scientific, and Cultural Organization (UNESCO). The participating countries are Colombia, Costa Rica, Cuba, France, Mexico, the United States and Venezuela. The initial mission of this project was to create new bathymetry for the Gulf of Mexico and the Caribbean Sea (IBCCA 2013).

Table 1 Specifics of metadata for each imagery dataset used in the project

Study Site	Date captured	Acquired via	Company	Sensor	Pixel Resolution	Bands	Projection	RMSEz
Fire Island	April 2010	USGS Earth Explorer	Sanborn Map Company, Inc.	Vexcel UCX	0.5 feet (0.15 m)	RGB + IR	New York State Plane, Long Island (feet)	1.48 ft (0.45 m)
Assateague Island	March 2010 – April 2010	USGS Earth Explorer	Axis Geospatial	ULTRACAM	0.5 feet (0.15 m)	RGB	Maryland State Plane (feet)	Unknown
Santa Rosa Island	October 2009 – January 2010	USGS Earth Explorer	Florida Dept. of Transportation	DMC	1.0 feet (0.31 m)	RGB	Florida State Plane, North (feet)	Unknown
Padre Island	February 2011	Google Earth	TerraMetrics	Unknown	< 1 m	RGB	Unknown	Unknown

The isobaths analyzed for this project were extracted from the NOAA CRM using tools in the Spatial Analyst extension of ESRI's ArcMap program. The contours were extracted at 5 m intervals, and only the -5 m, -10 m, -15 m, and -20 m on the sound side and the ocean or gulf side of the island were extracted. While initially the sound bathymetric contours were intended for inclusion in analysis, they were too spatially inconsistent or non-existent within the sound for all study sites, and thus there was not enough data to produce valid results. The result was analysis of only the gulf or ocean bathymetric contours.

Analysis was only performed to depths of 20 m because the 95% significant wave height (the tallest that might meet the shoreface within a given year) will not touch bottom any deeper than 20 m. This statistic was calculated from NOAA buoy data. The significant wave for each location in the year 2011 was: 1.3 m at Fire Island, 1.16 m at Assateague Island, 1.13 m at Santa Rosa Island, and 1.34 m at North Padre Island, as collected by NOAA buoys offshore. The dominant wave period for these buoys in 2011 was 7.2 seconds at Fire Island, 7.6 s at Assateague, 5.6 s at Santa Rosa, and 5.7 s at North Padre Island. Deep water waves do not touch bottom. A wave is a deep water wave when $\frac{2\pi h}{L} > 1$; where L is wave length and h is water depth. Substituting the dominant wave period for each study and a water depth of 20 m (the deepest isobath used at each study site) yields the following results for this equation:

- Fire Island: $\frac{2\pi h}{L} > 1\ ? \rightarrow \frac{2\times\pi\times 20m}{7.2s} = \frac{125.6}{7.2} = 17.4,\ 17.4 > 1 \therefore$ deepwater wave
- Assateague: $\frac{2\times\pi\times 20m}{7.6s} = \frac{125.6}{7.6} = 16.5,\ 16.5 > 1 \therefore$ deepwater wave

- Santa Rosa: $\frac{2\times\pi\times 20\text{m}}{5.6s} = \frac{125.6}{5.6} = 22.4,\ 22.4 > 1 \therefore$ deepwater wave
- North Padre: $\frac{2\times\pi\times 20\text{m}}{5.7s} = \frac{125.6}{5.7} = 22.0,\ 22.0 > 1 \therefore$ deepwater wave

For the 20 m isobath at each island, this means that the significant wave is still a deepwater wave, and waves will not touch the bathymetric surface at depths of 20 m or greater.

The resulting bathymetric maps for each study site are shown in Figure 11. The bathymetric contours were analyzed for shape signatures and spatial correlation with shoreline shapes. These contours inherit some artifacts of the 90 m square pixel resolution of the CRM, and so vector isolines produced by this method are not smooth at higher resolutions. It was determined that a smoothing algorithm might introduce a greater degree of interpretation or subjectivity to the data, as choice in smoothing algorithm would might affect patter analysis. Rather than introduce these additional artifacts to the data, the non-smooth 90 m spatial resolution isolines were used. Because of this 90 m resolution, the transects and intersection data used for input to the wavelet analysis were spaced 100 m apart. This ensures that location of an isoline in space does not artificially reinforce an isoline as derived from the edge of a single 90 m pixel (since a portion of isoline that is drawn from a single pixel will not be “picked up” by more than one transect).

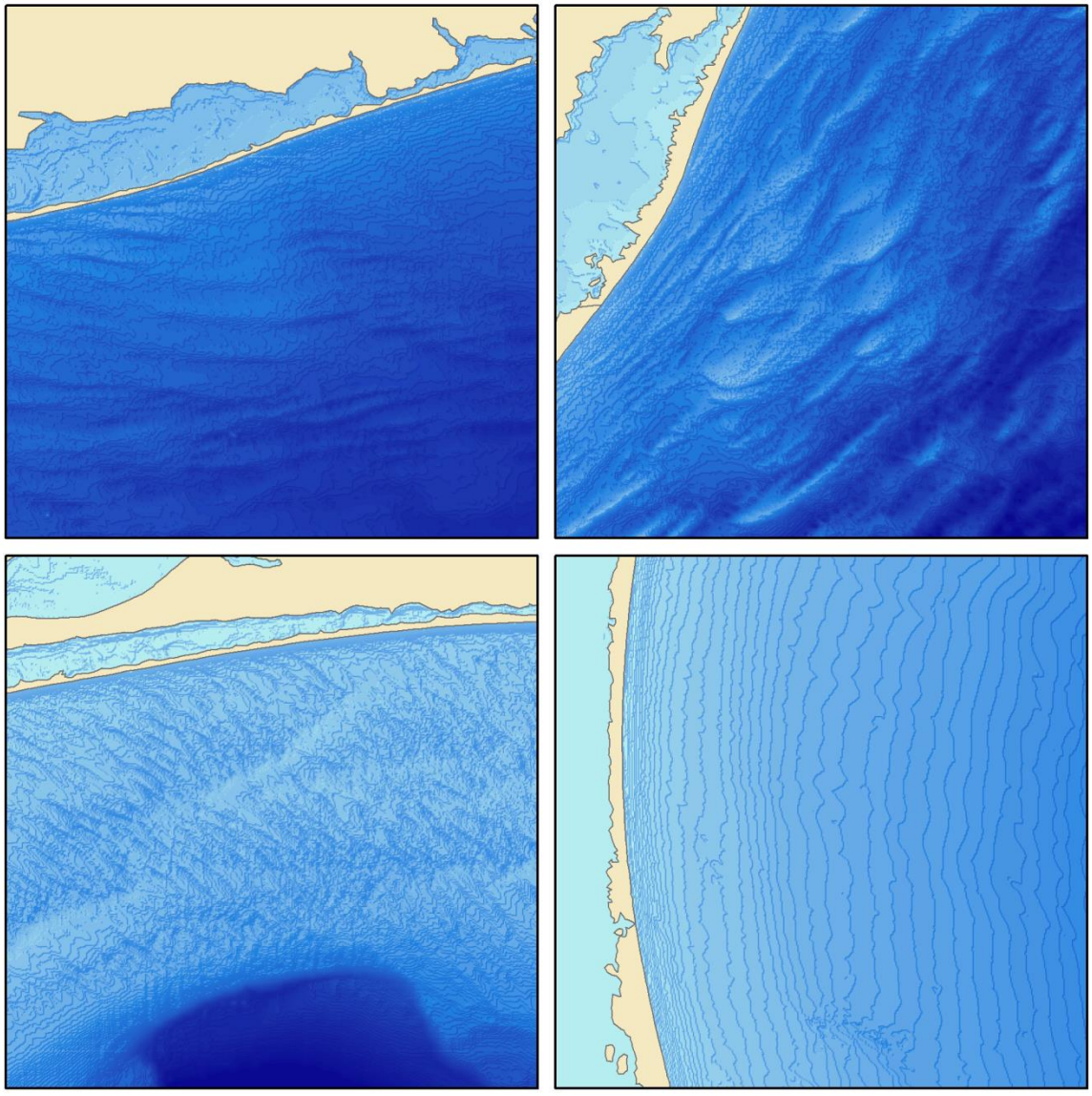

Figure 11 Bathymetric elevation models for all four study sites from which the bathymetric contours were extracted. Maps are all shown at a scale of 1:600,000 for direct comparison, and as a result these images depict only a central portion of each island, and not the entirety of each study site. Clockwise from top left they are: Fire Island, Assateague Island, North Padre Island, Santa Rosa Island.

Extracting the shoreline

In his dissertation and resulting publications, Borrelli (2008; 2009) compared multiple shoreline change rate statistics as measured by the DSAS program for Pleasant Bay, Massachusetts as recorded by different shoreline indicators. The results showed that when shoreline change was calculated as movement in the indicators most common for ocean-facing beaches (such as the MHWL), shoreline change rates within the bay were not statistically significant. In stark contrast, when shoreline change was calculated according to movement in the location of the marshline rates of change were significant, and in some instances quite high; the marshline is defined as the basinward extent of marsh vegetation. These findings suggest that the most commonly used shoreline indicators may not be appropriate when measuring change in low-energy, marshy coastlines such as those seen along the lagoonal side of many US barrier islands, including these four study sites.

In addition, valuable sediment deposits in the back-barrier may be stored or protected by the extent of marsh vegetation, and changes in the width of this ecosystem are indicative of corresponding changes in the geomorphology of the barrier island. Because one of the hypotheses of this study is that wider island widths spatially correlate to the nearshore geologic framework, the back-barrier shoreline was digitized in the GIS as the marshline, when it was present. None of the islands is entirely bordered by marsh on the back-barrier shoreline. Vegetation is sometimes absent (as for parts of Santa Rosa Island), or it does not extend further into the lagoon than the exposed, sandy beach (as along much of North Padre Island where there are wind tidal flats). In these cases, the

wrack line is digitized as the shoreline; the wrack line is a widely validated, widely used shoreline indicator.

Although all four study sites in this project are designated in part as National Seashores, they do contain some development and anthropogenic features. In certain cases, the back-barrier shoreline is artificially maintained by a man-made structure, such as rip rap or low walls. When these are present, they are the feature digitized as the shoreline. The shoreline was digitized as a man-made feature most commonly along the mainland coastline. It should be noted that the reinforced shoreline digitized in these instances varied little from the "natural" shoreline, as the reinforced shoreline is typically indicative of the natural shoreline location at some baseline point in time – typically the shoreline position within the last 20 years (which local landowners have chosen to artificially preserve). The variability in location of the shoreline as digitized by these different indicators is insignificant for the measurement of the alongshore variation at the mesoscale, and necessary due to the alongshore variation of shoreline type.

In summary, the shoreline was digitized as the marshline in all cases where this was possible. When there was no marshline, the shoreline position was digitized as the wrack line. If neither of these indicators was present, the artificially constructed barrier was digitized. For field photographs of each of these indicators, see Figure 12 (all three photographs are from one of the trips the investigator made to a study site: Santa Rosa Island, Florida).

Figure 12 The shoreline indicators used, as they appear in the field (across the top) and in the HRO as seen in the GIS. All examples from Santa Rosa Island, Florida, though the field photos are not of the exact location seen in the GIS images shown.

North Padre Island: A Special Methodology for Extracting Shorelines Using Google Earth

After the project was well underway, it was discovered that North Padre Island, while covered in certain areas with multiple HRO datasets between 2002-2012, was not covered in its entirety by any of these imagery representing a single year. Also, much of the middle of the island was not covered by HRO that could be acquired within the project budget. The only available dataset covering the whole of the island was single frame aerial photographs from 2002 that lacked georectification, and the investigator did not have adequate ground truth data to georectify these images within the timespan of the project. As an alternative, the vector data for the mainland and back-barrier shorelines were collected through the digitization in Google Earth of that system's imagery. These images are high resolution and were captured on 1 January, 4 February, and 22 November of a single year (2011), so they fall within the requirements for the project.

The digitization of the shoreline within Google Earth was performed at the same scale as for the other study sites (1:750), so they represent the same spatial resolution and accuracy as the shorelines digitized from HRO in ArcMap for the other three study sites. Over the wind-tidal flats, the position of the backbarrier and mainland shorelines are highly dependent on meteorological conditions at the time of photography because the effects of barometric pressure shifts, wind velocity and direction, and tides will be exaggerated by the extremely low gradient of these coasts. As a result, the most common shoreline indicator used for North Padre Island was the wrack line, following the precedent set by Prouty and Prouty (1989).

The Google Earth software program (which can be downloaded from Google for free) can be used to digitize surface features into *.kmz or *.kml filetype vector data with its "Add Path" tool. These data can then be converted in ArcCatalog to geodatabase files, which may then be imported into the DSAS geodatabase. The shorelines digitized in Google Earth were imported to the North Padre feature dataset in the DSAS database used for this project and all further steps of data processing followed the same procedure as the other three study sites.

The successful creation and processing of the North Padre Island shorelines via this adapted method are proof that future researchers may use freely available Google Earth to perform the methodology presented by this project. Such verification is a positive implication for the real-world application of this methodology.

Digital Shoreline Analysis System

The Digital Shoreline Analysis System is an ArcGIS extension program available at no cost from the USGS (Himmelstoss 2009). It is designed for the calculation of shoreline change rate statistics. It accomplishes this by measuring distances between the intersections of dated shoreline vectors along transects cast from a user-defined baseline, and performing a variety of rate calculations using these distances between dates as input. The statistics are calculated at the discretion of the user.

When using DSAS, it is common to define a baseline that is some distance offshore, and to cast transects along one side of this baseline towards the shoreline vectors. For this project, it was necessary to use a baseline that followed the entire length

of the barrier island with little alongshore variation. A perfectly straight line would fail to capture the natural alignment of the curvature of both the island itself and the offshore geologic framework, thereby failing to capture which features are spatially correlated. It is also impossible to draw a geometrically straight line that runs the entire length of the island while staying within the landmass of the island.

To ensure that the baseline was located completely within the barrier island, and between the back-barrier shoreline and the first isobaths (-5 m depth), the MHWL for each island was used. This vector was derived from multiple LiDAR surveys of the US coast performed by the USGS in 2000 for each of these study sites. In 2000, the USGS, and National Aeronautics and Space Administration (NASA) used the NASA Airborne Topographic Mapper (ATM II and III) to survey the US coastline. The raw LiDAR data were georeferenced and fitted to the North American Datum of 1983 (NAD83), the North American Vertical Datum of 1988, and projected coordinates (WGS 84 UTM zones appropriate to each state. DSAS will only run when all data are within a geodatabase that has a spatial reference to projection measured in meters (Brock, Nayegandhi1, and Duffy 2005; Weber, List, and Morgan 2005).

The MHWL was derived from this data by assessing 4 m wide shore-normal profiles at 20-meter intervals alongshore. An algorithm based on a regression fit through the foreshore of each profile produced the MHWL (Brock, Nayegandhi1, and Duffy 2005; Weber, List, and Morgan 2005). The resulting baseline as used in this study is a highly accurate (±2.3 m RMSEz) baseline that follows the ocean-facing beach with little

alongshore variation, remaining within the landmass of the barrier island – always oceanward of the back-barrier shoreline and always above the -5 m isobath.

This baseline was used to cast 20 km long transects at varying alongshore intervals. Each island has a transect file (used to capture the intersection data analyzed for shape signatures) at 100 m intervals along the baseline. To test whether patterns seen in the data were artifacts of this 100 m spacing, the Santa Rosa study site was also tested at 20.5 m intervals; although the signals produced by this 20.5 interval test differed from the signals produced by the 100 m interval test, the vectors showed the same spatial correlation of signal to each other. For example, the peaks in power on the global wavelet of the 5 m isobath were not at the same values as when the 5 m isobath was tested at the 100 m interval, and they did not align with the peaks of any other vector sampled at 100 m intervals. The peaks within the 20.5 m global wavelet for the 5 m isobath did show strong spatial correlation to all other vectors tested at 20.5 m. This is evidence that the vectors can be tested at multiple intervals, and so long as they are tested at the same intervals, the strength of spatial correspondence will not vary. The spatial correspondence exhibited by the wavelet analysis is valid as demonstrated by the shift in length-frequency signal's values with shifts in interval scale.

In this study, the DSAS was used as a measurement tool, solely to capture the alongshore variation in the distance between the user-defined baseline and the vector data: the mainland shoreline, the isobaths within the lagoon, the back-barrier shoreline, and the offshore isobaths. The DSAS program generates a text file output of the distance along each transect to the intersection between transect and the shorelines or isobaths.

These distances are representative of the distance between the baseline and each vector, and were used as the input data for the wavelet analysis portion of the project. Results are therefore indicative of variations in these widths.

In the case of the bathymetry, the curves in the isobaths sometimes loop back upon themselves as a result of the ridge and swale bathymetry present along certain portions of the study sites. The DSAS program can measure the distance along each transect from baseline to either the first or last intersection with a dataset, according to the user's preference. In the case of the shorelines (the back-barrier and mainland shorelines) this was not an issue. For the bathymetry, the distance was measured to the first intersection and these were the data analyzed. This was done because ridges in the nearshore are actually attached to the island when measured to the nearest intersection, and this nearshore geologic influence is the framework actually affecting the barrier island shape and transgression rate (as opposed to the farthest intersection of isobath and transect), which is a concern of this project's hypotheses.

Wavelet Analysis

Wavelet analysis is an increasingly common tool for analyzing localized variations of power within a data series (Torrence and Compo 1998). It also possible to substitute measurements of length for those of time, and thereby analyze spatial variations within a shape, as is done in this project for the shape of shorelines and isobaths. Such analysis allows for the determination of the dominant length scales of variability and how they vary within space (Torrence and Compo 1998).

Wavelet analysis is not the only choice for quantitative analysis of frequencies in a time or space series of data; it is, however, the best analysis for the data examined for this project. Fourier transform analysis, another common choice, is less appropriate for this shape signature analysis because it cannot account for frequencies at all scales; it missies signals occurring at scales significantly larger than or smaller than its window-step-size. When predetermined scaling, which is necessary for Fourier transform analysis, is inappropriate because of a wide range of dominant frequencies, which are present in shoreline or bathymetric isolines, wavelet analysis is a more appropriate choice because it is a scale independent method of length-frequency localization (Torrence and Compo 1998).

The Morlet wavelet is a commonly used complex transform for nonorthogonal functions. An orthagonoal wavelet analysis is to be used when data have discrete blocks of power, where the global wavelet has jumps in power value; nonorthogonal analysis is for those global wavelets with "smooth, continuous variations in amplitude," as is the case with shorelines and isolines (Torrence and Compo 1998). When the wavelet spectrum is highly correlated at adjacent times, as the bathymetry are, the Morlet wavelet is a good choice (Torrence and Compo 1998). Also, the ridges, which cause the undulations in the bathymetric isolines, are highly correlated to each other, and a hypothesis of this thesis is that the shape of the shorelines will exhibit similar shapes (perhaps out-of phase). The input data is the variations in each vector's distance from the baseline. The nonorthogonal Morlet wavelet can be employed as either a real or complex function. It is employed here as a complex function because: a) complex functions

(unlike real functions) are better adapted for capturing oscillatory behavior, and b) if used as a real function the analysis would only return power values when oscillations within the data were extreme or when a sharp discontinuity occurred, and these are not present in the continuous shorelines and isobaths (AutoSignal 2003). A real wavelet function is more appropriate for isolating peaks and discontinuities, but a complex function like the Morlet returns information about both amplitude and phase (Torrence and Compo 1998). For observation of presence or absence of pattern shared between shapes, it is more appropriate to identify oscillations at common length scales than to identify only peaks and discontinuities, and so the complex nonorthogonal Morlet is employed, because it provides the best combined resolution for both power and frequency (AutoSignal 2003).

When working with finite-length series, such as shorelines that end at inlets, errors produced at the edges of the global wavelet can be a concern. For this reason, and because the geomorphological forces at work along inlet shores present special circumstances, the first and last 500 m of shoreline were left out of analysis. To further analyze whether results were indicative of length-frequency signals or simply noise, the set of global wavelets produced for each island was compared to a plot of both white and red background noise, which are appropriate background spectra for most geophysical phenomena (Qiu and Er 1995; Torrence and Compo 1998). Only signals that fall outside the range of noise are considered significant (see Chapters III and IV, Results and Discussion).

The adjustable parameter for a Morlet mother wavelet is the wavenumber n which determines how many peaks are present in the mother wavelet. For consistency, this was kept low and was the same for all analysis – for all vectors at all study sites (n = 6). It was determined by the investigator that varying this value to experiment until finding the 'best' fit for each vector at each study site would introduce subjective bias , in addition to un-validating the comparison of signals between vectors and between study sites. Results described in Chapter III are therefore indicative of vectors' similarity at this step size (scale). Figure 13 shows the mother wavelet used for all analysis.

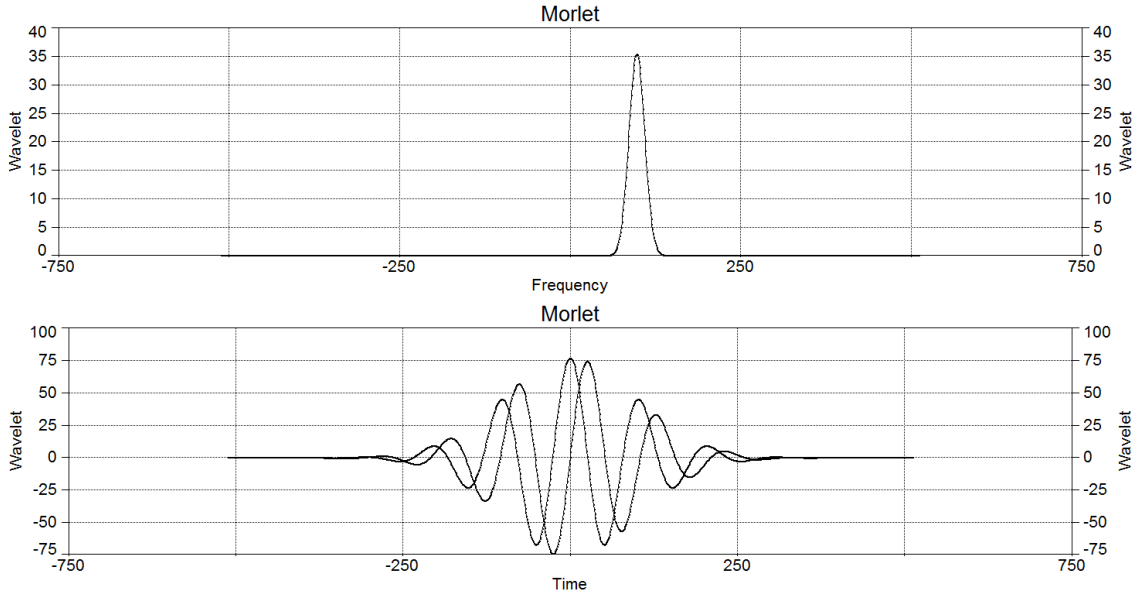

Figure 13 Mother wavelet used for analysis; n = 6

As previously mentioned, the DSAS outputs a text file of the distance along each transect to the point at which transect and vector (in this instance, shoreline or isobath) meet. The curvature of the baseline, the mean high water line (MHWL), follows the gentle curve of the barrier island and as a result, the record of the intersections between transects cast perpendicular to the MHWL remove any artifacts of this general shape (see Figures 14, 15, 16, and 17). The features captured by the wavelet analysis are indicative of variations in the shorelines and isobaths independent of this naturally occurring curvature and represent spatial correlation. Plotting the global wavelets against the red and white noise curves reveals which corresponding features are significantly different from the noise levels and are therefore shared shape signatures (and not coincidental; see Chapter III: Results).

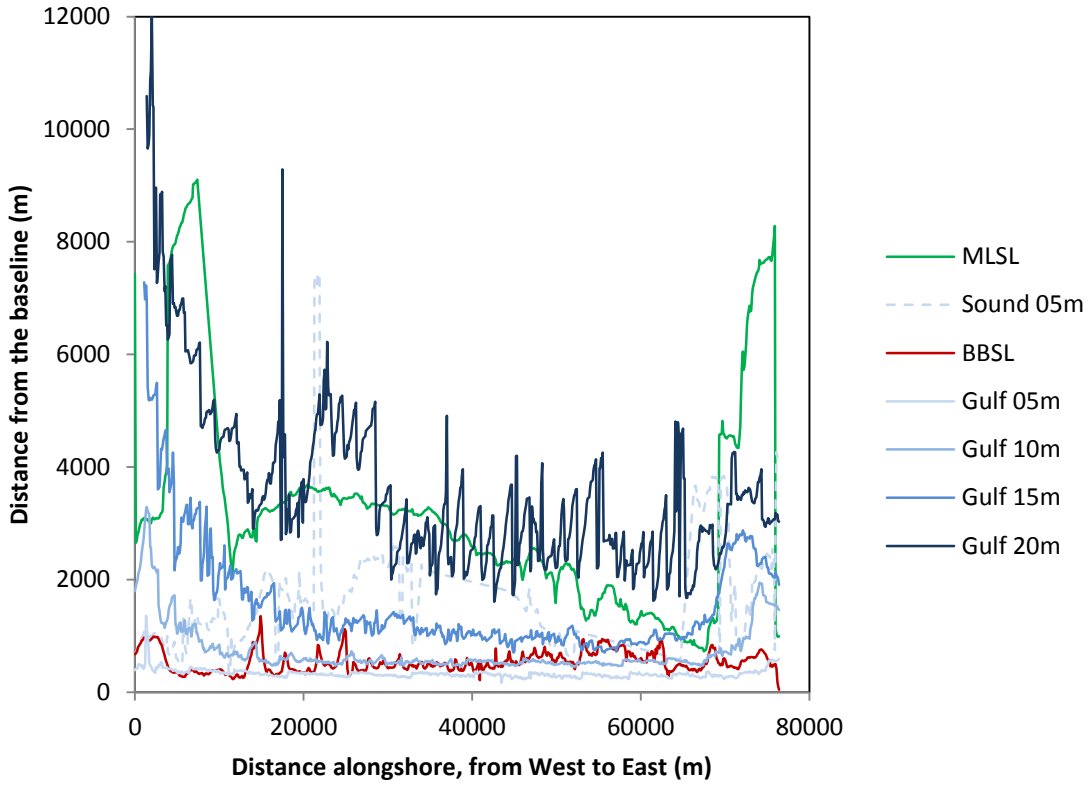

Figure 14 The output from the DSAS for Santa Rosa Island. Lines represent the alongshore variation in each vector with any curvature in the island removed.

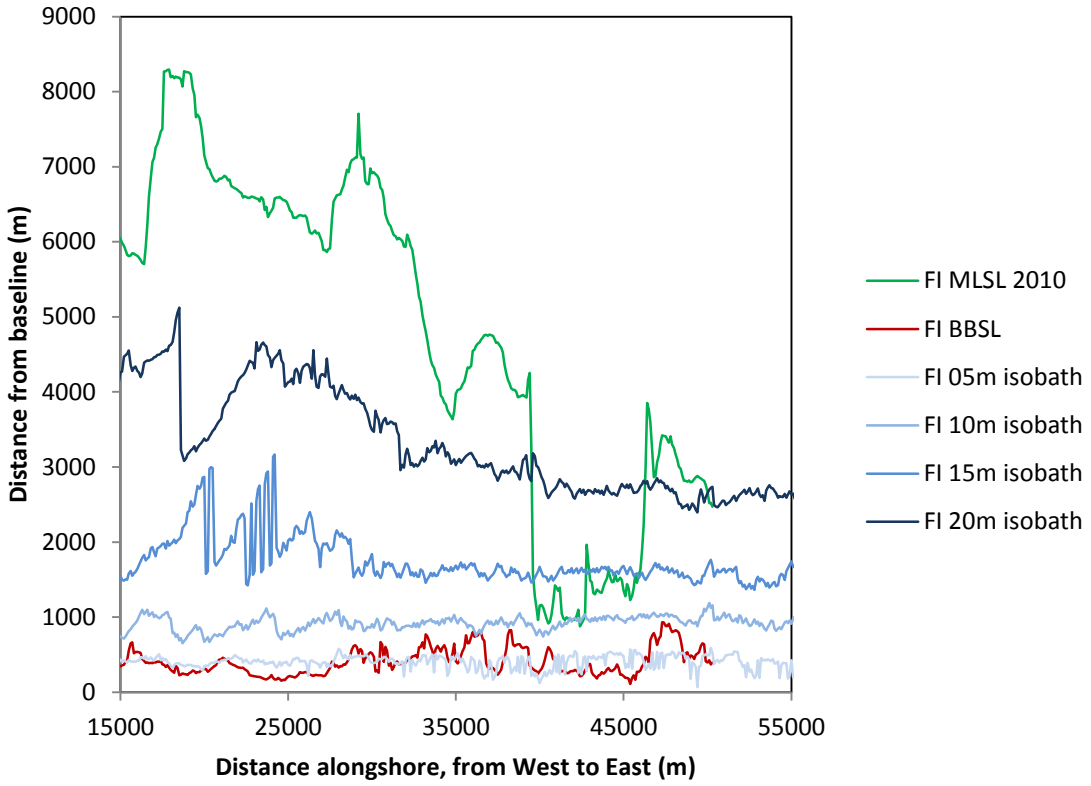

Figure 15 The output from the DSAS for Fire Island. Lines represent the alongshore variation in each vector with any curvature in the island removed.

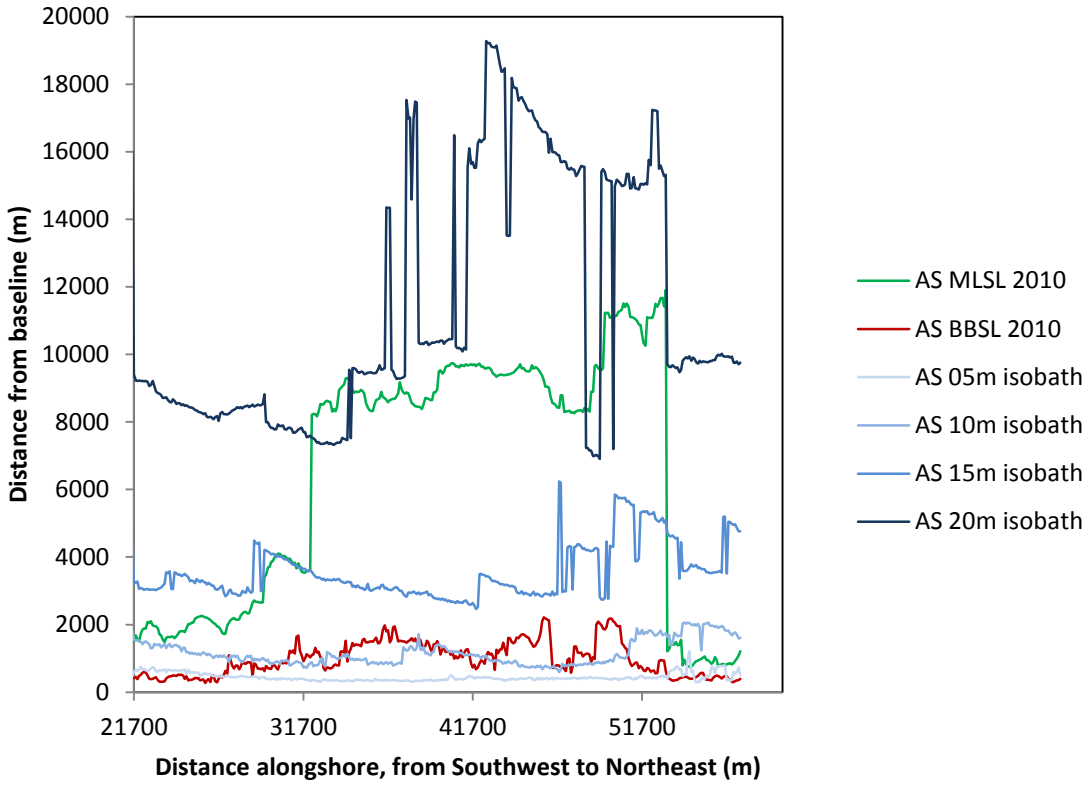

Figure 16 The output from the DSAS for Assateague Island. Lines represent the alongshore variation in each vector with any curvature in the island removed.

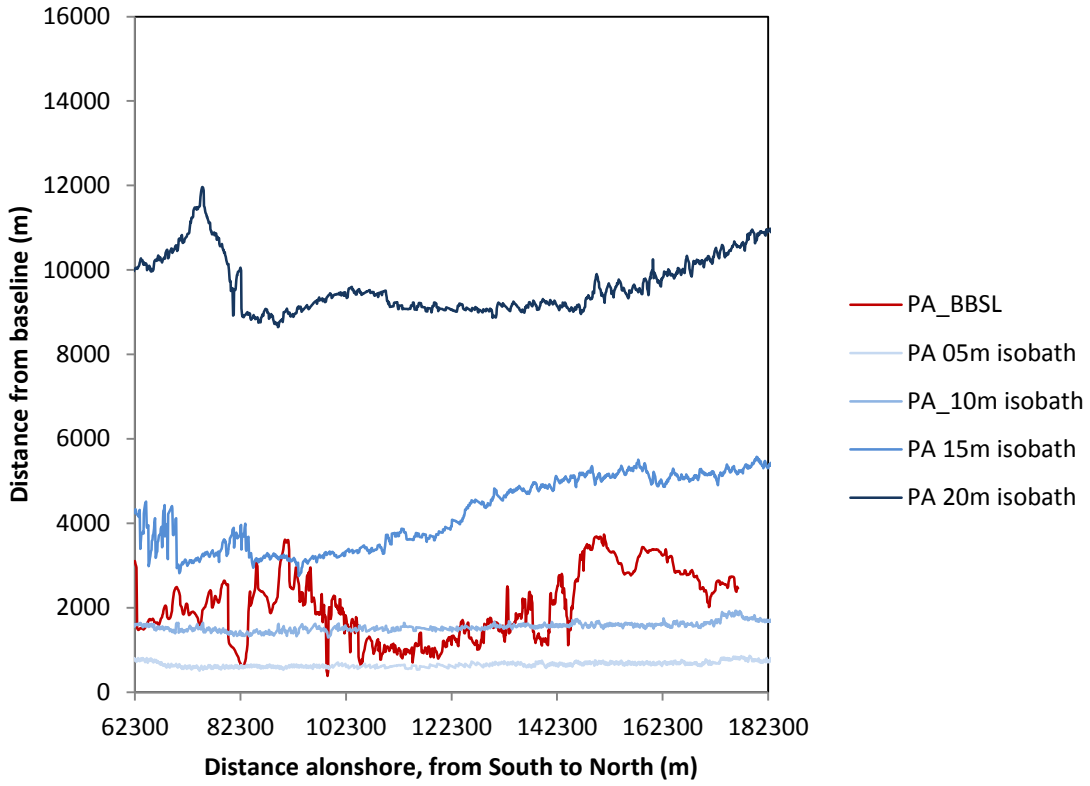

Figure 17 The output from the DSAS for North Padre Island. Lines represent the alongshore variation in each vector with any curvature in the island removed.

The wavelet analysis for this project was performed with the AutoSignal Program™ (version 1.7). This program allows for many user-defined parameters. For this project, the same wavelet and filter parameters were entered for each island. The output data from the DSAS was imported into AutoSignal™ in the form of (x,y) data, where x = the distance in meters from the westernmost/southernmost tip of the island (transect ID x 100 – 100) and y = the length of transect (in meters) between the baseline

(MHWL) and the intersection of the transect and the vector (either an isoline or shoreline). These input data were then analyzed by a continuous wavelet spectrum time range, a specialized wavelet procedure which computes power across all frequencies for a specified range; this produces a global wavelet spectrum (similar to a smoothed forward Fourier transform, or FFT).

CHAPTER III

RESULTS

Introduction

Wavelet analysis was successfully performed for all four study sites on the mainland shoreline, the back-barrier shoreline, and the offshore bathymetry isolines. Each of these vectors was run through wavelet analysis with the AutoSignal™ program as described in Chapter II: Methodology. Only Santa Rosa Island had isolines in the lagoon with enough data length for analysis, and this was only for the 5 m isobath. The methodology was successfully adapted to the use of Google Earth acquired data for the North Padre Island study site. The global wavelet produced by the Morlet function analysis of all vectors was converted from the power v. frequency (length scale) values output by the AutoSignal™ program back in to Fourier space for all plots, so that the correspondences in shape frequency shown by all figures are indicative of the power exhibited at a certain length scale (Torrence and Compo 1998). The resulting global wavelets have been converted from (frequency, power) to (length in km, percent contribution to total shape) so that they fall within the same range of values on the x and y axis. Each island exhibits shared shape signatures between some vectors, and there are also similar patterns exhibited between islands. The details of which signatures are shared (or not shared) are explained below, first for each individual study site, and then as a group.

Reading the wavelet analysis output

Shared peaks in global wavelets indicate a shared shape signature, where the x-coordinate of a peak in the global wavelet is the width, in kilometers, of the repeating wavelet shape. Two global wavelets may share a signal but the signals may not be in-phase. 'In-phase' means that a signal in one vector occurs at the same alongshore position in another vector. For example: two isobaths both exhibit a 10 km signal, which means a wavelet 10 km wide can be fit to portions of the data. If the signal is 'in-phase' then the heat map of both isobaths will have hot spots located at the 10 km equivalent on the x-axis (frequency = 0.0001) that are centered at the same alongshore locations, such as 0, 15, and 30 km alongshore. Note that the alongshore spacing of the 10 m signal does not have to equal 10 km – it also does not have to be continuous alongshore. A signal may be consistent for one part of the island, but not the other. The same two isobaths could share a 10 km signal out-of-phase if the signal was centered at 0, 15, and 30 km in one vector, but at 5, 25, and 45 km in the other.

It is important to note that the contribution by each frequency to the total power is partly dependent on the length scale of that frequency. The larger the length scale of the variation, the more that it contributes to the overall shape of the vector (independent of the variation within each variable). A shorter length scale variation may not occupy the entire length of the island, but may still represent a significant deviation of the variable despite having low power.

Santa Rosa Island, Gulf Islands National Seashore, Florida, US

The methodology was first tested by working with the Santa Rosa dataset. A qualitative correspondence between the width of the island (distance from seaward beach to back-barrier shoreline) and offshore ridges has been previously demonstrated by multiple publications (Houser, Hapke and Hamilton 2008; Houser and Hamilton 2009; Houser 2012). The study site in this series of studies was 11 km of the undeveloped central portion of the National Seashore. This thesis expands upon the previous findings by quantitatively investigating the presence of shared patterns for the entire 96 km of Santa Rosa Island (minus the 500 m adjacent to each inlet), and adds analysis of the mainland shoreline and lagoon bathymetry. A map of all input data for Santa Rosa is shown in Figure 18.

Testing the significance of interval spacing

The Santa Rosa dataset was examined at three different intervals of input data to observe whether vectors that shared features at one interval also shared signals when examined at other intervals, or if the difference in parameter caused significant changes in results, such as the loss or addition of shared signals. The Santa Rosa data were examined at a 100 m transect interval, a 20 m transect interval, and a 67 m interval. The 20 m test interval was used to observe the effect of introducing additional data (5x increase in data points) to the 100 m interval dataset. The 67 m 'test' interval was a randomly chosen interval employed to observe the effect of two similar-density intervals with no shared data points (none of the intersections between the 67 m and the 100 m transects with the vectors have the same coordinates, but input to the wavelet analysis

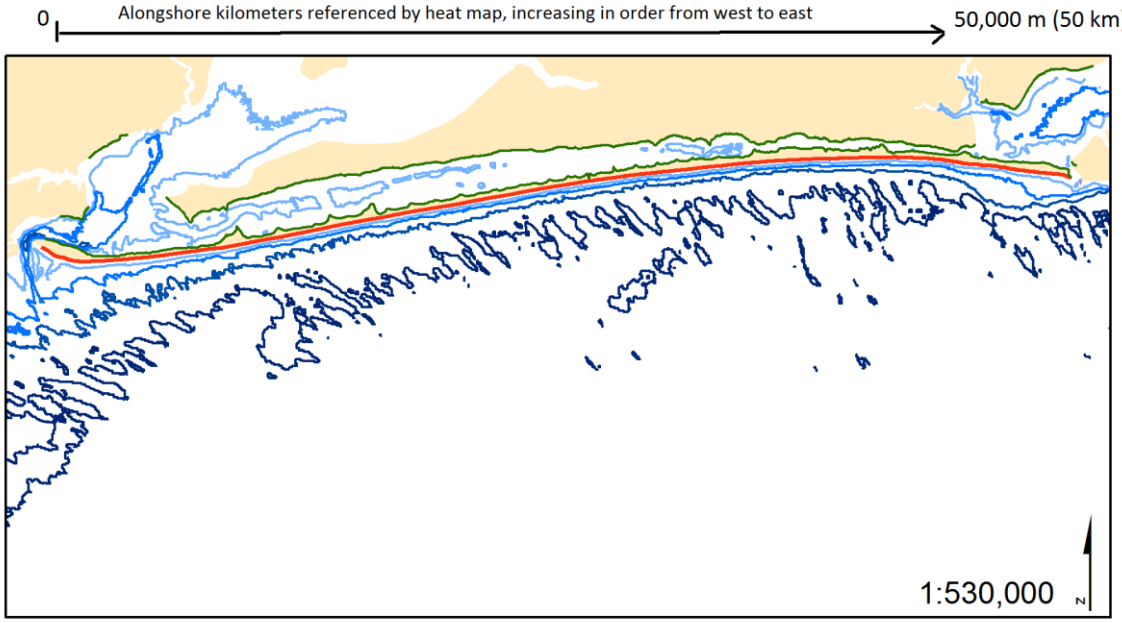

Figure 18 Map showing all input vectors for DSAS analysis. NOAA bathymetric isolines are shown in blues that increase with depth; the red line is the MHWL used as a baseline, and the green lines are the back-barrier and mainland shoreline. The heat maps are later reference to alongshore spacing; this spacing is indicated on those graphics to distance measure in 1000s of m (km), which in reference to the map above, increase from 0 in the west to 50,000 m (50 km) in the east.

contains a similar number of total data points for the series). The results described here support the theory that changes in transect spacing do not cause significant shifts in the global wavelet peaks or correspondence of the peak's frequency values between vectors.

It should be noted that the 20 m and 67 m intervals can intersect a single value for the 90 m resolution bathymetric isolines, as changes in the position of these vectors occur at 90 m intervals (according to the 90 m resolution CRM from which they were derived). This causes some artificial reinforcement of shape signatures exhibited at

smaller length scales. Testing a larger interval may have eliminated such artifcats in this part of the anaylsis, but the larger length scale patterns were not the primary patterns under investigation. The tests at 20, 67, and 100 m do sufficiently show that the small scale patterns seen at 100 m are seen at other transect intervals, and that was the goal of including this test in the methodology. The global wavelets produced by the 20 m interval method, 67 m interval method, and 100 m interval method are shown in for certain frequencies in Figures 19 and 20.

There are multiple points of evidence for concluding that interval spacing does not have a significant effect on demonstration of shape correspondence in wavelet analysis. Table 2 gives the frequency (in km) of the multiple signals exhibited by each vector, at each interval spacing. Concurring frequencies are stacked to emphasize signals that match between vectors. Red cells in the 20 m and 67 m sections of the table indicate values that are different from those returned by the 100 m interval test. Of the 37 signals identified at the 100 m interval, the 20 m dataset preserves all but one, and introduces no new signals despite a 5 times increase in data input. The dropped signal is the 3.48 km signal in the 5 m isobath. The 67 m interval misses the same 3.48 km signal in the 5 m isobath while also adding a 1.01 km signal to the 10 m isobath and a 7.41 km signal to the 20 m isobath. All signals greater than 9 km are preserved no matter the sampling interval, suggesting that at Santa Rosa Island, larger frequencies are unaffected by transect distance.

Figure 19 shows the global wavelet for the 5 m isobath as sampled by the three different transect intervals. The 3.48 km signal seen in the 100 m interval data is high-

Table 2 Values for the most dominant peaks produced by the Morlet analysis of each vector for Santa Rosa Island. Signals are spread out across multiple columns to highlight shared signals. An empty column for a given row indicates no strong variance at that length scale for that vector. Frequencies are in km.

	Vector	The strongest length scales (km) for each vector								
100 m	Back-barrier shoreline	38.42	25.08	19.33	11.20	6.23	3.86		1.52	
	Mainland shoreline	38.42	25.08		10.08			2.65	1.53	
	5 m isobath (Ocean)	38.42	25.08	19.33	12.59	6.55	3.48	2.85	1.70	
	10 m isobath (Ocean)	38.42	25.08			6.01	4.01		1.56	
	15 m isobath (Ocean)	38.29	25.03		9.33		5.26	2.41	1.50	1.07
	20 m isobath (Ocean)	38.21	24.99		11.43		5.05		1.88	
20 m	Back-barrier shoreline	38.40	25.07	19.32	11.19	6.31	3.83		1.52	
	Mainland shoreline	38.40	25.07		9.88			2.75	1.55	
	5 m isobath (Ocean)	38.41	25.08	19.33	12.59	6.55		2.72	1.71	
	10 m isobath (Ocean)	38.41	25.13			6.01	3.98		1.55	
	15 m isobath (Ocean)	38.30	25.03		9.33		5.26	2.39	1.48	1.06
	20 m isobath (Ocean)	38.22	25.00		11.18		5.05		1.90	
67 m	Back-barrier shoreline	39.43	24.87	19.20	11.03	6.29	3.85		1.53	
	Mainland shoreline	38.40	25.07		9.69			2.62	1.51	
	5 m isobath (Ocean)	38.42	25.08	19.33	12.59	6.55		2.65	1.71	
	10 m isobath (Ocean)	38.42	25.08			6.01	4.01		1.55	1.01
	15 m isobath (Ocean)	38.30	25.03		9.33		5.31	2.39	1.48	1.06
	20 m isobath (Ocean)	38.23	25.00		11.43	7.41	5.10		1.91	

lighted by a vertical gray column. Note that there are still slight undulations in the global wavelets for the 20 m and 67 m sampled data within ±0.5 km on either side of the 3.48 km signal. These are not output as definite frequencies because at these intervals they are present, but not strong enough to stand out as a greater perturbation than might exist within red noise (at a 95% confidence level). The sampling interval has a "dampening" effect, but does not erase the signal.

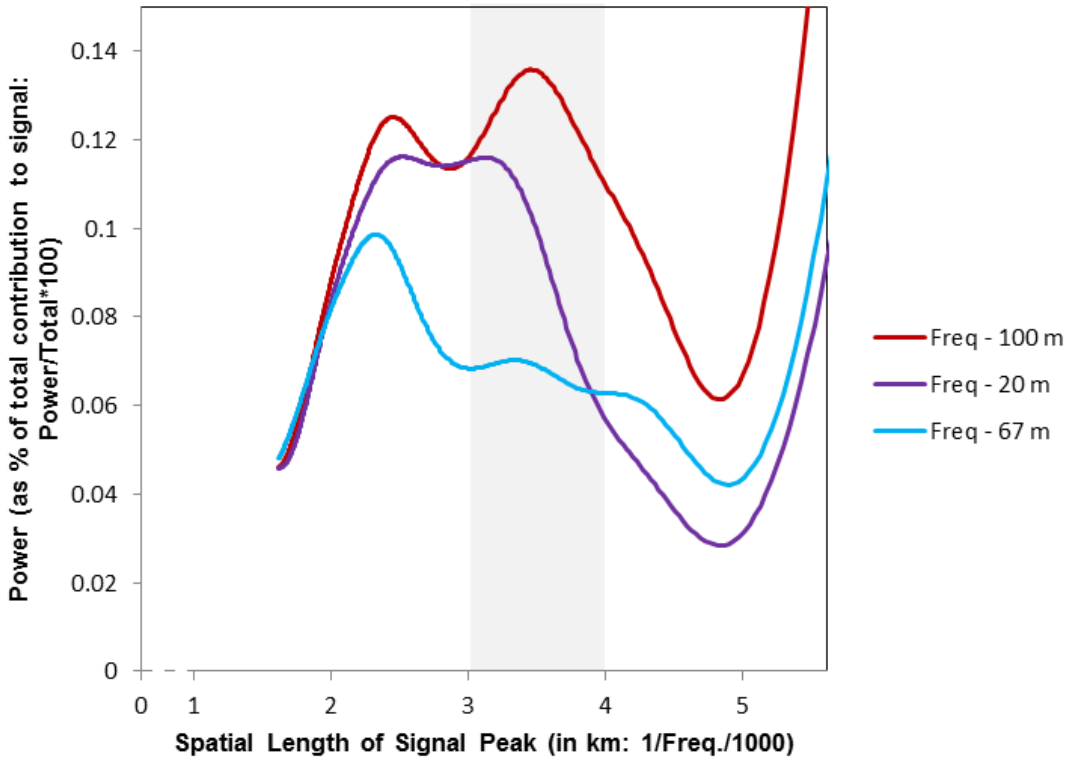

Figure 19 The global wavelets for the 5 m isobath as sampled at 100 m (red), 20 m (purple), and 67 m (turquoise); plot shows only the lowest frequencies (< 4 km).

In the 10 m isobath, an additional signal at < 2 km was added by the 67 m sampling that is not seen in the 100 m interval data (Figure 20). This additional signal, at 1.01 km is less than 500 m different from the 1.57 signal seen in the 10 m isobath by all sampling intervals. It accounts for 0.0029% of the entire isobath shape, but is supplementary to the 1.57 km signal (which accounts for 0.0086%, a fraction of the shoreline's overall shape but 296% more power than the 1.01 signal).

The introduction of the 7.41 km signal to the 20 m isobath by the 67 km dataset is the most significant change between the differing transect interval methods. In the graph of the global wavelets for all frequencies less than 10 km, the 7.41 km signal is not a stand out. There are still undulations in the 100 m and 20 m dataset at this frequency. The difference is in the 67 km global wavelet is that the wavelet has a greater decrease in power for surrounding frequencies, which makes the peak at 7.41 stand out as more significant.

It stands to reason that the smallest frequencies are potentially the most affected by transect spacing, yet these tests produced nearly the same signals even at frequency lengths of less than 9 km. The overall shape of the global wavelet at all sampling intervals is, however, largely indistinguishable. Sampling with either the 20 m or 67 m transect spacing does not affect the shape signature exhibited by each vector. When sampled at the 100 m interval, the global wavelets exhibit the same signals seen at 20 m and 67 m, though each peak has a greater degree of power over the signal as a whole because there are fewer input data points. The width of each peak in the global wavelet also encompasses a greater portion of the x-axis, and so some minor information is not preserved at this sample frequency, but the shape signature identified by the signals (peaks) are preserved.

The more efficient 100 m spacing is the only transect interval used for the remaining three study sites because: 1) the 100 m spacing shows greater qualitatively observed alignment of peaks in the global wavelets, 2) it takes the least time to calculate for both the DSAS and AutoSignal™ portions of the methodology, and 3) the different

sampling intervals preserved the same signal peaks and the same pairings between vectors. For ease of comparison between islands, the correspondence of geomorphological characteristics is discussed for only the 100 m transect data for Santa Rosa Island.

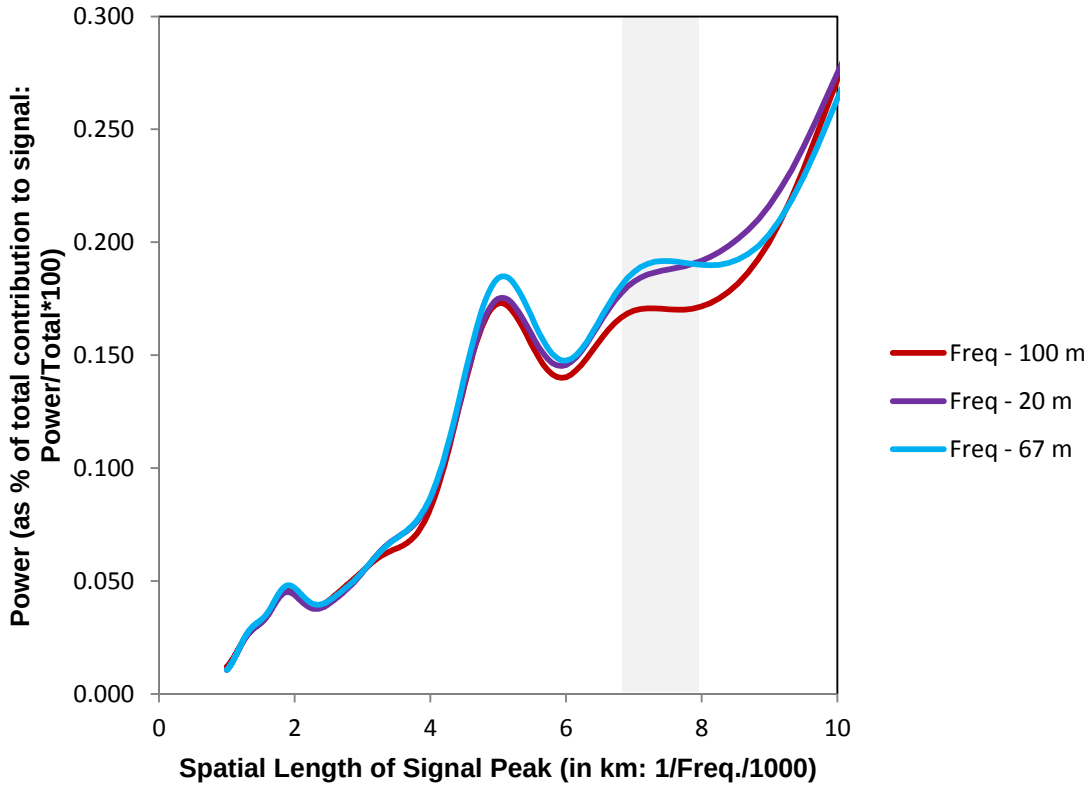

Figure 20 The global wavelets for the 20 m isobath produced by analysis with each transect spacing.

Wavelet Analysis of Santa Rosa Island data

The table data highlights the values of the most prominent signals controlling the shape of each vector and their exact length scale in km. Not all undulations in the global wavelet are apparent as signals in the peak value data (Table 3). These small undulations are sometimes indicators of minor trends in the data that correspond between vectors when viewed in the global wavelet – but are not necessarily large enough to be considered more than red noise. They do not, therefore, appear in the data's output or as hot spots within the heat map because they may not me more significant than red noise at a 95% confidence level. However, they can indicate that a correspondence between each vector's global wavelet at that scale should not be completely ruled out.

A more intensive look at the Santa Rosa dataset sampled at 100m reveals all vectors share their two largest signals, at approximately 38 km and 25 km (see Figure 21 and Table 3). The third most commonly shared signal occurs at 9–12 km, which is shared by all vectors except the 10 m nearshore isobath (this can also be seen by the cluster of peaks in the global wavelet in the Figure 22 showing the global wavelets for all vectors at frequencies less than 15 km). Only the back-barrier shoreline and 5 m isobath also share a signal of 19.33 km length. The back-barrier shoreline and 5 m isobath also share a frequency at 6 km, and are joined by the 10 m isobath. At approximately 3 – 5 km the backbarrier displays a signal shared by all vectors except the mainland shoreline. The mainland shoreline, 5 m sound isobath and 15 m gulf isobath have a frequency between 2 – 3 km. All vectors have a signal at 1 – 2 km.

Table 3 The strongest length scales seen in the 100 m sampled Santa Rosa data (in km). The signal caused by the ridges is outlined in black.

	Vector	The strongest length scales (km) for each vector								
100 m	Back-barrier shoreline	38.42	25.08	19.33	11.20	6.23	3.86		1.52	
	Mainland shoreline	38.42	25.08		10.08			2.65	1.53	
	5 m isobath (Ocean)	38.42	25.08	19.33	12.59	6.55	3.48	2.85	1.70	
	10 m isobath (Ocean)	38.42	25.08			6.01	4.01		1.56	
	15 m isobath (Ocean)	38.29	25.03		9.33		5.26	2.41	1.50	1.07
	20 m isobath (Ocean)	38.21	24.99		11.43		5.05		1.88	

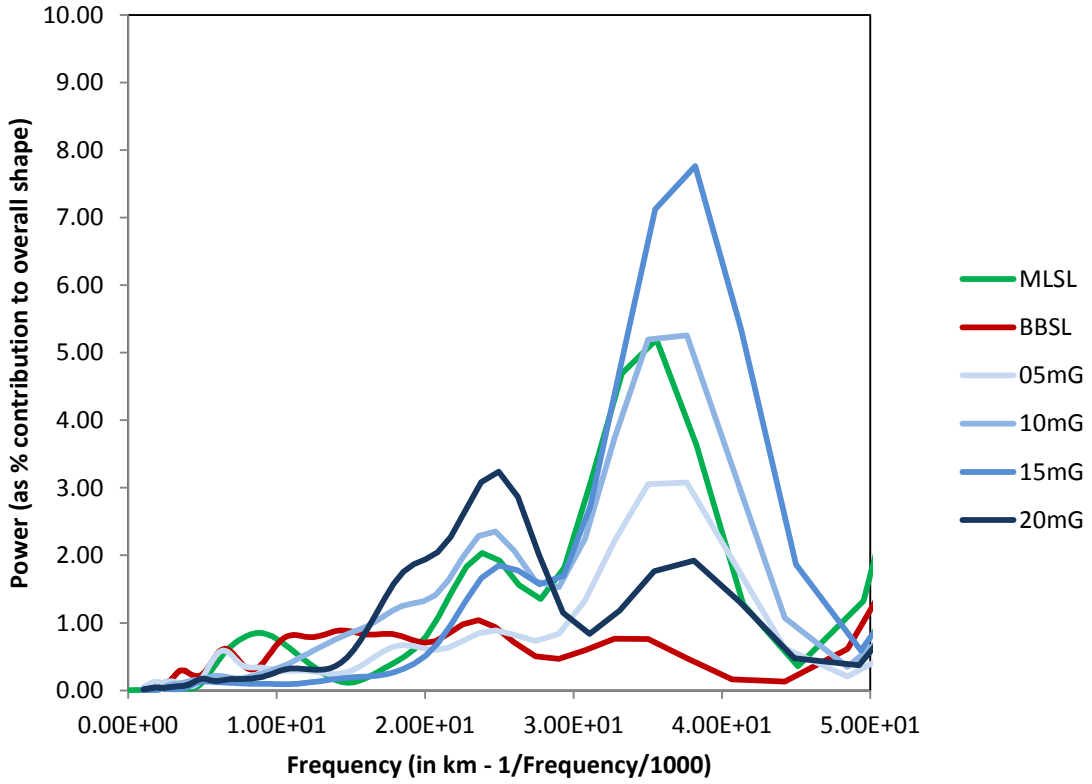

Figure 21 Global wavelets for all Santa Rosa data.

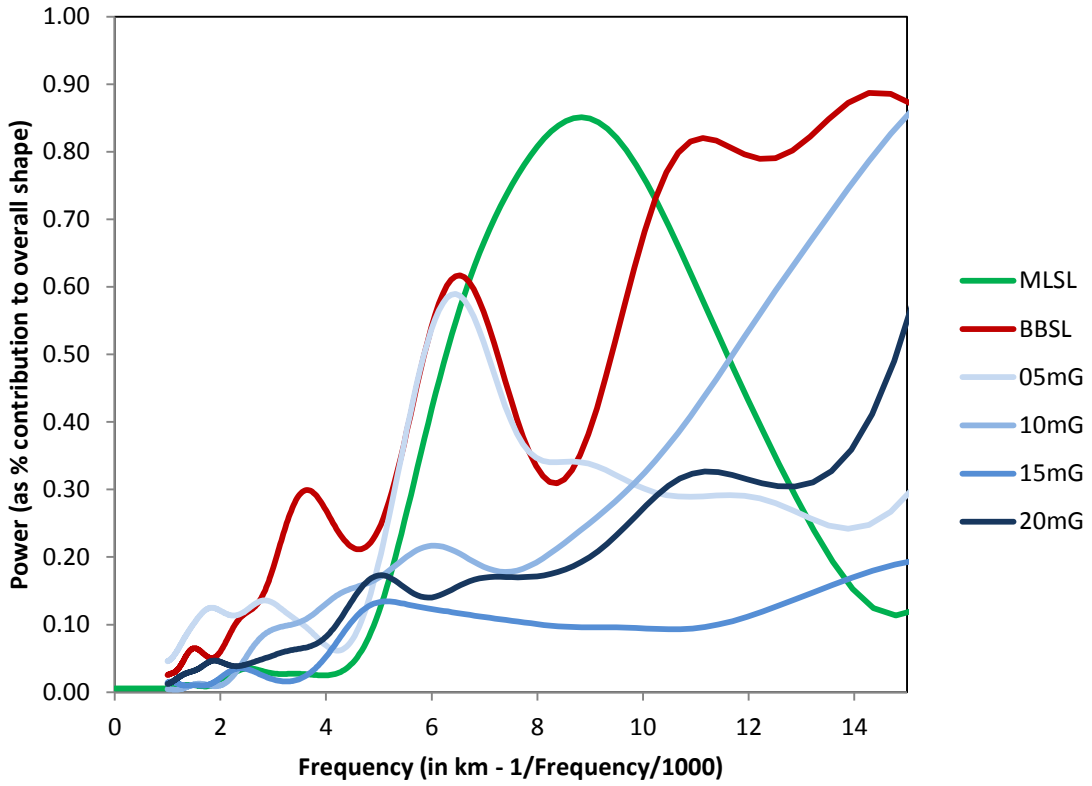

Figure 22 Frequencies of less than 15 km for the global wavelets of all Santa Rosa data.

Qualitative analysis of the heat maps generated by wavelet analysis can also be beneficial in for interpreting the spatial correlation of each signature. The heat map for the back-barrier shoreline of Santa Rosa Island is shown in Figure 23. Red areas represent mathematically calculated 'red' background noise (which are statistically insignificant at the 95% confidence level), with colors progressing in rainbow order toward the hot spots of strongest signal in fuchsia (most significant), which represent areas of strong signal and their alongshore location. The hot spots are a visualization of

the center of each global wavelet peak. The peak in the global wavelet indicates the length scale of the wavelet shape seen as a shape signature, and the hot spots aligned with it in the heat map show the alongshore location of each one of these shapes.

For example, in the heat map of the back-barrier shoreline for Santa Rosa (Figure 23), the peak at frequency $2.603e^{-5}$ is equivalent to a 38 km pattern of shape, which is the longest scale frequency exhibited by all vectors (see Table 3). The hot spots aligned with this peak in the global wavelet are located 20 km apart alongshore, starting at the first transect (bottom of the primary y axis). This is because the Morlet function can occur at irregular intervals, and in this instance represents a curvature of the back-barrier shoreline shape with an independent length scale of 38 km, meaning that the 38 km shape is seen at multiple, overlapping sections of the island and is in this instance centered at several alongshore locations: at approximately 0, 20, 40, 58, and 75 km in the BBSL. This signal is not particularly strong in the BBSL, as indicated by the lack of intensity in the hot spots and the low power, indicated by the limited peak in the global wavelet. The 38 km hot spots grow in intensity from the deeper waters to the mainland: in the BBSL (Figure 23) they are the first row of light red circles, which is also how they appear in the 20 m isoline, then they are stronger in the 15 m heat map and strongest in the 10 and 5 m heat maps and the MLSL (Figures 24 – 28). This means that they contribute more to the overall shape of these vectors. In each heat map, this signal is located in the same space alongshore, indicating that the signal is in-phase for each vector.

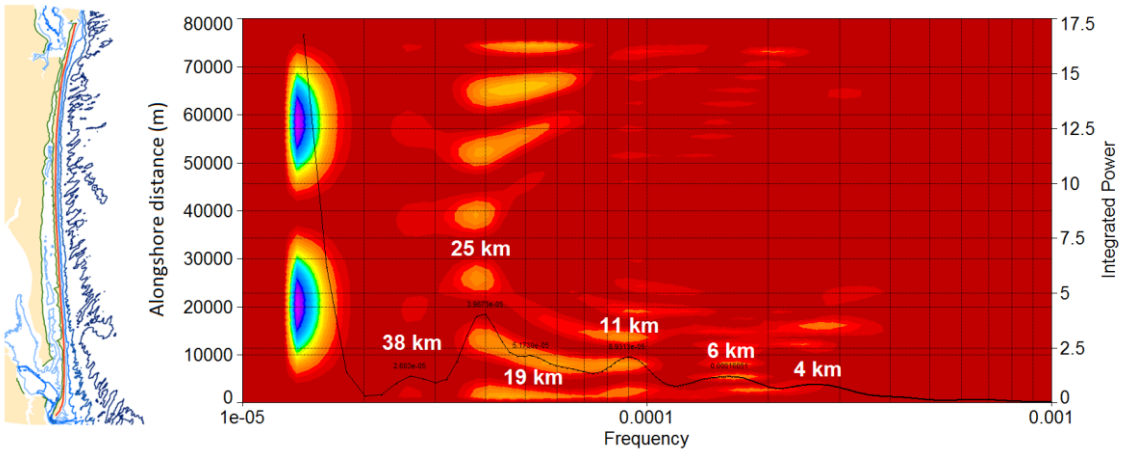

Figure 23 Heat map of the back-barrier shoreline at Santa Rosa Island, FL.

The second longest signal, the 25 km frequency scale seen in all vectors, is spaced ~ 11 or 12 km apart in the BBSL, starting at the first transect. This 25 km pattern is demonstrated by all global wavelets but is weakest in the 15 m sound isobath (Figure 25). The hotspots associated with this length scale are located at relatively even alongshore intervals and in-phase with each other, meaning that this particular shape signature is continuous alongshore.

In contrast, the 11 – 12 km pattern is not continuous alongshore. It appears in the western 25 km of the island, and very faintly in the easternmost 25 km (both times spaced about every 5 – 6 km alongshore), but is absent from the center. The 12 km signal is strongest in the BBSL and MLSL (where is shows the same alongshore variation; see Figure 28). Despite being indicated by the table output as present in each isobath (except the 10 m), and being visible in the plot of global wavelets, it is less

recognizable in the heat maps for the isobaths. This is reason for investigating all three versions of the wavelet analysis data to identify signals.

Also in the BBSL heat map several hot spots indicative of the 6 km signal are clustered at the western end of the island (lower 15 km of the primary y axis) and slightly visible at the eastern end as well (top of the primary y axis). These high-frequency shapes are not apparent in the other heat maps, and so their alongshore spacing cannot be determined, but their presence is indicated on the global wavelets and table output. For the three highest-frequency shape signatures seen on the BBSL heatmap (the 11, 6, and 4 km length scales) the gap in their alongshore distribution coordinates with their farther distance from shore, between alongshore kilometers 20 and 40.

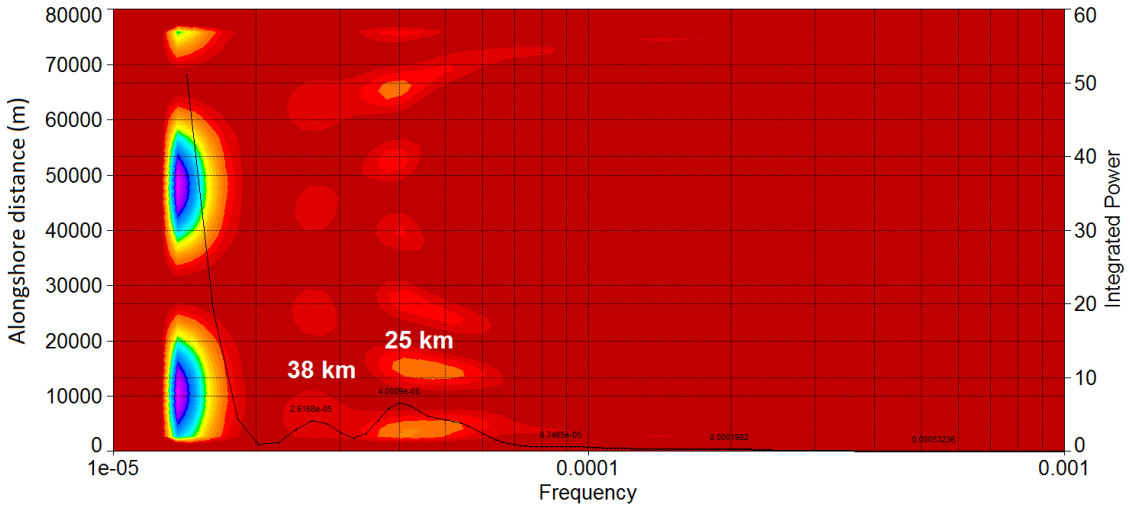

Figure 24 Heat map for the 20 m bathymetric isoline in the nearshore of Santa Rosa Island.

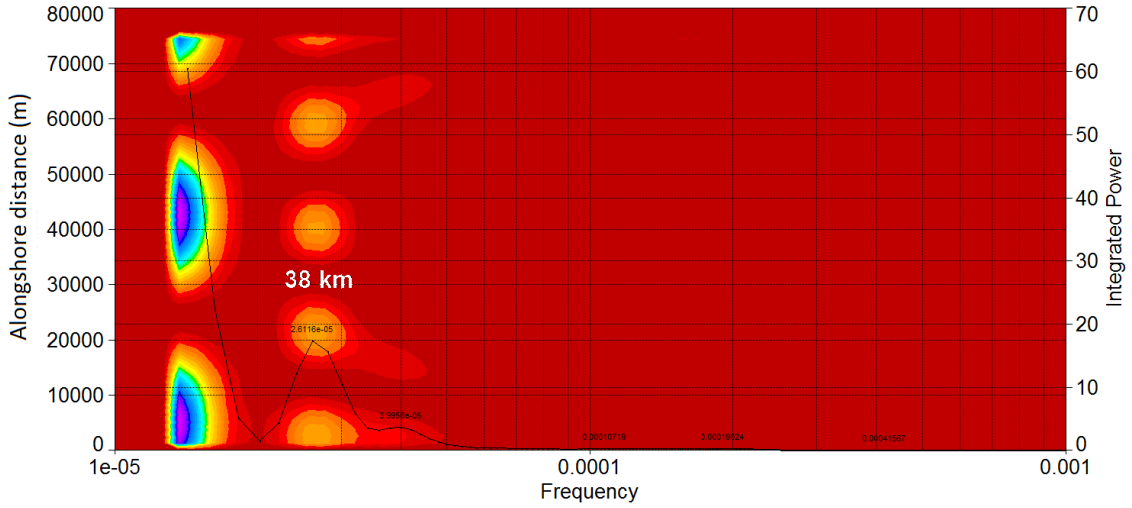

Figure 25 Heat map for the 15 m bathymetric isoline in the nearshore of Santa Rosa.

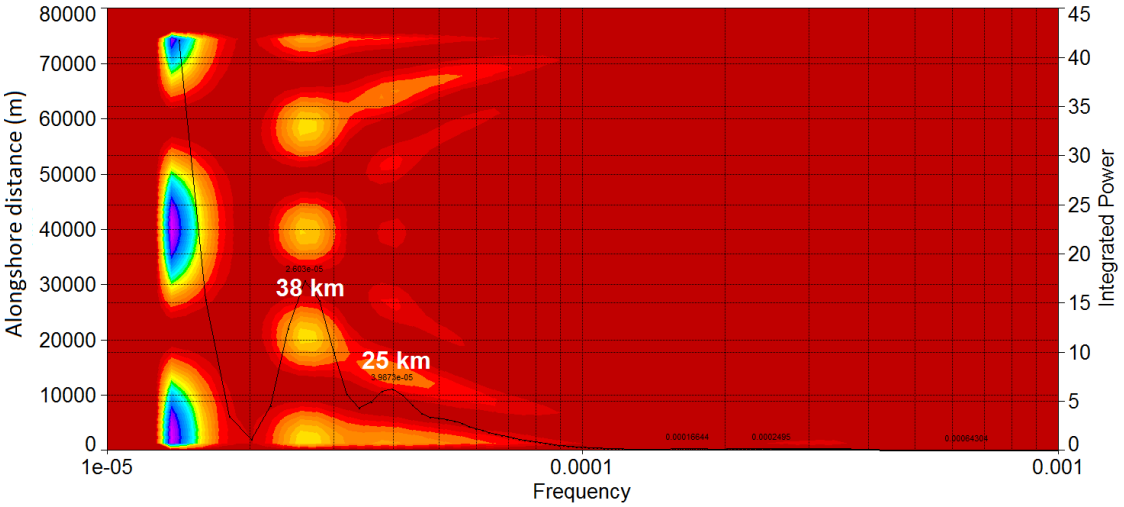

Figure 26 Heat map for the 10 m bathymetric isoline in the nearshore of Santa Rosa.

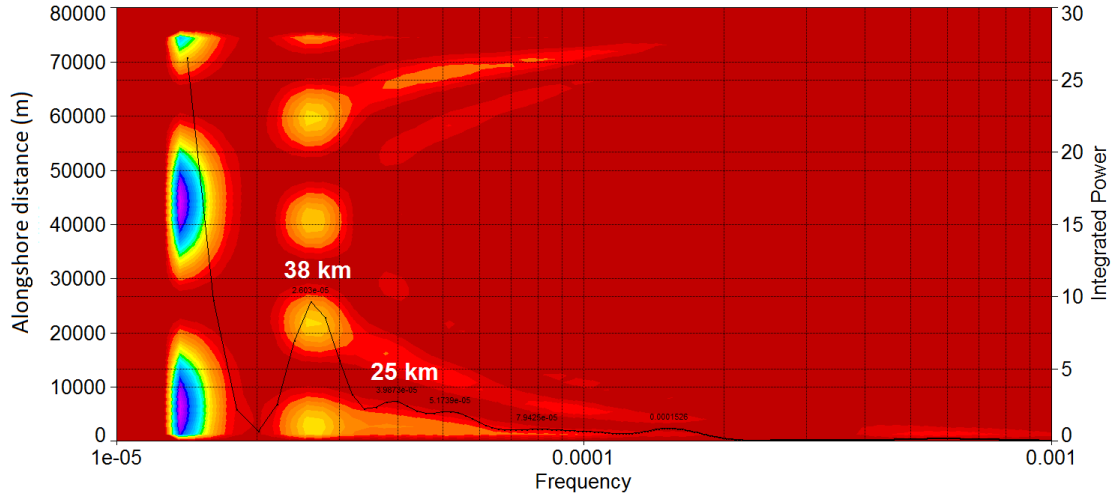

Figure 27 Heat map for the 5 m bathymetric isoline in the nearshore of Santa Rosa.

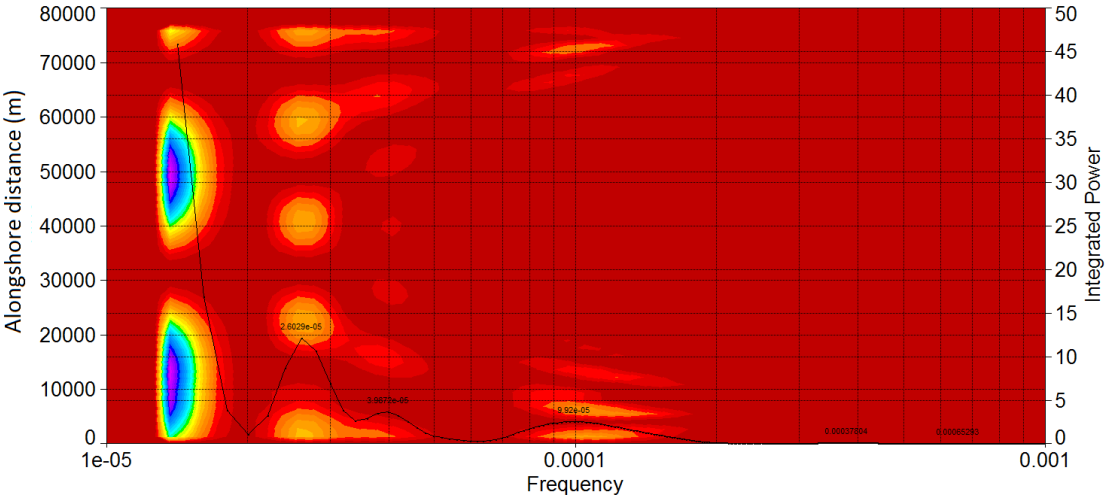

Figure 28 Heat map for the mainland shoreline of Santa Rosa Island.

Fire Island National Seashore, New York, US

Previous studies of Fire Island, NY have shown a potential correspondence between the nearshore geologic framework and the back-barrier shoreline shape (Hapke et al. 2010), generally associating narrower parts of the island with ridges (and wider sections with swales), suggesting that the ridges are repeatedly focusing wave energy onto certain regions of the island. This thesis introduces the mainland shoreline to the analysis. The ridge and swale topography is well defined at Fire Island; ridges are generally 2 – 4 km apart and attached to the shoreface along the western half of the island. In the map showing all input data (Figure 29), the ridges can be seen most clearly in the 20 m isobath on the western half of the island. They are less defined or absent on the eastern half. The table highlighting the strongest frequencies in the shape of each vector are highlighted in Table 4, and stacked apart so that matching signals line up vertically within each column.

All nearshore bathymetry shares a 38 km signal, but the shorelines do not. Every vector has a 24 km signal. The nearest-shore 5 and 10 m isobaths share an 18 – 19 km frequency, which may or may not be associated with the 16.57 km signal in the back-barrier. The back-barrier shoreline shares its 10 km signal with all but the 15 m isobath. The alignment of these signals can be seen in the plots of all global wavelets, Figures 30 and 31 (which show the same information at two different scales). All vectors except the mainland shoreline have a frequency of length 6 – 8 km.

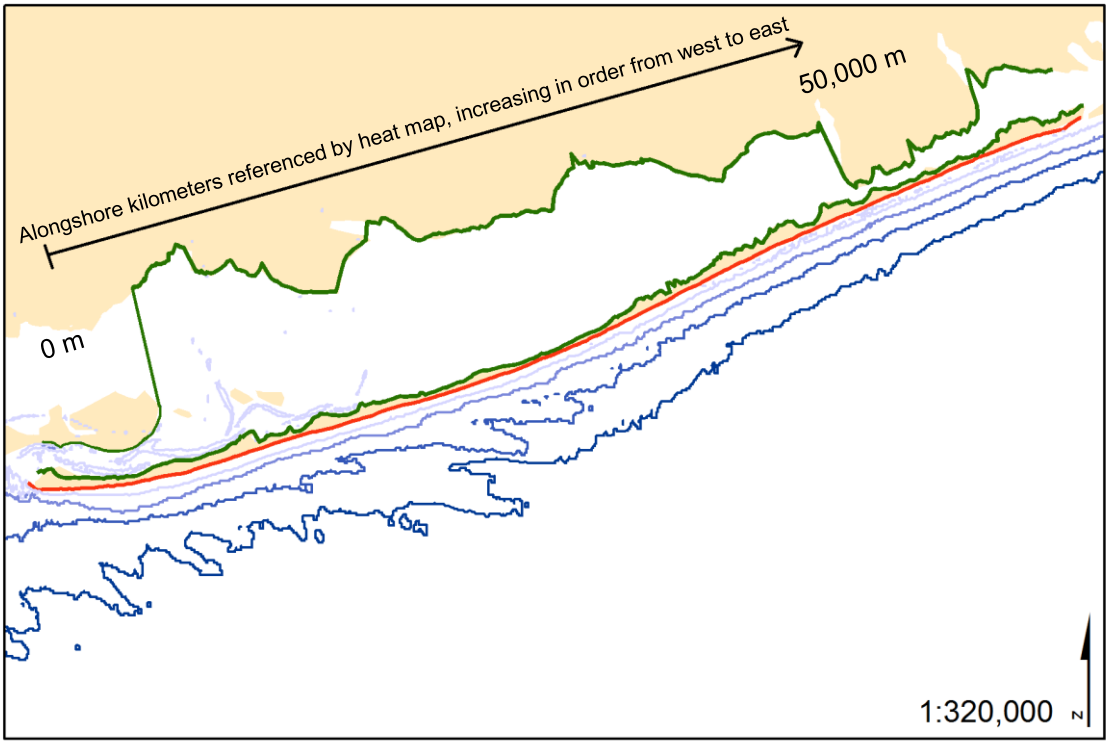

Figure 29 Map of all vectors analyzed for Fire Island, New York

Table 4 Values for the most dominant peaks produced by the Morlet analysis of each vector for Fire Island. Signals are spread out across multiple columns to highlight shared signals. An empty column for a given row indicates no strong variance at that length scale for that vector. Frequencies are in km.

Vector	The strongest length scales (km) for each vector							
Back-barrier shoreline		24.57	16.57	10.24	6.64	3.99		
Mainland shoreline		24.57		9.30				
5 m isobath (Ocean)	38.01	24.73	18.52	12.55	8.12	3.16		1.42
10 m isobath (Ocean)	38.01	24.92	19.23	10.05	6.15		2.07	
15 m isobath (Ocean)	38.06	24.93			7.52	3.85	2.10	
20 m isobath (Ocean)	38.01	24.91		11.96	7.19	3.28	2.51	1.03

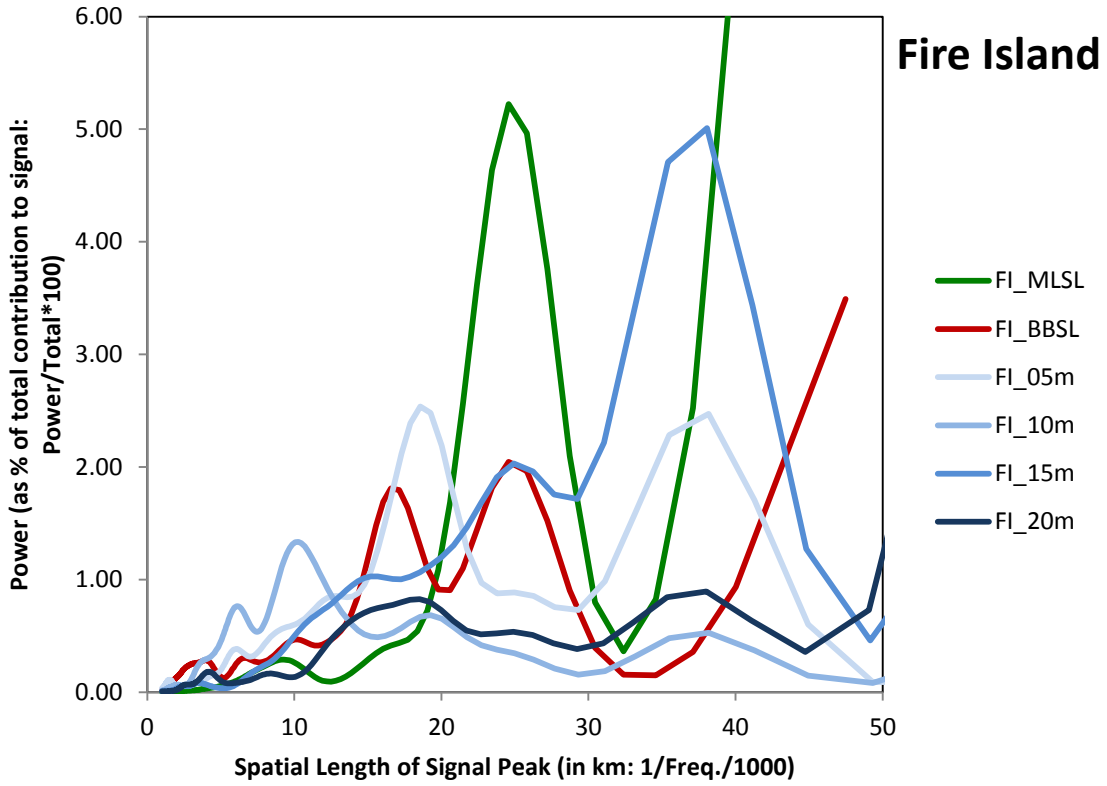

Figure 30 The global wavelets produced by analyzing the mainland shoreline, back-barrier shoreline, and offshore bathymetry at 5 m intervals for Fire Island National Seashore.

In the global wavelets, a definitive peak is shared by all nearshore isobaths at 38 – 40 km (which matches the table output) and it becomes apparent that the shorelines had fewer input data points and so the 38 km signal was beyond their reach. Signals at ~ 10 km are shared by all vectors and the 20 m isobath, which is also apparent from the table. In the plot of global wavelets, it can be seen that the 15m isobath has the smallest

of undulations at this same scale, but that it is absorbed by the strength of a signal at 15 km, which in turn is overwhelmed by the 25 km signal. The 15 km signal is also exhibited by the BBSL, 5 and 10 m isobaths in the table output, but aligns with small undulations in the MLSL and 20 m isobath.

Higher frequencies within the global wavelet are exhibited at 3 – 4 km by the BBSL and the 5, 15, and 20 m isolines, but not the MLSL or 10 m isoline (Figure 31). A signal at 2 km is shared by the 3 deepest isobaths, and the smallest frequency signal identified is a 1 km signal in the 5 and 20 m isobaths (but not those in between). Previous studies of Fire Island have shown that ridges in the nearshore are spaced about 1 – 3 km apart, extending approximately 20 km offshore, and oriented about a 120 – 130º northwest to southeast azimuth (Schwab et al. 2000; Hapke et al. 2010). These are the frequencies in shape < 5 km (Figure 29) seen in the nearshore bathymetry. In the graph of the global wavelets for higher frequencies (Figure 31), the 5 m isoline has a defined peak at 1.5 km and another smaller undulation at about 3 km, which aligns with the ridge spacing described by previous research. The 10 m isoline has peaks at 1.5 and 2 km. The 15 m and 20 m isolines have a peak near 2.5 km. The BBSL has a series of peaks which appear as a broad shoulder over a range of frequencies from 1 – 4 km, but with noticeable undulations at 1.8, 2.5, leading to the highest peak at 4 km.

The heat map for the back-barrier shoreline of Fire Island is shown in Figure 32. The back-barrier shoreline has repeating patterns which appear in the heat map as a series of hot spots at length frequency of 25 km (closest to the primary y axis), 16 km (middle series), and 10 km (only between alongshore km 9 and 30) and 6 km (only at the

ends of the island). The 4 km signal appears along the westernmost third of the island at an alongshore spacing of 1 – 2 km; the same location and spacing of the well-documented nearshore ridges, which are attached on the western half of the island but located further offshore in the eastern half, where the back-barrier heat maps does not show hotspots for the 4 km signal.

The 16 and 10 km hot spots are stronger at the eastern most end of the island (the top of the primary y axis), where the mainland is closer to the bayshore of the island. Cross-sound distances here are only 0.3 – 2.5 km, while for the western 2/3rds of the island they are 3 – 8 km, except at the very westernmost end where they return to < 2 km due to overlap with the next island in the barrier chain (and here there is also a return in strength for the hotspots). The other high frequency signals are also clustered at both ends of the island. Of the high frequency signals, only the 4 km signal is stronger in the middle of the island.

The mainland shoreline heat map exhibits a similar alongshore pattern that aligns somewhat with the second level variance seen in the back-barrier shoreline at 13 – 15 km, but it does not share the 10 km pattern. Also, it does exhibit alongshore nodes at 25 km but they are exactly opposite phase from the same frequency seen in the back-barrier shoreline; these hotspots occur alongshore precisely between the alongshore locations of the hotspots for the same frequency in the back-barrier. This is indicative of an earlier stage of the model presented in Ashton et al. (2009), where cusps forming at the edges of the elongate water body are not symmetrical across the lagoon until later in the self-organization process.

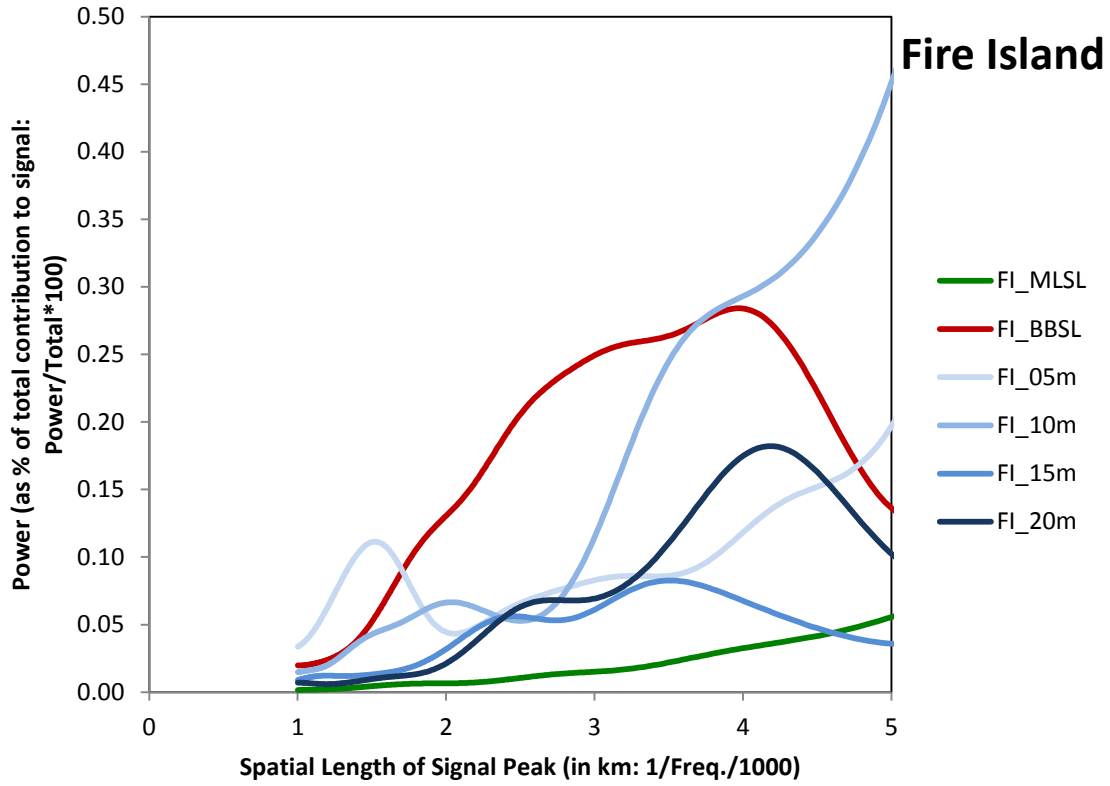

Figure 31 A closer look at signals for frequencies lower than 5 km in the global wavelets produced for Fire Island National Seashore.

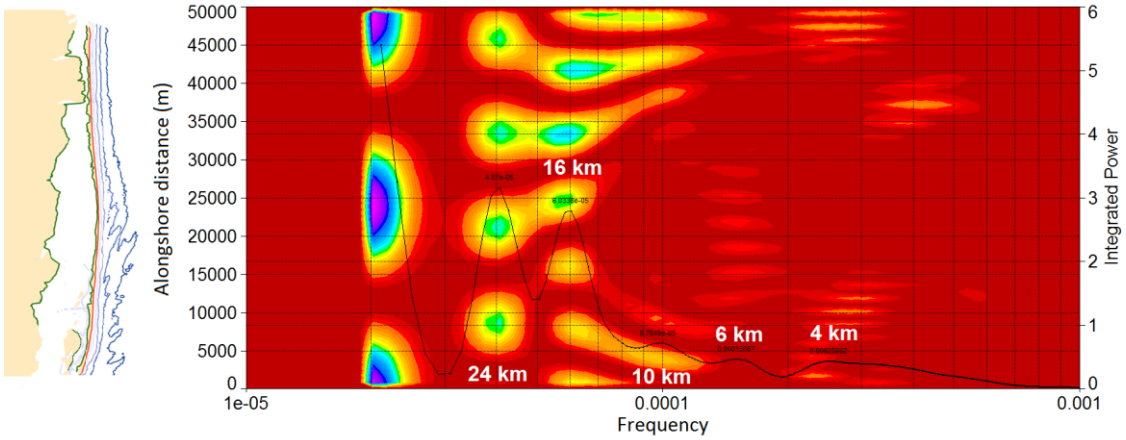

Figure 32 Heat map of the back-barrier shoreline global wavelet generated by Fire Island, New York

The 5 m nearshore isobath exhibits patterns that are very similar to the back-barrier shoreline, with three series of nodes but with slightly different alongshore spacing: one at 40 km, one at 25/27 km, and one at 10 km. The 10 km nodes are in direct spatial alignment with those seen in the back-barrier shoreline, and are strong at the eastern end of the island (where they were strongest for the back-barrier shoreline) but have equal significance along the western end of the island. This western variation is in concurrence with the findings of Hapke et al. (2010), who observed that the ridges and swales are attached in the west, but they did not see these ridges attached in the east. Strength of variance in the 5 m isobath corresponds spatially with the inlets at the ends of the island. In the east the variations trend along a slight NW/SE axis (white dashed line), that corresponds to the predominant angle of approaching waves.

The ridges described by Hapke et al. (2010) are most visible in the 5 and 10 m heat map (Figure 33). They are concentrated on the westernmost third of the nearshore and spaced at about 4 km (which was also apparent in the table output and global wavelet plot shown in Figure 30). They can barely be inferred from the 15 m heat map and are not visible in the 20 m heat map, despite their visibility in the map shown in Figure 29.

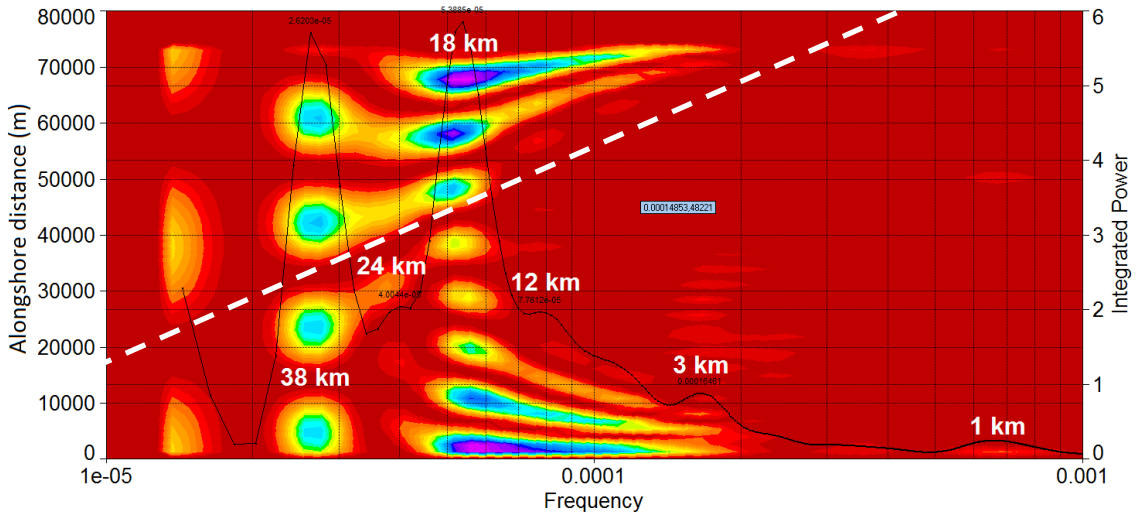

Figure 33 Heat map of the 5 m isobath variations at Fire Island, New York.

Assateague Island National Seashore, Maryland, US

Previous research has suggested that paleochannels exist For the Assateague Island dataset, though their precise locations and structure are still not well defined (Kehrin 1989, Krantz et al. 2004), but they are evidence that washover has been the dominant process determining island morphology for several thousands of years. The bathymetry at Assateague presents what may be called ridges at a highly oblique angle to the coast, but these linear features in the isobaths are discontinuous and sporadic at best (see Figure 34). No previous works have shown links between coastline morphology and nearshore bathymetry for the island as a whole, though many have investigated these links for the northernmost 10 km of the island, just south of the Ocean City Inlet. In this portion of the island, a general trend was seen in island volume for that

stretch of beach: the center was degrading, trasngressing with loss of volume, while the outer edges were transgressing while maintaining volume (Brock, Krabill and Sallenger 2004). This pattern mirrors that seen at Santa Rosa Island, where the repeating cuspate shape favors repeated washover in the center, but maintains island width at the wide cusp tips (Houser, Hapke and Hamilton 2008).

The longest shape signal exhibited in the global wavelets is at ~ 28 km, and this frequency is shared by all nearshore bathymetry (see Figure 35 and Table 5). This signal is exhibited by the isolines but not the MLSL or BBSL, because they do not have enough input points to calculate lengths at such a large frequency (they top out at about 28 km; see Figure 35). All vectors but the deepest isobath have a signal between 18 – 20 km (Figures 35, 36, and 37). The MLSL and 20 m isobath share a 13 km signal not seen in other data. A 7.87 km signal in the 20 m isobath could either be the smallest end of the spectrum in a ~ 8 km signal shared by all vectors, or the upper end of the spectrum in a signal ~ 7 km shared by all vectors. The highest frequency signals are the least shared. The 1.83 km signal in the BBSL could ether be shared with the ~ 2km signal in the deepest isobaths or the 1 – 2 km signal seen in all but the 5 m isoline.

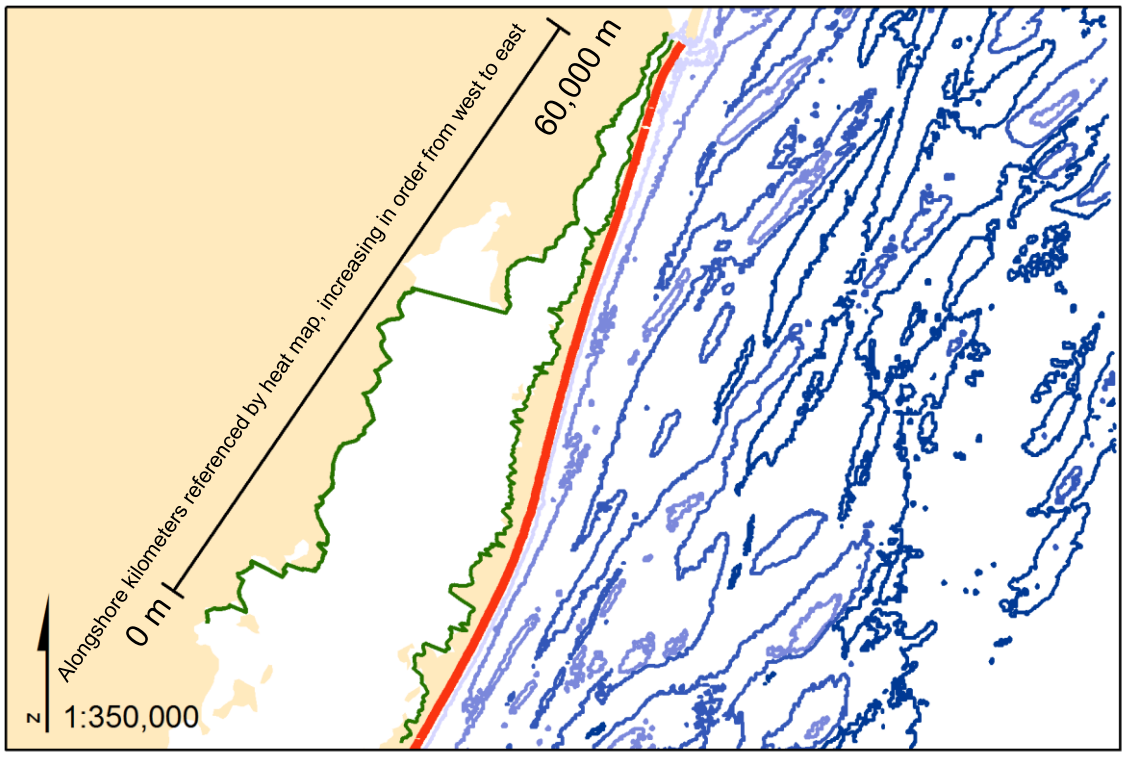

Figure 34 Map of all data input to wavelet analysis of Assateague Island.

Table 5 Values for the most dominant peaks produced by the Morlet analysis of each vector for Assateague Island. Signals are spread out across multiple columns to highlight shared signals. An empty column for a given row indicates no strong variance at that length scale for that vector. Frequencies are in km.

Vector	The strongest length scales (km) for each vector							
Back-barrier shoreline		17.82		11.99	6.86	4.76	1.83	
Mainland shoreline		20.19	13.34	9.78	7.49		2.04	1.07
5 m isobath (Ocean)	29.33	19.30		8.56	5.75	4.44		
10 m isobath (Ocean)	27.38	18.44		11.15	5.80	4.40		1.42
15 m isobath (Ocean)	27.38	18.44		8.98	5.80			1.22
20 m isobath (Ocean)	27.38	18.44	13.90	7.87		3.54	2.62	1.70

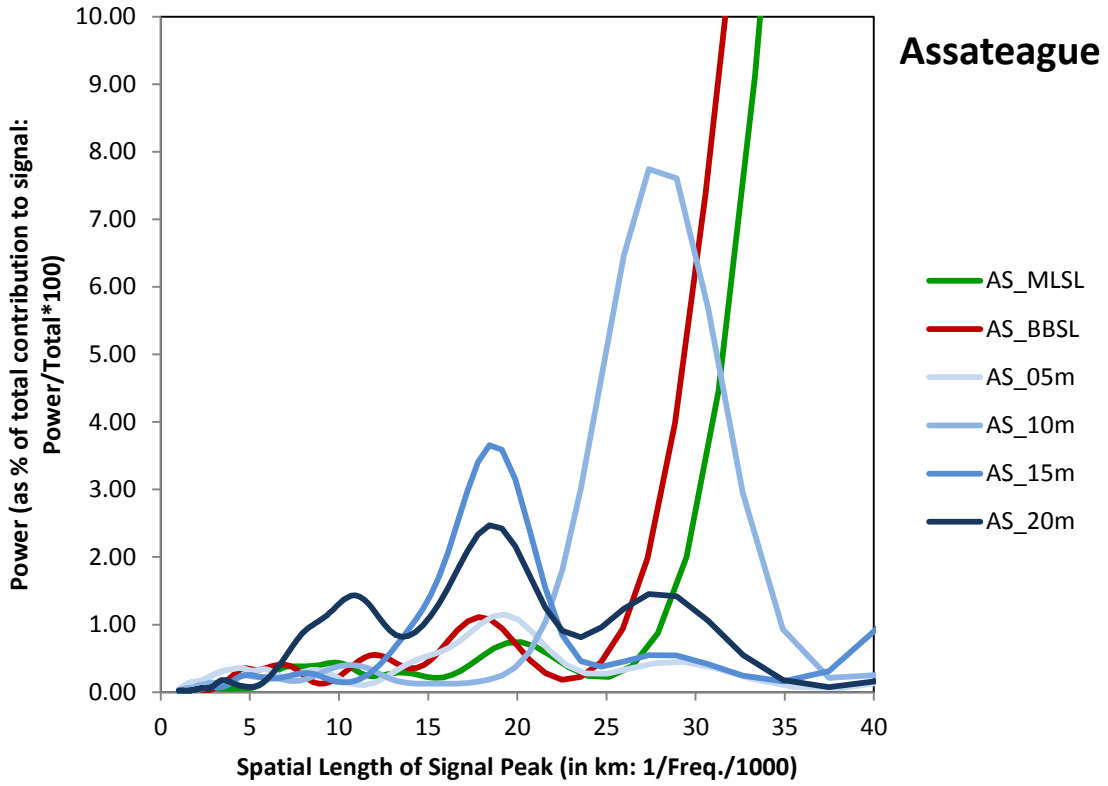

Figure 35 The global wavelets produced by analyzing the mainland shoreline, back-barrier shoreline, and offshore bathymetry isobaths for Assateague Island National Seashore.

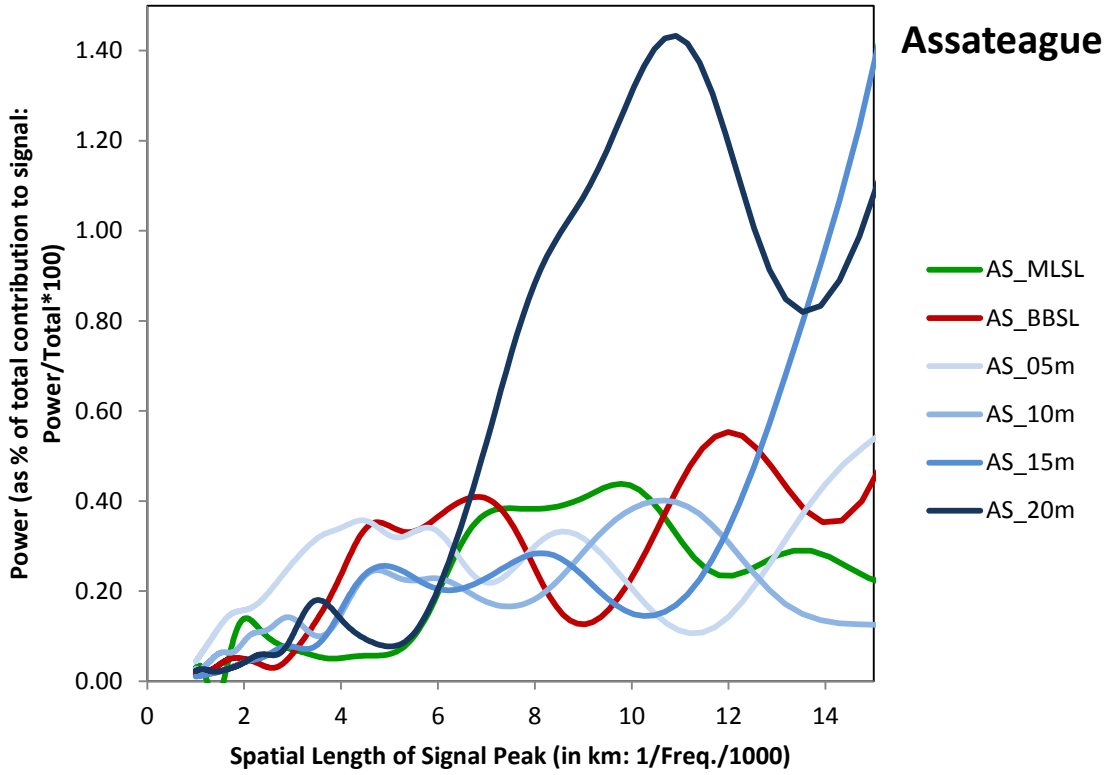

Figure 36 The global wavelets for frequencies lower than 15 km seen in the global wavelets produced by analyzing the data for Assateague Island National Seashore.

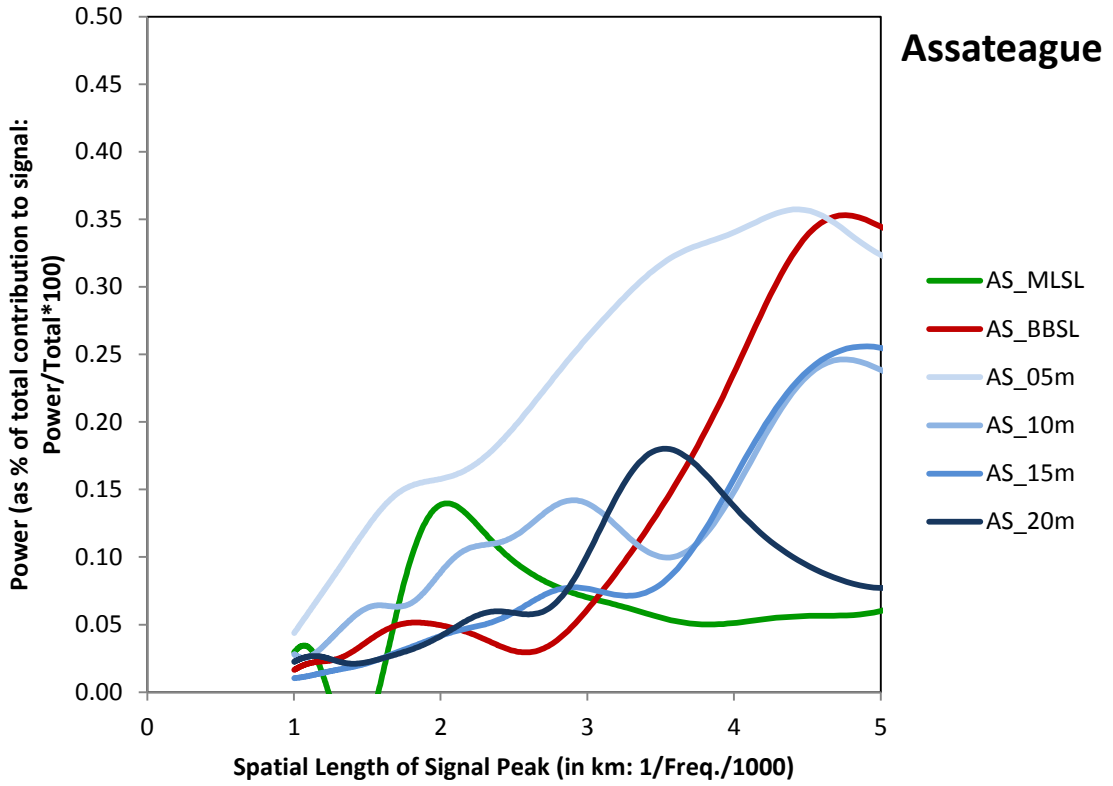

Figure 37 The global wavelets for frequencies lower than 5 km seen in the global wavelets produced by analyzing the data for Assateague Island National Seashore.

The heat map for the back-barrier shoreline reveals the weakness of any particular signal (Figure 38). The only other hot spots visible are weak. The 18 km signal occurs approximately 4 times alongshore, and a faint hint of the 4.76 km signal can be seen along the northern most part of the island. The mainland shoreline has equally low variance within the heat map.

In contrast, the nearshore bathymetry heat maps have many strong hot spots. The 5 m isobath heat map (Figure 39) exhibits 4 hot spots at the 38 km frequency as identified in Table 5. They are distributed at the same regular alongshore distance as the 18 km signal in the BBSL, but are stronger and oriented to the northwest of the signal seen in the back-barrier (about 500 m north along the y axis + west of the back-barrier shoreline = northwest). The 18 km signal is clearly defined in the 5 m isobath as a series of hotspots that begin at the first transect and repeat with regular alongshore spacing every 10 km for the length of the island. The more frequent signals (8.56, 5.75 and 4.44 km) are seen at the southern end of the island, but barely register in the north.

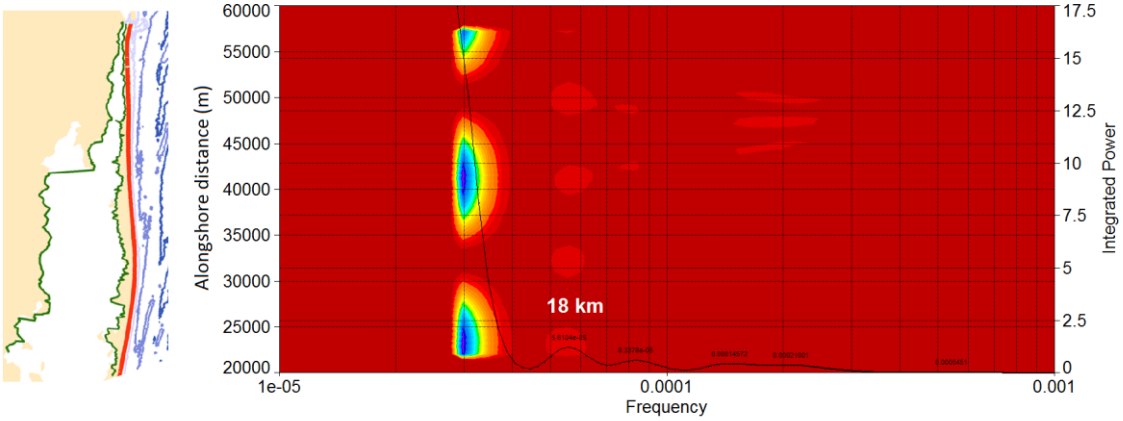

Figure 38 Heat map of the Assateague Island back-barrier shoreline.

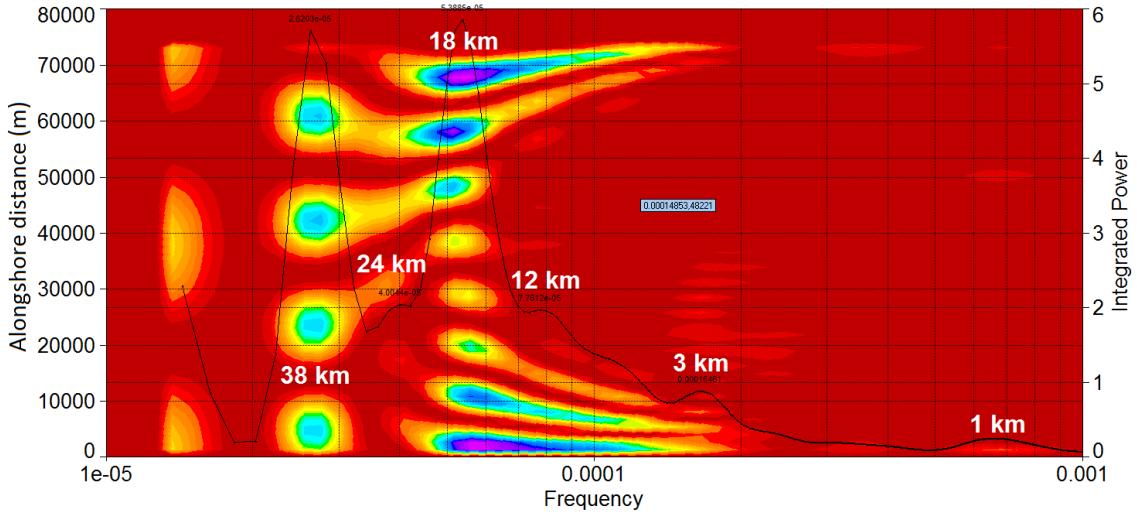

Figure 39 Heat map of the 5 m isobath at Assateague Island**.**

In the heat map of the 10 m isobath, the 28 km signal is much stronger than in any of the other vectors (Figure 40). The 18 km signal is weak in the 10 m isobath, present only in the northern half of the island and spaced every 5 km alongshore. In the 15 m isobath heat map it is stronger, occurring more frequently alongshore location than in the BBSL. The 15 m isobath has only a weak hot spot series at the 18 km signal, with regular alongshore variation in phase with the 5 m isobath (Figure 41). The 20 m isobath has the most variation, including a 14 km signal that is only shared with the MLSL. It also shows the 29 km signal with a slight northwest shift from the hot spots in the 5 and 10 m isobath heat maps. The 8 km signal is also very strong in the 20 m isobath, with dense alongshore variation (about every 5 km) and is concentrated in the southern half like it is in the 5 m isobath. The 8 km signal is located alongshore at opposite phases in

in the 5 m and 20 m isobaths. Where this signal repeats near each 10 km mark alongshore in the 5 m isobath, it repeats directly in between these in the 20 m isobath (Figure 42). This is in agreement with previous studies, which have shown that the ridges are not normal to shore, but angled at about 65º; this causes alongshore shifts in signal location with increasing depth in the nearshore.

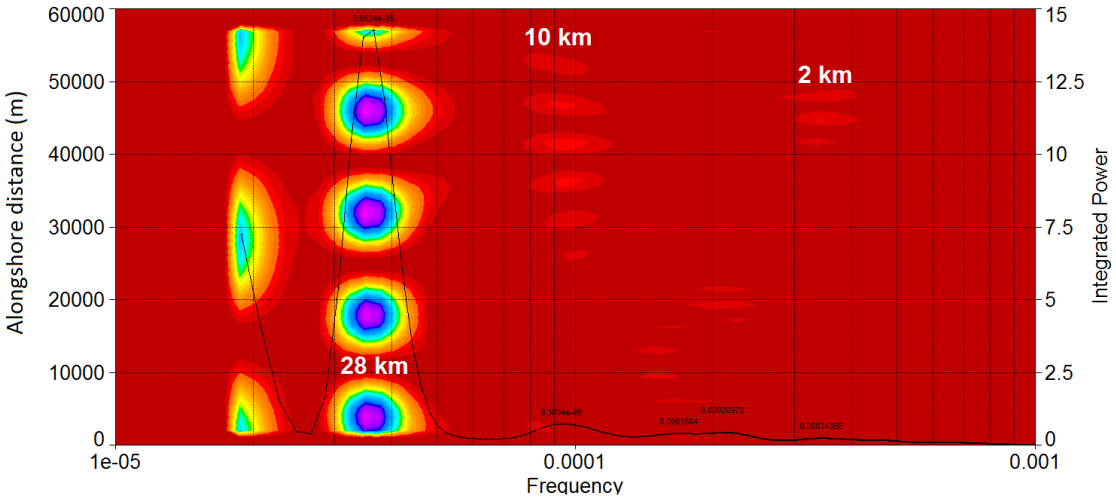

Figure 40 Heat map of the 10 m isobath at Assateague Island.

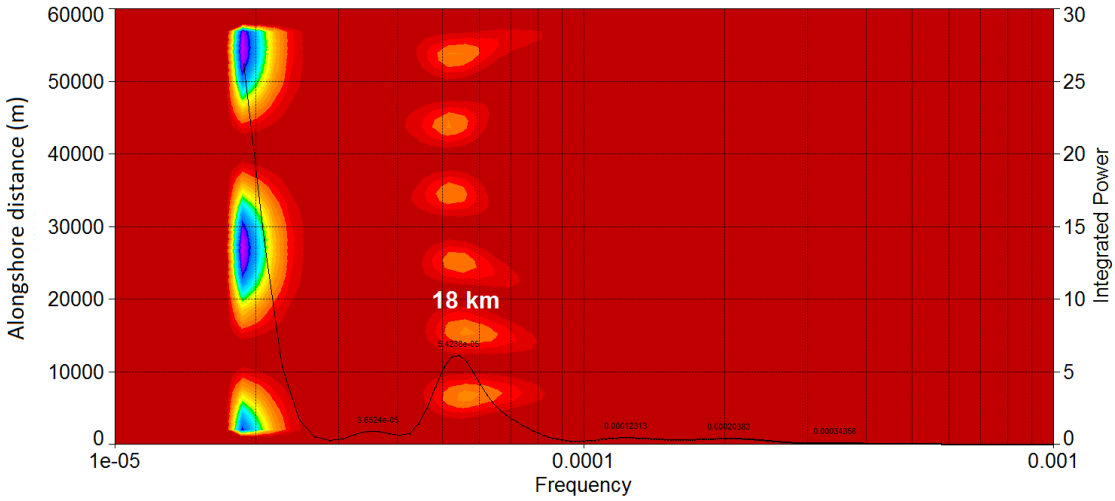

Figure 41 Heat map of the Assateague Island 15 m isobath.

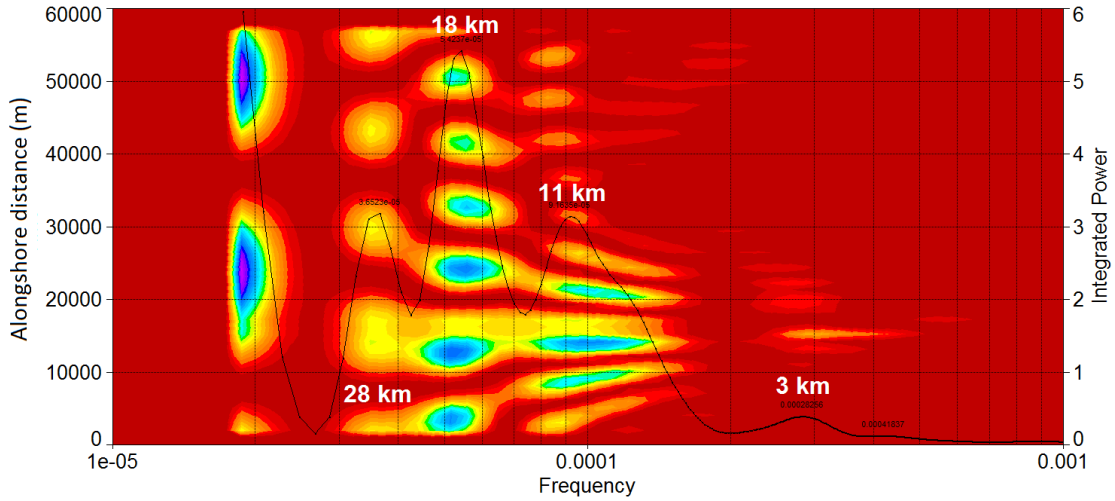

Figure 42 Heat map of the Assateague Island 20 m isobath.

Padre Island National Seashore, Texas, US

The data for North Padre Island includes the bathymetric isolines derived from NOAA data, as for all study sites, but for this dataset the mainland and back-barrier shoreline were digitized using Google Earth tools and imagery rather than using ArcMap to capture shorelines shown in High Resolution Orthoimagery. Although the exact details of the Google Earth imagery resolution, capture method and RMSEz vary throughout the study area, they are always consistent with the criteria for the project. The spatial resolution is 1 m or less, the bands are either RGB or RGB+NIR, and the imagery was all captured within a single year (2011) and within 10 years of the project (post 2002). The vectors digitized in Google Earth (the mainland and back-barrier shoreline) were captured at a scale of 1:750, which is consistent with the digitization in ArcMap of the HRO for the other three study sites. Figure 43 is a map of all North Padre data input to the analysis. The bathymetry here is almost entirely parallel to shore, with a few ridges at the southernmost end of the island that are visible in the 15 m isobath and are spaced about 1.2 km apart alongshore (Figure 43).

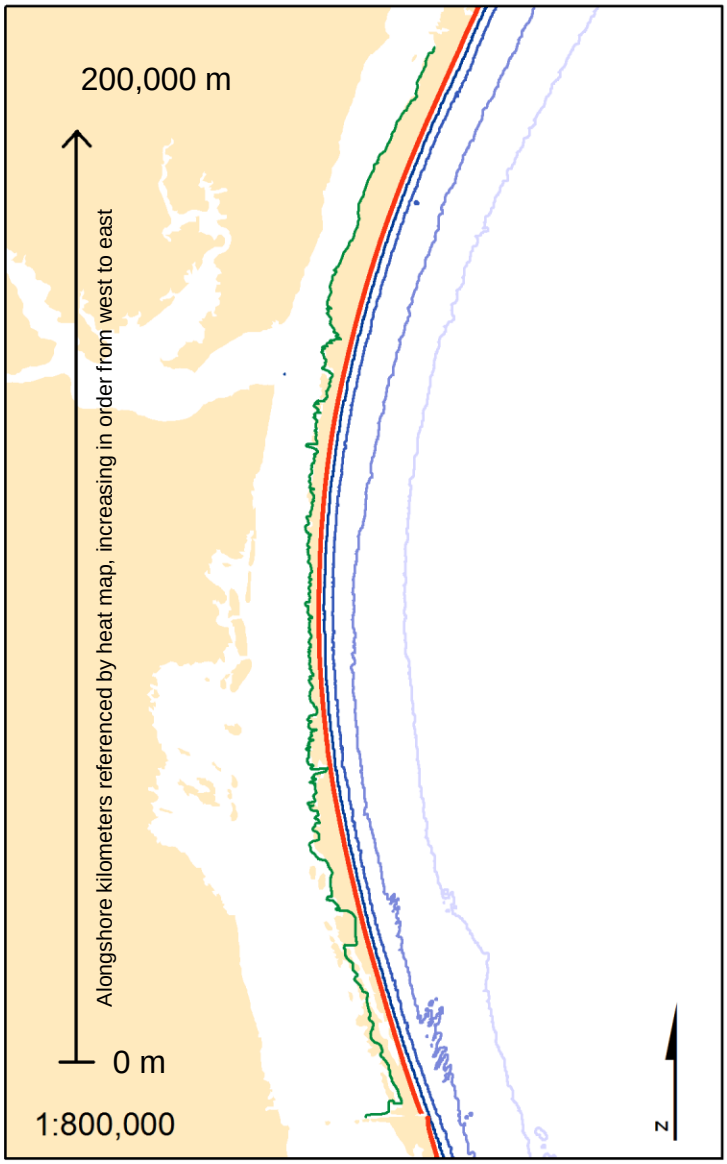

Figure 43 Map of all vectors analyzed for North Padre Island, TX.

The back-barrier shoreline's longest frequency shape signature occurs at 59 km, and this signal is shared by the 5, 10, and 20 m isobaths but not the 15 m isobath (see Table 6). The 15 m isobath is the vector that captures the offshore ridges located in the southernmost portion of the island. The 59 km signal does appear as an undulation in the 15 m global wavelet shown in Figure 44. The nearshore bathymetry vectors share a signal at 37.22 km (absent from the 20 m isobath) but this signal is not present in the BBSL. The 28 km signal defined in the BBSL and the 20 m isobath are relatively similar to the 20 – 24 km signal peaks shared by the other bathymetry when viewed as stacked mother wavelets (Figures 44, 45, and 46). The 15.49 km signal in the BBSL is most closely shared by a 14.55 signal in the 15 m isobath.

Table 6 Values for the five most dominant peaks produced by the Morlet analysis of each vector for Padre Island. Signals are spread out across multiple columns to highlight shared signals. An empty column for a given row indicates no strong variance at that length scale for that vector. Frequencies are in km.

Vector	The strongest length scales (km) for each vector									
Back-barrier shoreline	59.02			28.74	18.99	15.49	7.93	6.03	2.92	2.32
Mainland shoreline										
5 m isobath (Ocean)	59.02		37.22		24.54		8.47			1.99
10 m isobath (Ocean)	59.02		37.22		20.54		9.59	5.63		2.22
15 m isobath (Ocean)			37.22		22.36	14.59		6.85	3.80	1.77
20 m isobath (Ocean)	59.02	47.82		27.19		12.13	8.06		3.04	

The 8 – 10 km signal is shared by all but the 15 m vector in the table data, but the 15 m isobath global wavelet does have a slight undulation at 10 km that leads into the more dominant 14 km signal (Figure 45). In addition, close examination of the global wavelets reveals that the 5.63 and 6.85 km signals highlighted for the 10 and 15 km isobaths are also exhibited by the global wavelets for the 20 m and BBSL, though they are weak (Figure 45). The peak at ~ 2 km identified for the 5 m isobath and BBSL is also apparent in the 15 m isobath.

The heat map of the back-barrier shoreline is very consistent alongshore, and dominated by the 28 km signal (Figures 47 to 51). In these bathymetry, hotspots at more frequent intervals (the 20 – 28 km frequencies) are apparent, closely linked to the 15 – 18 km signals, and attached to the southern end of the island, expanding northward with deeper bathymetry. These frequencies are also present at the northern end of the island but to a lesser extent.

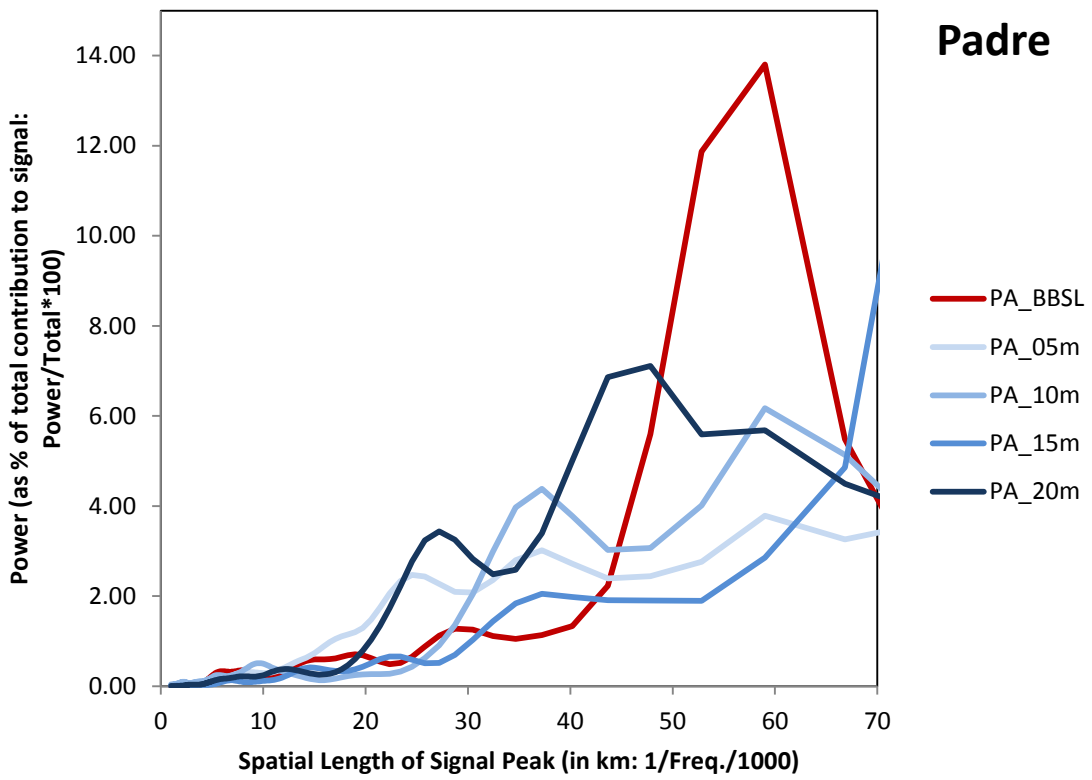

Figure 44 North Padre Island global wavelets.

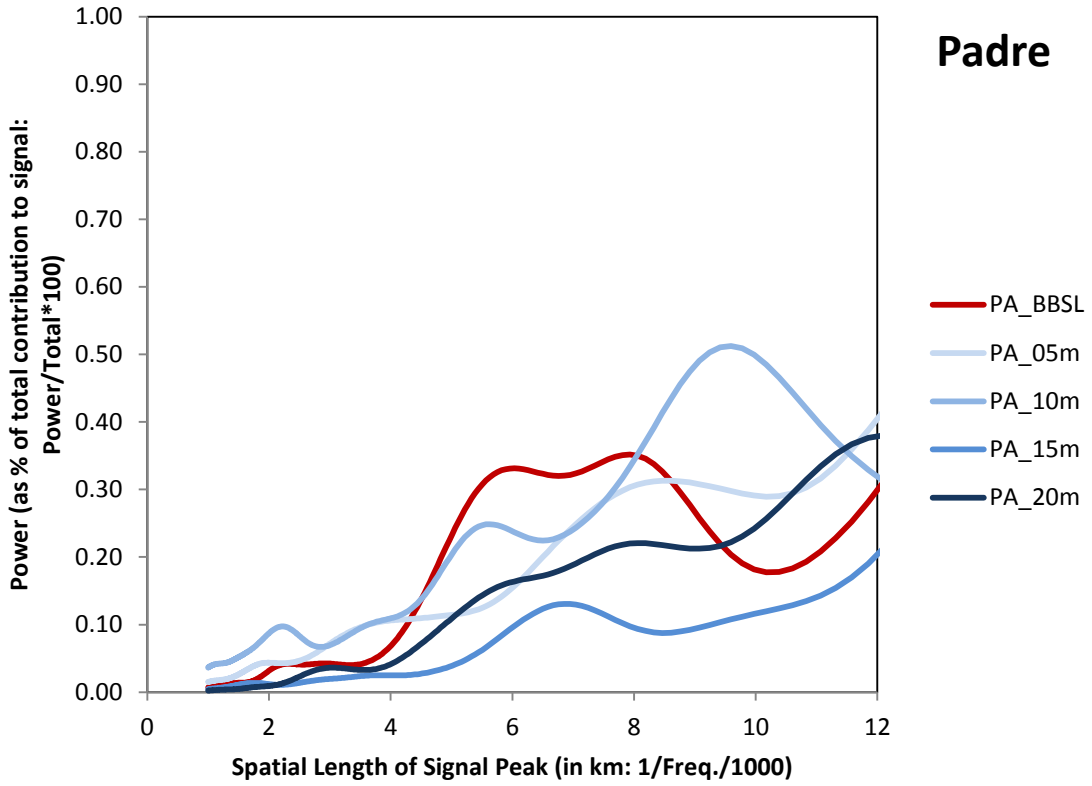

Figure 45 North Padre Island global wavelets at frequencies lower than 20 km seen in the global wavelets produced by analyzing the data for Padre Island National Seashore.

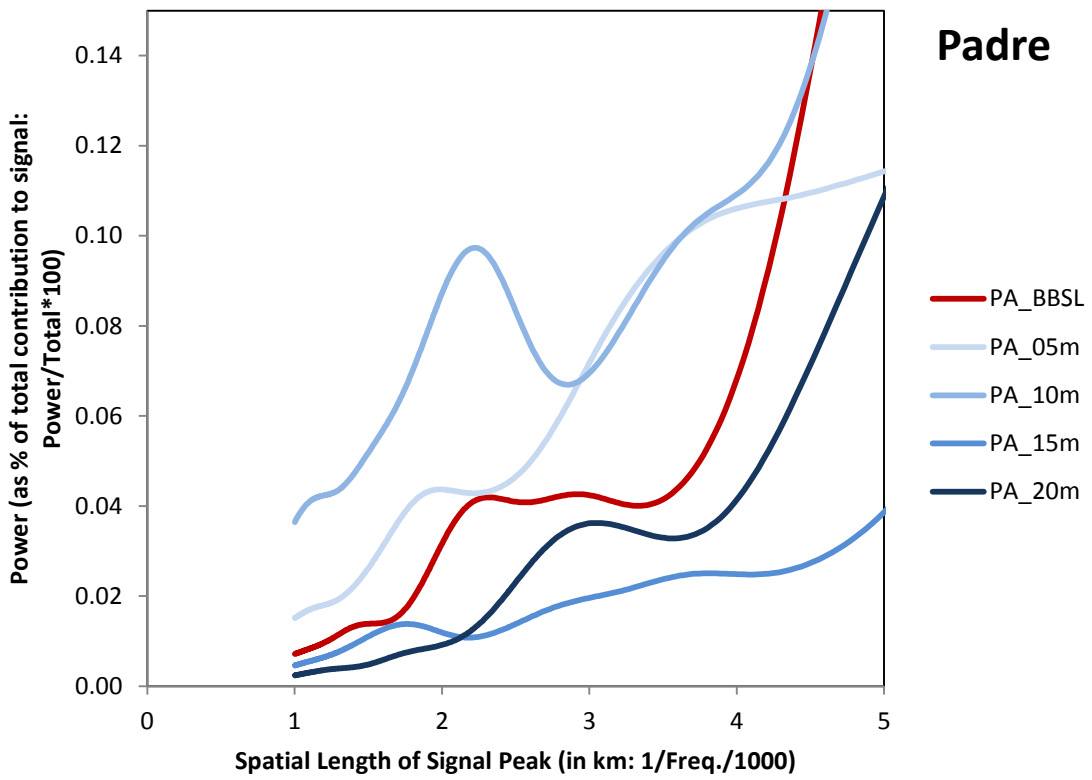

Figure 46 Global wavelets produced by analysis of vectors at North Padre Island, TX.

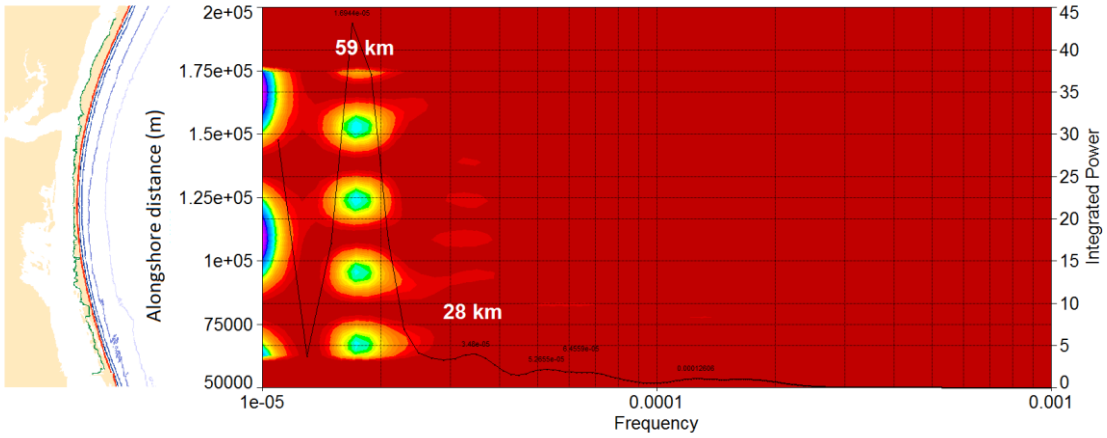

Figure 47 Heat map of the alongshore position of variances seen in the North Padre Island back-barrier shoreline.

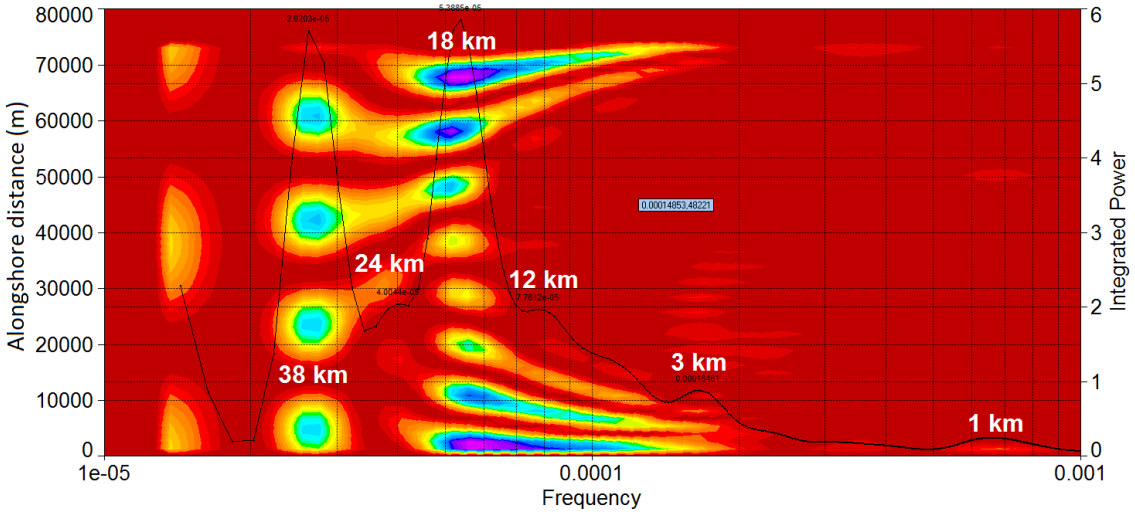

Figure 48 Heat map of variance in the 5 m isobath at North Padre Island, TX

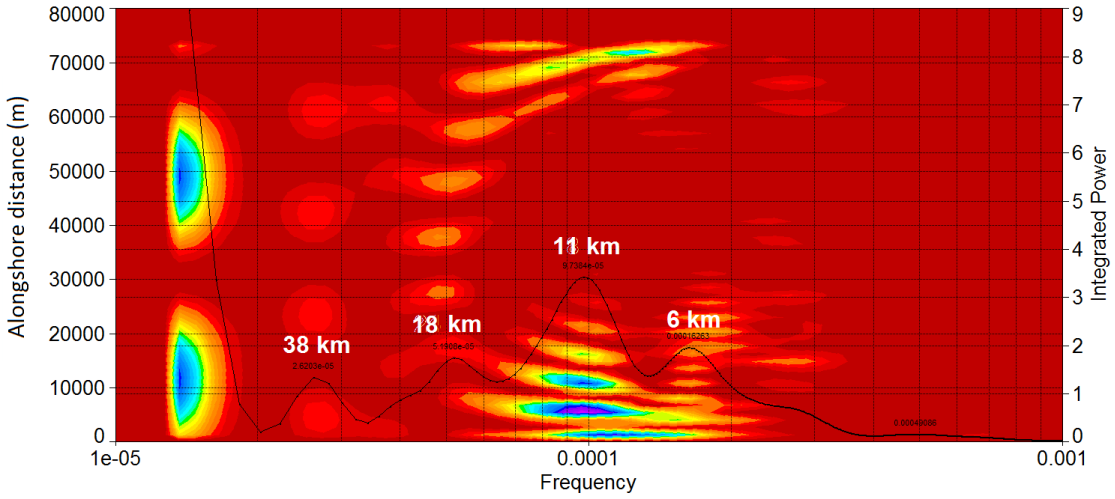

Figure 49 Heat map of variance in the 10 m isobath of North Padre Island.

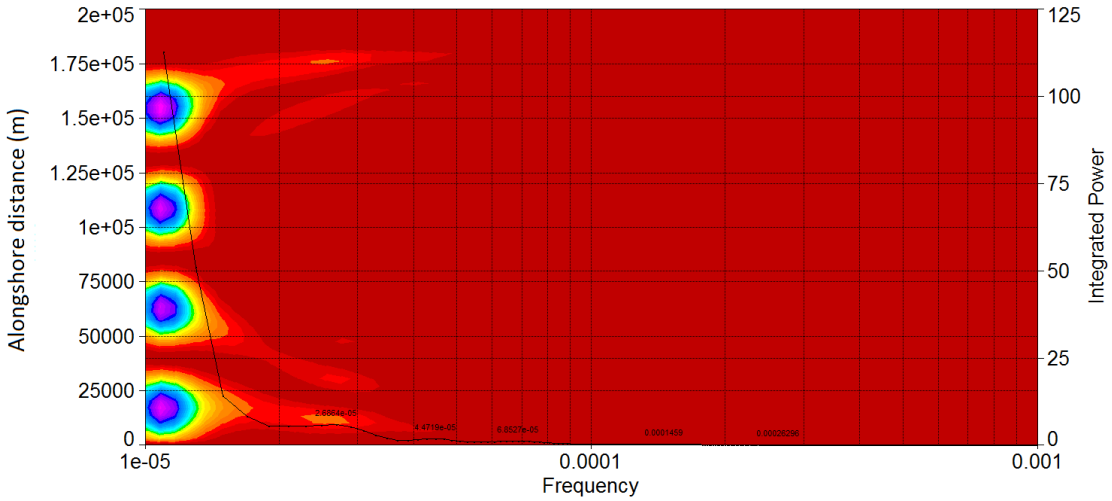

Figure 50 Heat map of the 15 m isobath of North Padre Island, TX.

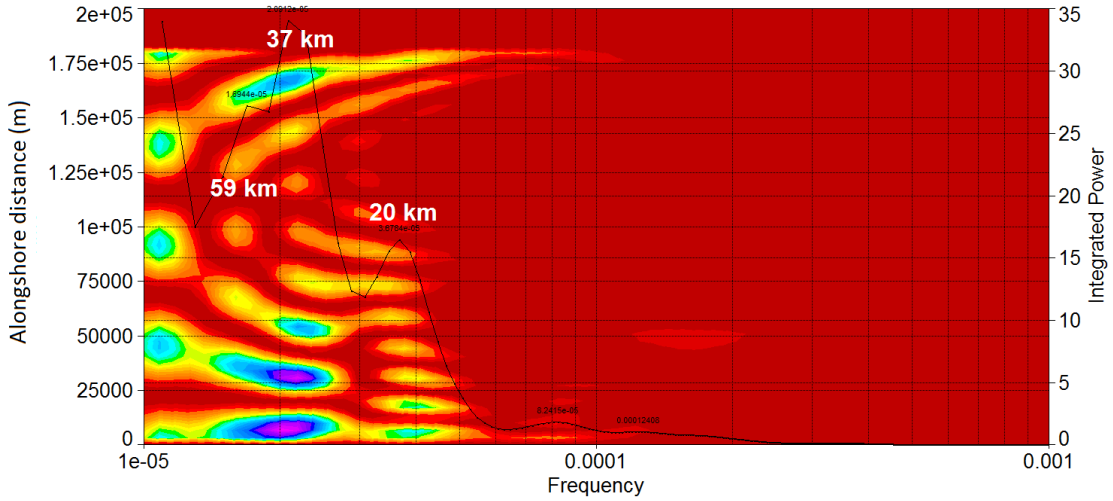

Figure 51 Heat map of the 20 m isobath at North Padre Island.

CHAPTER IV

DISCUSSION

The primary hypothesis of this study is that the dominant mechanisms responsible for the development and evolution of the back-barrier shoreline will generate an empirically identifiable shape signature indicative of that particular geomorphology. If the back-barrier shoreline is controlled by the geologic framework, then the scales of variation in its shape will be directly related to the offshore bathymetry and in some cases, also the mainland shoreline. Vectors will share signatures, and islands with similar geologic framework will share patterns. If the back-barrier shoreline is shaped independently of the geologic framework, there will *not* be shared variations beyond those that occur by chance (defined here as red noise at 95% confidence level). The results of this project show that pattern similarity occurs at all scales and between islands with similar nearshore bathymetry. This evidence adds substantial information to the presently thin literature regarding the source of back-barrier structure, and offers some of the first empirical evidence that an island's Holocene past is recorded in this structure.

In this thesis, alongshore variation in back-barrier shoreline shape was used as a proxy for dune height or structure, to examine if it reflected the same scales and frequency of variations as nearshore bathymetry and could thereby be used in future studies to expand the time and spatial scale that may be considered in future research (the coring, LiDAR, and GPR surveys that led to these conclusions are spatially restricted). The results here presented may be used as a space-for-time substitution,

interpreting the history of an island's formation (time) from its current shoreline shape and position (space). This substitution is known as the Ergodic principle and is commonly used in geology, geomorphology, and related studies of the Earth surface in which a controlled experiment is not always possible (Gardener 2004).

To test the hypothesis, four objectives were completed. First, extensive profiles for four US National Seashores were compiled from their extensive geomorphological literature (see Chapter I). Second, high resolution orthoimagery taken within the last decade was acquired for each location and the back-barrier shoreline and mainland shorelines of each study site were digitized according to the marshline (where present). Third, the shoreline shape signature of each island was quantified using wavelet analysis, so that the length frequency and alongshore variation of features in the back-barrier shoreline, the mainland shoreline, and isobaths in the lagoon and nearshore were empirically identified. In this final chapter, correspondence between these shape signatures and observed geomorphological processes (or lack thereof) is attributed to the geomorphic features and geologic framework present at each island.

Each island exhibits a variation in the BBSL at a range of spatial scales, and for each island variations are seen at the same scales in other vectors, sometimes with corresponding alongshore variation evidenced by heat maps. In many cases this correspondence is in-phase (as with the 2 km ridges at Santa Rosa). When this spatial correspondence occurs, it implies that the forces creating the vector's shape, and the controls on said forces, are shared between features. For all islands, variations that are continuous alongshore are indicative of self-organizing forces, such as the predominant

wind and wave directions that develop cuspate features on the shore of elongate water bodies (Ashton et al. 2009). In a self-organizing system, units in a landscape are pre-determined to reach only one possible outcome state, and entropy in the system is zero. In this environment, landscape evolution reflects progression towards the zero entropy state, and this process is manifested by alongshore regularity in features (Phillips 1995). When variations are localized alongshore, they represent a localized control by geologic forcing in that space and on a local direction. Some of the self-similarity seen in each vector is indicative of the fractal nature of these shapes. Indeed, Benoît Mandelbrot coined the term 'fractal' after publishing his paper "How Long Is the Coast of Britain? Statistical Self-Similarity and Fractional Dimension" (1967). Unfortunately the timeline of this project did not allow for fractal analysis of the vectors examined for determining the degree to which self-similarity contributes to overall shoreline shape, but this could be an interesting direction for future research

Implications of alongshore variation in signals

At Santa Rosa Island, offshore ridges of 3 m relief have been identified by bathymetric survey, GPR, and sediment coring for examination of their sedimentary layers. Findings reveal that ridges are interspersed with organic material that is seen in the wider cuspate sections of the modern barrier island. Also, the near-horizon mud and sand layers resemble those seen in the back-barrier of islands, bolstering the conclusion that the ridges were once the back-barrier of the island (Houser 2012). The swales are spatially correlated with narrower island sections, and cores taken in the swales also

possess the interspersed mud, sand and clay layers that result from multiple, overlain washover fan deposits, but these cores are absent the woody material seen in the ridge cores (Houser 2012). This evidence further substantiates the theory that ridges and swales in the nearshore bathymetry are not only spatially correlated to wider and narrower parts of the island today, but have been through the Holocene.

The geologic framework at Santa Rosa is a controlling factor on island morphology, including the shape of the back-barrier shoreline. The ridges are oriented to the gulf-facing beach shoreline in parallel with the typical incoming wave field. They are nearly normal to the shoreline, and the wave action of incoming waves under normal or storm conditions will be focused by this nearshore bathymetric topography. The wave alongshore variation in wave action forces alongshore variation in erosion and deposition of the beach, which leads concurrent alongshore variation in eolian transport potential and sediment supply to the dune system (Houser 2012). The result is variations in dune height and stability, which leads to self-reinforcement of the narrow and wide sections of the island by causing some areas (the narrow portions that spatially correspond to swales) to be routinely more prone to washover events, and others areas (wide sections with more stable dunes) to experience less.

In addition, the self-organizing system described by Ashton et al. (2009) that is generated in the narrow back-barrier lagoon moves sediments away from the cusps that form at the narrow island sections and transports them to the cusps which form at wider parts of the island (Ashton et al. 2009). Washover events that breach the narrow island widths bring sediment deposits to the back-barrier. These are not well consolidated at

first, and what few waves are possible to form in the back-barrier preferentially moves them toward the wider cusps (Ashton et al. 2009). The back-barrier shoreline is typically a low-energy coast, bordering a narrow, shallow lagoon where few waves can form that are capable of moving sediment or reworking the shoreline. These transport-capable waves that do form are generate by the predominant wind direction in Santa Rosa Sound, either from the northeast into the southwest (onshore to the back-barrier shoreline) or from the southeast into the northwest (offshore to the back-barrier shoreline but onshore to the mainland shoreline). Neither of these is aimed directly down the long axis of the lagoon, but they can form waves strong enough to refract down the elongated water body, and it is these refracted waves that form the self-organizing system, which is organized enough by the westernmost end of the lagoon (the endpoint of the travelling refracted waves and area which experience the most focused and organized wave activity). It is not coincidental that the cusps are most clearly formed at this end of the lagoon.

The cusp tips along the Santa Rosa back-barrier and mainland shorelines in the eastern km of the island are spaced ~ 2 km apart. Wavelet analysis of these two shorelines reveals a 2 km signal in both shorelines, though they are too small to be seen as hot spots in the heat map; filtering and closer examination of only these coastline portions might reveal alongshore correspondence in signal, which would confirm that this location fits the model proposed by Ashton et al. (2009). The 2 km signal seen in the shorelines is also present in the nearshore isobaths; if a more highly filtered or focused wavelet analysis of this part of the island revealed alongshore correspondence of these

features as well, then there is evidence that the winds and low-energy wave environment as described by Ashton et al. (2009) is not the only geologic control on the shoreline shape at that scale. Ridges previously identified for the length of Santa Rosa Island (Houser 2012) are typically spaced 1 – 3 km apart along the nearshore. An alternative geologic framework may be responsible for the back-barrier shoreline shape if the 1.5 – 2 km (identified in all vectors) and 2.4 – 2.8 km (identified in some vectors) signals identified by the wavelet analysis are distributed continuously alongshore (as the ridges are known to be).

The cuspate shoreline is also seen in the back-barrier shoreline of Assateague Island, though to a lesser extent. Here, the winds blow predominantly from the north to the south, directly along the long axis of the narrow north end of the lagoon. The most clearly formed cusps are again present at the shorelines farther down the axis of the predominant wind direction: the cusps at the wider southern end of the Assateague mainland shoreline are formed where the waves have had longer space and time to refract and organize, preferentially eroding the cuspate bays and accreting alongshore sediment transport at the cusp headlands.

At the northern end of Assateague Island, the cusps along the mainland and back-barrier shores of narrow Sinepuxent Bay are between 1 and 3 km wide, with greater variation in width seen in the mainland shoreline (Figure 52). These features may be the shape captured by the 1 km signal in the back-barrier shoreline and the 1 & 2 km signals extracted by the wavelet analysis in the mainland shoreline. At such small length scales, neither is apparent in the heat maps generated – but if they appeared in more highly

filtered wavelet analysis to be concentrated along the northern coasts of these two shorelines (and with the correct alongshore spacing) then it could be hypothesized that in Sinepuxent Bay, Assateague also exhibits some of the self-organizing alongshore sediment transport described by Ashton et al. (2009). For the rest of the island, where the sound is wider, the cusps are not present. The larger 18 km length signal shared by all vectors (except the 10 m isobath) is located at ~10 km intervals alongshore for all datasets, but is not perfectly in phase for any of these. This finding matches the qualitative assessment that any ridges seen in the Assateague bathymetry are highly oblique to the shore, but highlights a periodicity in their shape not easily proven by qualitative observation. The regularity of this 18 km signal suggests self-organization over geologic control, perhaps driven by the longshore current and wave actions along this part of the coast. If the precise locations of the paleochannels could be mapped for the length of Assateague Island, then the alongshore location of these features could be examined for relationship to the alongshore variations seen in the data developed here, but this has not been accomplished by previous works.

What ridges and swales are seen in the nearshore bathymetry of Assateague Island are not as well defined as at Santa Rosa. The geologic framework here is the result of paleo-channels that have become submerged submarine features during the Holocene. Unfortunately, clear maps of the alongshore locations of these channels do not yet exist, though several research project are currently underway at several American universities in an attempt to clarify their location and formation.

Figure 52 Cuspate shorelines seen at Assateague Island (top) and Santa Rosa Island (bottom). Wind roses have been rotated to match the orientation of the photographs. The wind roses indicate the direction the wind *is blowing* – so longer sections of red indicate persistent winds into that direction. Although the strongest winds are not necessarily in the same direction as the long axis of these sounds, one of three dominant wind directions is in line.

Results of this study show that the 2 km spacing of the ridges can be identified via wavelets analysis in both the bathymetry and the back-barrier shoreline. The mainland shoreline also exhibits this length scale in its shape signature. At Fire Island, the BBSL reflects the nearshore bathymetry directly. The ridge and swale topography of the shelf formed independently of the barrier island during the Pleistocene or early

Holocene. These types of ridges are "ubiquitous features of the Mid-Atlantic Bight continental shelf" but the origin and evolution of these features in the modern ridges and swales is not fully documented (Hapke et al. 2010). It is known that the barrier island formed after this geologic framework and as a result, forces (such as the persistent waves from the southeast) have shaped the island into a feature reminiscent of the same alongshore variations seen in the bathymetry. Where the ridges are attached to the shore at angles near 45º in the western half the island, the overall trend for the shoreline in the last century has been accretion, which suggests that the ridges may be a sources of sediment for the beach, or that they dissipate wave energy in such a way that accretion is encouraged (or both; Hapke et al. 2010). This is a similar pattern to that seen at Santa Rosa Island, where ridges also spatially correspond to wider parts of the beach.

In the eastern half of the island the ridges are present but they are farther offshore, and spatially correspond to an overall net erosion of the beach. Within the two halves of the beach, there is higher frequency pockets of erosion and accretion that occur in 2 – 4 km intervals. These zones spatially correspond to the 2 – 4 km spacing of the ridges offshore (Hapke et al. 2010). A 2 or 3 km signal is revealed by the wavelet analysis of the Fire Island data in all bathymetric data as well as in the back-barrier shoreline. In the heatmap of the back-barrier shoreline the hot spots representing the alongshore variation of the 2 km signal are concentrated on the western side of the island, and spatially correlated in-phase alongshore with the same signal in the isobaths. This is further evidence that the back-barrier reflects the geologic framework of the

nearshore because in the western half of the island, where the ridges are attached to the shoreface, the ridges are spatially correlated to the wider portions of the back-barrier.

Hapke et al. (2010) found that areas of accretion were spatially correlated to ridges; the results presented here show that the back-barrier shoreline shape is wider at these accretionary coasts. This is also in concurrence with the alongshore transport modeled by Ashton et al. (2009) which proposes that alongshore sediment transport in the back-barrier will be concentrated toward cusps or protruding parts of the coast, and matches the evidence seen in the data for Santa Rosa Island, Florida and Assateague Island, Maryland. The cuspate features described in Ashton et al. (2009) are not seen along either shoreline of Fire Island because the sound here is wide; it is the widest water body of these four study sites and does not meet the "elongated" requirement for the self-organizing shape to develop, though the general alongshore transport described by Ashton et al. (2009) may be present. Combining the findings of previous studies with the findings of this study implies that the wider sections of the back-barrier result from a combination of multiple forces within the geologic framework: the ridges and swales in the nearshore control alongshore variation in sediment supply and wave impact on the coast, which restricts dune development and supply to the back-barrier, while the fetch-limited back-barrier experiences alongshore transport that also preferentially erodes narrower island sections and accretes wider sections.

Previous research at three of the four islands has identified a similar series of geologic traits. Along much of the US East and Gulf Coasts, bathymetric shoals exist on the inner shelf, where they modify sediment supply, incoming wave energy, and

alongshore current energy that affects the patterns of sediment erosion, transport, and deposition on their adjacent beaches (Riggs et al. 1995). Of the four study sites, only Santa Rosa, Fire Island, and Assateague have these ridges.

At Santa Rosa Island the ridges are a tread left by wider parts of the island as it transgressed through the Holocene. Their slightly curved shape is reminiscent of the spit that forms at the westernmost end of the island. It is possible that the ridges are not only evidence of transgression of the island northward toward the mainland, but also of deposits of the longshore current that moves from the east to the west. This elongating spit theory of barrier island formation is one theory put forth to explain the origin of Santa Rosa Island and others in the Gulf Islands National Seashore Chain (Otvos ####).The widest signal seen at Santa Rosa and the other islands may be the remnants of tidal inlet deltas as the westernmost island end migrated westward with the transport of sediment by the longshore current.

At Fire Island, the geologic origin of the ridges is not well-defined. They are clearly in-phase with the wider parts of the island are likely a tread left by the transgression of the island towards Long Island through the Holocene. Their angle (parallel to the predominant incoming waves) and spatial correspondence to erosion and accretion on the ocean-facing beach, as well as self-reinforcement of breaches over modern time, are geomorphological evidence that the shape signatures shared between the back-barrier shoreline and nearshore bathymetry are indicative of a transgressional tread.

At Assateague Island, the few, scattered ridges are the result of in-filling of a surface previously dissected by paleochannels, though the specific alongshore locations of these channels are not entirely well-mapped. Here, the self-reinforcement of island washover locations is dictated by the lower dune heights and narrower island widths, created as an antecedent morphology at an unknown time.

Each of these three islands has exhibited transgression through the Holocene and migration through overwash, for which the alongshore variation is controlled either directly or indirectly by the nearshore ridges. At Santa Rosa, these troughs appear to focus washover so that narrower island sections spatially correspond to swales, and ridges correspond to wider island cusps. Potential causes of this alongshore variability include the ability of storm surge to advance closer to the beach and overtop the narrower island (Houser, Hapke and Hamilton 2008; Houser 2012). At Fire Island, the same conditions appear to be true, as the ridges have been shown to spatially correspond with wider sections of the island (Hapke et al. 2010). Alongshore variability in washover frequency at Assateague Island appears driven by the location of previous inlets and breaches in the island chain, and has not yet been tied to nearshore geologic framework (Krantz et al. 2008).

Like these three islands, North Padre Island has also transgressed throughout the Holocene, but it is so abundantly supplied with sediment by the convergence of longshore currents in the Gulf of Mexico that it transgresses not by wave action and overwash events controlled by the nearshore bathymetry, but instead as a result of eolian transport that leads to dune migration and dune blowouts (Weise and White 1980). This

process results in a lack of the back-barrier variation seen at the other three sites. The more subtle undulations in this back-barrier shoreline are evidence of consistent transport of sands into the back-barrier by eolian transport caused by persistent winds. The winds are persistent, driving dunes and dune blowouts consistently in the same shore-normal direction and moving sands from the beach to the back-barrier. The back-barrier shoreline has variations on the same minor scale as the bathymetry, as evidenced by shared signals at Padre, but relative to those seen at the other islands these are minimal and lack the larger-scale alongshore variation seen in geologically controlled forces. Also, when these high frequency variations are seen in the other islands it is due to wave action along the low-energy back-barrier shoreline. Laguna Madre is so incredibly shallow that even the low-energy waves shaping the Santa Rosa, Assateague, and Fire Island cannot form. Instead, rising and falling tides and winds that are rarely directed down the long axis of the lagoon maintain the dominance of eolian transport normal to the shore. Such environments can result from persistent wind (Padre) or wave action (Santa Rosa) and are evidenced by cuspate features along the shorelines of Santa Rosa Island and Assateague Island (Figure 52).

At North Padre Island, there are a few small ridges spaced about 2 km apart are present along the southernmost 15 km of shoreline of the study site, near the artificially maintained Mansfield Inlet. Their signal is too high frequency to be apparent in the heat-map, but the table output and global wavelets indicate that this 2 km signal is present in the back-barrier shoreline. To identify alongshore correspondence with these ridges would require higher filtering during the wavelet analysis. The ridges are evidenced in

the heat maps of the 5 and 10 m isobaths, where they appear as hotspots spaced 3 km (for the 5 m isobath) and 6 km (for the 10 m isobath) alongshore. This spacing suggests that the ridges widen at a 1:2 rate with increasing depth, making them indistinguishable in the 15 m and 20 m isobath heat maps, despite being identified as signals in these vectors by the table output. The ridges here are indicative of the ridges seen at the other islands, in that they may represent remnants of the tidal inlet delta present here before North Padre Island was cartographically surveyed. The Mansfield Inlet was likely created at an already narrow part of the island. A narrow portion that, perhaps, was previously an inlet but was since in-filled by the convergence of the Gulf of Mexico alongshore currents. There is not at present primary literature sources to cite this theory, but it is a possibility and if true, would indicate the same processes observed at the other study sites.

The two primary reasons the back-barrier shoreline may strongly reflect patterns at the same scales and alongshore placement as the isobaths is if:

1. The ridge and swale topography of the shelf, which formed independent of the barrier island during the Pleistocene or early Holocene, forces alongshore variation in washover and dune morphology through wave forcing during storms
2. The backbarrier shoreline developed in a particular pattern early in the Holocene, and is responsible for creating the ridge and swale morphology as a tread left by the island as it transgressed.

The higher frequency features shared between bathymetry and the mainland or back-barrier coastlines are identified above, but larger scales of variation are also strongly shared among datasets. At Santa Rosa Island, a 38 km and 25 km signal shared by all vectors is also in-phase for all vectors and located at consistent interval alongshore. These signals are oriented parallel to the island's historic path of transgression, through the shallower isobaths show some influence of an axis that parallels the modern day predominant incoming waves. If the ridges are a tread left by the island as it moved closer to the mainland, this would explain why they are in-phase for all vectors, and oriented normal to the shore (and not to incoming waves). The slight re-working of the shallower isobaths by the wave direction is a modern feature.

Shape signatures of 18 km and larger are shared at all study sites between multiple vectors. These are sometimes in-phase (as at Santa Rosa and North Padre Island), and sometimes occur with a slight alongshore shift in center (as at Fire Island) or with a shift in both alongshore center and spacing (at Assateague). These large scales of variation are more likely attributed to the geologic environment, while smaller scales are more likely attributed to the morphologic environment.

Conclusions

When the passive margin coastlines of the United States are confronted with limited sand supply, such as the restrictions placed on Assateague Island by the jetties at the Ocean City Inlet, or the less extreme removal of sands by strong alongshore currents at Fire Island and Santa Rosa, the coast will typically develop barrier islands that

become “perched upon pre-modern stratigraphic units that occur beneath and seaward of the shoreface” (Riggs et al. 1995). The stratigraphy created by this process on a geologic time scale then manifests as a modern control on the morphology of the shoreface, beach dynamics, sediment composition and budget flux of the beach and the island as whole (Riggs and O’Connor 1974; Pearson 1979; Riggs 1979; Crowson 1980). In this way it influences both the large-scale and smaller-scale variations seen in the back-barrier shoreline. Also, when these complex submarine headlands are composed of softer, layered rock types such as compacted muds or peats, limestone, or sandstone (as at Fire Island, Assateague Island, and Santa Rosa), they will have a greater effect on the morphology of the shoreface than if the inner shelf is composed of unconsolidated sands or soft muds (Riggs et al. 1995) as it is at North Padre Island.

At the four study sites, signals in the back-barrier shoreline shape spatially correspond to signals seen in both the nearshore bathymetry and, at some scales, the mainland shoreline. This correspondence supports the theory that the ridges may be a tread left by the transgression of the island since the Holocene. For Santa Rosa and Fire Island, the alongshore variation in the back-barrier shorelines are an appropriate proxy for alongshore variation in bathymetry and the forces acting on the beach face (and the island has a whole). The back-barrier may be reasonably used to estimate the morphological history and future response of the island to geomorphologic forces, as long as the segmentation of the narrow lagoon shores is accounted for, according to the Ashton et al. (2009) model. It is possible, at Santa Rosa and Fire Island, to make a space-for-time substitution where variations in geologic forces are concerned.

The same proxy relationship exists for Assateague Island and North Padre Island, despite the differences in their geomorphologic history from the other two study sites and from each other. To strengthen the correspondence between Assateague Island alongshore distribution of shape signatures, a more defined map of paleochannels in the nearshore must first be created, then compared to the trends seen in the data presented here. At North Padre Island, though back-barrier shoreline shape is more driven by the winds and abundant sediment supply than by nearshore bathymetry, these are still evidenced in the global wavelets and alongshore variations that are present. Despite a different morphological history and present suite of conditions, the back-barrier shoreline is still a possible record of geologic framework.

"The complex variability in this underlying geologic framework, in consort with the physical dynamics of each specific coastal system, ultimately determines the 1) 3-D shoreface morphology, 2) composition, and texture of beach sediments, and 3) shoreline recession rates" (Riggs et al. 1995). The most shoreline variability occurs where there is the most variability in the geologic framework, both in the nearshore underwater topography (as at Fire Island and Santa Rosa Island) and in sediment texture being supplied (as at Assateague). Where these are absent (Padre) you see less variability and more stability. Although the sediments being so abundantly supplied to North Padre Island are from the convergence of longshore currents brings very different sediments, there is such homogeneity of substrate and nearshore bathymetry that these are the controlling factors and the resulting back-barrier shoreline has alongshore-consistent, medium to large scale variability.

The antecedent structural and nearshore stratigraphic characteristics of "the pre-barrier island surface interacts in a complex way with modern coastal processes to determine the barrier beach, morphology and nearshore dynamics" seen today (Riggs et al. 1995). This antecedent geologic framework of a barrier island controls and influences the present morphology, nearshore dynamics, and rates of transgression in response to sea-level rise so that it produces a signature that can be seen in the shape of the back-barrier shoreline.

Research published since 2000 has suggested that antecedent morphology, and the geomorphological history in general, are recorded in the back-barrier of islands (Houser, Hapke, and Hamilton 2008).This history is evidenced in the present landscape, which is in turn controlled by the geologic framework (Riggs, Cleary and Snyder 1994; Houser 2012). In other words, there is a multi-scale feedback in which the response of barrier islands to storms defines and is defined by the geologic framework. The methodology tested here attempts to make a space-for-time substitution of the shape and location of the back-barrier shoreline for geomorphological history of the barrier island. The shape signature of the back-barrier shoreline of four islands is empirically identified and coupled to each island's nearshore geologic structure, as well as the geomorphological profile assembled from the ample literature available for each island.

These methods can then be applied to new locations in future research projects; investigators will be able to quantify the back-barrier shoreline shape of unstudied or poorly understood barrier islands and deduce information about that island's geomorphologic history. Understanding the correspondence between shoreline shape

signatures and known morphological processes will extend geologic surveys and actuate projects on less-investigated barrier islands.

REFERENCES

Ashton, A.D., A. B. Murray, R. Littlewood, D. A. Lewis, and P. Hong. 2009. Fetch-limited self-organization of elongate water bodies. Geology. 37: 187-190.

AutoSignal Users Guide, version 1.7. 2003. SeaSolve Software Inc. Framingham, MA, USA.

Brock, J. C., W. B. Krabill, and A. H. Sallenger. 2004. Barrier island morphodynamic classification based on LiDAR metrics for north Assateague Island, Maryland. Journal of Coastal Research. 202: 498-509.

----------, A. Nayegandhi1, and M. Duffy. 2005. Extracting Shorelines from NASA Airborne Topographic Lidar-Derived Digital Elevation Models. U.S. Geological Survey, Open-file report 2005–1427

Bricker-Urso, S., S. W. Nixon, J. K. Cochran, D. J. Hirschberg and C. Hunt. 1989. Accretion rates and sediment accumulation in Rhode Island salt marshes. Estuaries. 12: 300-317.

Bullard, F. M. 1942. Source of beach and river sands on Gulf Coast of Texas. Geological Society of America Bulletin. 53(7): 1021-1043.

Claudino-Sales, V., P. Wang, and M. H. Horwitz. 2008. Factors controlling the survival of coastal dunes during multiple hurricane impacts in 2004 and 2005: Santa Rosa barrier island, Florida. Geomorphology. 95: 295-315.

Cooper, J. A. G., and F.Navas. 2004. Natural bathymetric change as a control on century-scale shoreline behavior. Geology. 32: 513-516.

Courrat, A., J. Lobry, D. Nicolas, P. Laffargue, R. Amara, M. Lepage, M. Giardin, and O. Le Pape. 2009. Anthropogenic disturbance on nursery function of estuarine areas for marine species. Estuarine, Coastal, and Shelf Science. 81: 179-190.

Crossett, K. M., P. C. Culliton, T. R. Wiley, and B. L. Godspeed. 2004. Population trends along the coastal United States: 1980-2008. Coastal Trends Report Series. National Oceanic and Atmospheric Association, National Ocean Service, Management and Budget Office, Special Projects. 86p.

Davis, R. A. and W. T. Fox. 1975. Coastal Dynamics along Mustang Island, TX. Western Michigan University Technical Report No. 9. ONR Contract #388-092. 68 p.

Davis Jr., R.A.1997. R.A. Davis Jr. Geology of the Florida coast. In The Geology of Florida, eds. A.F. Randazzo and D.S. Jones. Gainesville, FL: University Press of Florida. pp. 155–168

Demarest, J. M. and S. P. Leatherman. 1985. Mainland influence on coastal transgression: Delmarva Peninsula. Marine Geology. 63(1): 19-33.

Dickinson, K., H. L. Berryhill and C. W. Holmes. 1972. Criteria for Recognizing Ancient Barrier Coastlines. In Recognition of ancient sedimentary

environments, ed. J. K. Rigby and W. K. Hamblin. Society of Economic Paleontologists and Mineralogists.

Donnelly, J. P., P. Cleary, P. Newby, and R. Ettinger. 2004. Coupling instrumental and geological records of sea-level change: Evidence from southern New England of an increase in the rate of sea-level rise in the late 19th century. Geophysical Research Letters. 31 L05203.

----------. 2005. Evidence of past intense tropical cyclones from backbarrier salt pond sediments: A case study from Isla de Culebrita, Puerto Rico, USA. Journal of Coastal Research. 42: 201–210.

Ebersole, B. A. 1982. Atlantic Coast Water-Level Climate: Wave Information Study. Vicksburg, Mississippi: U.S. Army Waterways Experiment Station Report No. 7. 35p.

Edgar, G. J., N. S. Barrett, D. J. Graddon, and P. R. Last. 2000. The conservation significance of estuaries: a classification of Tasmanian estuaries using ecological, physical and demographic attributes as a case study. Biological Conservation. 92: 383-397.

Emery, K. O. 1969. A Coastal Pond Studied by Oceanographic Methods. Woods Hole, Massachusetts: Oyster Pond Environmental Trust Inc.111 pp.

Foster, E. R., D. L. Spurgeon, and J. Cheng. 1999. Shoreline change rate estimates: Escambia and Santa Rosa Counties. Florida Department of Environmental Protection, Office of Beaches and Costal Systems, Report BCS-99-03. 85 p.

French, P. W. 2006. Managed realignment – the developing story of a comparatively new approach to soft engineering. Estuarine, Coastal and Shelf Science. 67: 409-423.

Gardner, L. R. 2004. Geologic History and the Ergodic Principle: Foundations for Long-Term Ecological Research in Salt Marshes. In *The Ecogeomorphology of Tidal Marshes,* Eds S. Fagherazzi, M. Marani and L. K. Blum. Washington, D. C.: American Geophysical Union.

Goodnough, A. 2005. Intense storms of ’05 may become the norm. The New York Times. 30 November 2005. p. A19

Hapke, C. J., E. L. Lentz, P. T. Gayes, C. A. McCoy, R. Hehre, W. C. Schwab, and S. J. Williams. 2010. A review of sediment budget imbalances along Fire Island, New York: Can nearshore geologic framework and patterns of shoreline change explain the deficit? Journal of Coastal Research. 26(6): 510-522.

Hayes, M.O. 1965. Sedimentation on a semiarid, wave-dominated coast (South Texas) with emphasis on hurricane effects: Univ. Texas, Austin, Ph.D. dissertation. 350 p.

Hennessy, J. T., and G. A. Zarillo. 1987. The interrelation and distinction between flood-tidal delta and washover deposits in a transgressive barrier island. Marine Geology. 78:35-56.

Himmelstoss, E. A. 2009. DSAS 4.0 Installation Instructions and User Guide. in: Thieler, E.R., E.A. Himmelstoss, J. L. Zichichi, and A. Ergul. 2009.

Digital Shoreline Analysis System (DSAS) version 4.0 – An ArcGIS extension for calculating shoreline change: U.S. Geological Survey Open File Report 2008-1278. *updated for version 4.3

Houser, C., C. Hapke, and S. Hamilton. 2008. Controls on coastal dune morphology, shoreline erosion and barrier island response to extreme storms. Geomorphology. 100(3-4): 223-240.

---------- and S. Hamilton. 2009. Sensitivity of post-hurricane beach and dune recovery to event frequency. Earth Surface Processes and Landforms. 34: 613–628.

---------- and S. Mathew. 2011. Alongshore variation in foredune height in response to transport potential and sediment supply: South Padre Island, Texas. Geomorphology. 125(1): 62–72.

----------. 2012. Alongshore Variation in the Morphology of Coastal Dunes: Implications for Storm Response. Geomorphology. (in press, a corrected proof) Available online 17 November 2012.

Hubertz, J. M., E. F. Thompson, and H. V. Wang. 1996. Annotated Bibliography on Coastal and Ocean Data Assimilation. WIS Report 36. Vicksburg, Mississippi: U.S. Army Waterways Experiment Station Report. 31p.

Hyne, J. H., and G. H. Goodell. 1967. Origin of the sediments and submarine geomorphology of the inner continental shelf off Choctawhatchee Bay, Florida. Marine Geology. 5(4): 299-313.

International Bathymetric Chart of the Caribbean Sea and the Gulf of Mexico (IBCCA). 2013. <http://www.ngdc.noaa.gov/mgg/ibcca/> Visited 19 April, 2013.

Jackson, N. L., K. F. Nordstrom, I. Eliot, and G. Masselink. 2002. 'Low-energy' sandy beaches in marine and estuarine environments: a review. Geomorphology. 48: 147-162.

Kemp, A. C., B. P. Horton, J. P. Donnelly, M. E. Mann, M. Vermeer, and S. Rahmstorf. 2011. Climate related sea-level variations over the past two millennia. Proceedings of the National Academy of Sciences of the United States of America. 108(27): 11017–11022.

Kennish, M. J. 2001. Coastal salt marsh systems in the U.S.: A review of anthropogenic impacts. Journal of Coastal Research. 17(3): 731-748.

Leatherman, S. P. 1979 Migration of Assateague Island, Maryland, by inlet and overwash processes. Geology. 7(2): 104-107.

----------. 1983. Barrier dynamics and landward migration with Holocene sea-level rise. Nature. 301:415-417.

----------. 1985. Geomorphic and stratigraphic analysis of Fire Island, New York. Marine Geology. 63:173-195.

---------- and J. R. Allen. 1985. Geomorphic analysis of the South Shore Barriers of long island, New York. Boston, Massachusetts: Technical Report, National Park Service, 350p.

Leblanc, R. J. and W. D. Hodgson. 1959. Origin and Development of the Texas Shoreline.

Liu, K and M. L. Fearn. 1993. Lake-sediment record of late Holocene hurricane activities from coastal Alabama. Geology.21(9): 793-796.

Lohse, E. A. 1953. Dynamic geology of the modern coastal region, northwest Gulf of Mexico. Journal of Sedimentary Research. 23: 100-105

Lonard, R. I. and F. W. Judd. 1980. Phytogeography of South Padre Island, Texas. The Southwestern Naturalist. 25(3): 313-322.

Mackintosh, B. 1982. Assateague Island National Seashore: An Administrative History. Department of the Interior: Washington, D.C. 165p.

Mandelbrot, B. 1967. How Long Is the Coast of Britain? Statistical Self-Similarity and Fractional Dimension. *Science*. 156 (3775): 636-638.

McBride, R. A., M. R. Byrnes, and M. W. Hiland. 1995. Geomorphic response-type model for barrier coastlines: a regional perspective. Marine Geology. 126: 143–159.

----------. 1997. Regional variation in shore response along barrier island systems of the Mississippi River delta plain: historical change and future prediction. Journal of Coastal Research. 13(3): 628–655.

McCaffrey, R. J., and J. Thompson. 1980. A record of the accumulation of sediment and trace metals in a Connecticut salt marsh. Advances in Geophysics: Estuary Physics and Chemistry: Studies in Long Island Sound, vol. 22, ed. B. Salzman. New York: Elsevier. pp. 165–235.

Milliken, K. T., J. B. Andersen, and A. B. Rodriguez. 2008. A new composite Holocene sea-level curve for the northern Gulf of Mexico; in Andersen, J. B. and A. B. Rodriguez, eds. Response of Upper Gulf Coast Estuaries to Holocene Climate Change and Sea-Level Rise: Geological Society of America Society of America Special 443, p.1-11.

Moore, L. J., P. Kerlinger, and T. R. Simmons. 1990. Stopover on a Gulf coast barrier island by spring trans-gulf migrations. Wilson Bulletin. 102(3): 487-500.

Morton, R. A. 1994. Texas Barriers. In Geology of Holocene Barrier Island Systems, ed. R. A. Davis, 75-114. New York: Springer-Verlag.

----------, T. L. Miller, and L. J. Moore. 2004. National Assessment of Shoreline Change: Part 1, Historical shoreline changes and associated coastal land loss along the U.S. Gulf of Mexico. U.S. Geological Survey Open File Report, 2005-1213. p. 116.

National Park Service. 2013a. "Assateague Island National Seashore: Nature & Science." http://www.nps.gov/asis/naturescience/index.htm (last accessed 18 March 2013).

----------. 2013b. "Fire Island National Seashore: Nature & Science." http://www.nps.gov/fiis/naturescience/index.htm (last accessed 18 March 2013).

----------. 2013c. "Gulf Islands National Seashore: FL, MS." http://www.nps.gov/guis/index.htm (last accessed 18 March 2013).

----------. 2013d. “Padre Island National Seashore: History & Culture.” http://www.nps.gov/pais/historyculture/index.htm (last accessed 19 March 2013).

----------. 2013e. “Padre Island National Seashore: Nature & Science.” http://www.nps.gov/pais/naturescience/index.htm (last accessed 19 March 2013).

----------. 2013f. “Post-Hurricane Sandy: What's Happening on Fire Island.” http://www.nps.gov/fiis/post-hurricane-sandy-on-fire-island.htm (last accessed 18 March 2013).

National Research Council. 2007. Mitigating Shore Erosion Along Sheltered Coasts. Washington, D.C.: National Academic Press. p. 188.

Navarro, M. “Resisted for Blocking the View, Dunes Prove They Blunt Storms.” The New York Times. 4 December 2012. p. A1.

New York Times, Late Edition (East Coast). “Hurricane Sandy's Rising Costs: Editorial.” The New York Times. 28 November 2012. p. A.32.

NOAA National Geophysical Data Center, U.S. Coastal Relief Model, Retrieved February 2013, http://www.ngdc.noaa.gov/mgg/coastal/crm.html

Nordstrom, K. F., N. L. Jackson, J. R. Allen, and D. Sherman. 1996. Wave and current processes and beach changes on a microtidal estuarine beach at Fire Island, NY. In Estuarine Shores: Evolution, Environments, and Human Alterations. London: John Wiley & Sons. p. 213-232.

---------- and N. L. Jackson. 2005. Bay Shoreline Physical Processes (Fire Island National Seashore Science Synthesis Paper). Technical Report NPS/NER/NRTR–2005/020. National Park Service: Boston, MA.

"NPS Stats: National Park Service Visitor Use Statistics." https://irma.nps.gov/Stats/ (last visited 18 May 2013).

Orson, R. A., R. S. Warren, and W. A. Niering. 1998. Interpreting sea level rise and rates of vertical marsh accretion in a southern New England tidal salt marsh. Estuarine Coastal Shelf Science. 35: 453–471.

Otvos, E. G. 1981. Tectonic lineaments of Pliocene and Quaternary shorelines, northeast Gulf coast. Geology. 9: 398–404

Panageotou, W. and S. P. Leatherman. 1986. Holocene-Pleistocene stratigraphy of the inner shelf off Fire Island, New York: Implications for barrier-island migration. Journal of Sedimentary Petrology. 56(4): 528-537.

Parris, A., P. Bromirski, V. Burkett, D. Cayan, M. Culver, J. Hall, R. Horton, K. Knuuti, R. Moss, J. Obeysekera, A. Sallenger, and J. Weiss. 2012. Global Sea Level Rise Scenarios for the US National Climate Assessment. NOAA Tech Memo OAR CPO-1. 37 p.

Penland, S., P. F. Connor Jr., A.Beall, S. Fearnley, and S. J. Williams. 2005. Changes in Louisiana's shoreline: 1855–2002. Journal of Coastal Research. SI 44: 7–39.

Pilkey, O.H. and M. E. Fraser. 2003. A Celebration of the World's Barrier Islands. Columbia University Press. 309 pp.

Prouty, J. S. and D. B. Prouty. 1989. Historical back barrier shoreline changes, Padre Island National Seashore, Texas. Transactions – Gulf Coast Association of Geological Societies. 39: 481-490.

Psuty, N. P., M. Grace, and J. P. Pace. 2005. The coastal geomorphology of Fire Island: a portrait of community and change. Technical Report NPS/NER/NRTR–2005/021.

Qiu, L.-J. and M.-H. Er. 1995. Wavelet spectrogram of noisy signals. International Journal of Electrical Engineering. 79: 665-677.

Rampino, M. R. and J. E. Sanders. 1980. Holocene transgression in south-central Long Island, New York. Journal of Sediment Petrology. 50:1063-1079.

----------. 1981a. Evolution of the barrier islands of southern Long Island, New York. Sedimentology. 28:37-47.

----------. 1981b. Upper Quaternary stratigraphy of southern Long Island, New York. Northeast Geology. 3:116-128.

Redfield, A. C. 1965. Ontogeny of a salt marsh estuary. Science. 147: 50–55.

Redfield, A. C. 1972. Development of a New England salt marsh. Ecological Monographs. 2: 201–237.

Riggs, S. R., D. V. Ames, S. J. Culver, and D. J. Mallinson. 2011. The Battle for North Carolina's Coast: Evolutionary History, Present Crisis, & Vision for the Future. Chapel Hill, N.C.: The University of North Carolina Press. 142 p.

Roman C. T., J. A. Peck, J. R. Allen, J. W. King, P. G. Appleby. 1997. Accretion of a New England (U.S.A.) salt marsh in response to inlet migration, storms, and sea-level rise. Estuarine Coastal and Shelf Science. 45(6): 717– 727.

Rosati, J. D., R. G. Dean and G. W. Stone. 2010. A cross-shore model of barrier island migration over a compressible substrate. Marine Geology. 271: 1-16

Sallenger, A. H. Jr. 2000. Storm impact scale for barrier islands. Journal of Coastal Research. 16(3): 890-895.

----------, C. W. Wright, P. A. Howd, K. S. Doran, and K. K. Guy. 2009. Extreme coastal changes on the Chandeleur Islands, Louisiana, during and after Hurricane Katrina. In Sand resources, regional geology, and coastal processes of the Chandeleur Island coastal system – An evaluation of the resilience of the Breton National Wildlife Refuge: Lafayette, LA, U.S. Geological Survey Scientific Investigations Report 2009-5252, ed. D. L. Lavoie. p. 27-36.

Sanders, J. E. and N. Kumar. 1975. Evidence of shoreface retreat and in-place drowning during Holocene submergence of barriers: Continental shelf off Fire Island, N.Y. Geological Society of America Bulletin. 85:65-76

Schupp, C.A., G.P. Bass, and W.G. Grosskopf. 2007. Sand bypassing restores natural processes to Assateague Island, Maryland. In Proceedings Coastal Sediments '07. eds. N.C. Kraus and J.D. Rosati. Reston, VA: America Society of Civil Engineers.

Schwab, W. C., E. R. Theiler, J. R. Allen, D. S. Foster, B. A. Swift, and J. F. Denny. 2000. Influence of inter-continental shelf geologic framework on the evolution and behavior of the barrier-island system between Fire Island Inlet and Shinnecock Inlet, Long Island, New York. Journal of Coastal Resources. 16(2):408-422.

Scileppi, E. and J. P. Donnelly. 2007. Sedimentary evidence of hurricane strikes in western Long Island, New York. Geochemistry Geophysics Geosystems. 8(6):Q06011.

Sirigan, F. P. and J. B. Anderson. 1994. Modern shoreface and inner-shelf storm deposits off the east Texas Coast, Gulf of Mexico. Journal of Sedimentary Research. B64(2): 99–110.

Shepard, F. P. 1956. Late Pleistocene and recent history of the central Texas coast. The Journal of Geology. 64(1): 56-69.

Stapor, F. W. 1975. Holocene beach ridge plain development, N.W. Florida. Zeitschrift fuer Geomorpholog, Supplemenband 22. p. 116–144.

Stockdon, H.F., Sallenger, A.H., List, J.H., and Holman, R.A., 2002. Estimation of Shoreline Position and Change using Airborne Topographic Lidar Data. Journal of Coastal Research. 18(3): 502-513.

Stone, G. W. 1984. Mathematical modeling of the nearshore and implications for coastal management, Northwest Florida. Unpublished MSc thesis, Department of Environmental Studies, University of West Florida, 140 pp.

----------. 1991. Differential sediment supply and cellular nature of longshore sediment transport along coastal Northwest Florida and Southeast Alabama since the late Holocene. PhD Dissertation, University of Maryland, College Park, MD.

----------, F. W. Stapor Jr., J. P May, and J. P. Morgan. 1992. Multiple sediment sources and a cellular, non-integrated, longshore drift system: Northwest Florida and southeast Alabama coast, USA. Marine Geology. 105: 141-154.

----------, and F. W. Stapor. 1996. A nearshore sediment transport model for the northeast Gulf of Mexico coast, USA. Journal of Coastal Research. 12: 786-792.

----------, and R. A. McBride. 1998. Louisiana barrier islands and their importance in wetland protection: forecasting shoreline change and subsequent response of wave climate. Journal of Coastal Research. 14(3): 900-915.

----------, B. Liu, D. A. Pepper, and P. Wang. 2004. The importance of extratropical and tropical cyclones on the short-term evolution of barrier islands along the northern Gulf of Mexico, USA. Marine Geology. 210: 63-78.

Swift, D. J. P. and T. F. Moslow. 1982. Holocene transgression in south-central Long Island, New York-Discussion. Journal of Sedimentary Petrology. 52:1014-1019.

Torrence, A. and G. P. Compo. 1998. A practical guide to wavelet analysis. Bulletin of the American Meteorological Society. 79(1): 61-78.

United States Geological Society. 2012. High Resolution Orthoimagery (HRO). < https://lta.cr.usgs.gov/High_Resolution_Orthoimagery> Page last updated 24 January 2012. Visited 3 May 2013.

Wallace, D. J. and J. B. Anderson. 2013. Unprecedented erosion of the upper Texas coast: Response to accelerated sea-level rise and hurricane impacts. Geological Society of America Bulletin. Published online 29 January 2013.doi: 10.1130/B30725.1

Watson, R. L. 1971. Origin of shell beaches, Padre Island, TX. Journal of Sedimentary Petrology. 41(4): 1105-1111.

Weber, K. M., J. H. List, and K. L. M. Morgan. 2005. An Operational Mean High Water Datum for Determination of Shoreline Position from Topographic Lidar Data. U.S. Geological Survey, Open-file Report 2005-1027

Weise, B. R. and W. A. White. 1980. Padre Island National Seashore: A guide to the Geology, Natural Environments, and History of a Texas Barrier Island. Austin, TX: The University of Texas at Austin.

Williams, S. J. 1976. Geomorphology, Shallow Subbottom Structure, and Sediments of the Atlantic Inner Continental Shale off Long Island, New York. Fort Belvoir, Virginia: U.S. Army Corps of Engineers, CERC, Technical Paper No. 76-2. 123p.